Coarse-grained simulations of nanometer-sized devices for drug delivery

TESIS DOCTORAL

Programa de Doctorado en Física y Ciencias del Espacio

Luis Pérez Mas

Directores

Alberto Martín Molina

Manuel Quesada Pérez

Universidad de Granada

2021

Editor: Universidad de Granada. Tesis Doctorales
Autor: Luis Pérez Mas
ISBN: 978-84-1306-852-7
URI: http://hdl.handle.net/10481/68165

A mis padres.

Tabla de contenido

Abstract

It is well known that certain polymers and polyelectrolytes can be synthesized forming cross-linked networks (commonly referred to as polymer/polyelectrolyte gels). Some of these polymers are thermo-sensitive and are characterized by their ability to change reversibly from a swollen to a shrunken state with temperature. This phase transition makes the synthesis of thermo-responsive microgels (micrometric -sized cross-linked polymer particles) very interesting. However, it should be noted that both gels and microgels are sensitive to other environmental conditions (such as pH and ionic strength). As its own name implies, a microgel is a kind of "small gel", ergo, a polymer network with the entity of particle. Specifically, particles in the colloidal range of 10 to 1000 nm. They are often referred to as nanogel if their equivalent diameter is less than 100 nm.

Therefore, a great interest has surged around the microgels and nanogels as soft active materials. They could be used in a variety of applications such as super-absorbers, or as stimuli-responsive nanoreactors for controlled catalysis. In fact, these particles can be easily penetrated by solvent molecules, ions, and other types of small reactants. This opens the door for its use as drug delivery, biosensor, chemical separation, and catalysis, among others.

Although many studies have been conducted on the synthesis and characterization of microgels and nanogel dispersions, the number of articles directly related to effective interactions between constituent particles is relatively small. Computer simulation can be very helpful in clarifying these problems. Furthermore, they can be used to test theories and improve the understanding of the processes involved. More specifically, coarse-grained simulations can provide valuable information about steric and electrostatic effects on different single-particle properties without requiring detailed information on the chemical nature.

In the present thesis, different aspects of micro- and nanogels are studied with help of coarse-grained simulations, that will allow us to understand their behavior in order to be used as drug transporters. For this purpose, the equilibrium absorption of nanometric cosolutes (which could represent drugs,

reactants, small globular proteins and other kind of biomacromolecules) inside neutral hydrogels has been studied. We have explored, for different swelling states, the competition between the steric exclusion induced by the cross-linked polymer network constituting the hydrogel, and the solvent-induced short-range hydrophobic attraction between the polymer chains and the cosolute particle. For this purpose, the cosolute partition coefficient is calculated by means of coarse-grained grand canonical simulations, and the results are compared to theoretical predictions based on the calculation of the excluded and binding volume around the polymer chains. The interplay between hydrophobic adhesion and the steric exclusion leads to different behaviors depending on the hydrophobic attraction or the size of the cosolutes.

Simulations with charged nanogels have also been carried out where their ability to absorb different electrolytes or polyelectrolyte is explored. On the one hand, coarse-grained simulations of nanogels in the presence of three different electrolytes were performed. Aiming to evaluate the effect of dispersion forces on different properties of nanogels, such as size, net charge and surface electrostatic potential. This model allowed us to explicitly consider the dispersion interactions between ions inside the nanogel and monomer units rather than interactions between the ions and the nanoparticle as a whole. On the other hand, coarse-grained simulations of nanogel–polyelectrolyte complexes were carried out, where our simulation results capture two phenomena reported in experiments with real complexes: the charge inversion detected through electrophoretic mobility data, which our simulations only shows if the polyelectrolyte charge is large enough; and the reduction in size after absorbing just a few chains. These results allow us to delve into the application of nanogels as nano-sized devices for drug delivery.

Resumen

Es bien sabido que ciertos polímeros y polielectrolitos pueden sintetizarse formando redes reticuladas (comúnmente denominadas geles de polímeros/polielectrolitos). Algunos de estos polímeros son termosensibles y se caracterizan por su capacidad de cambiar reversiblemente de un estado hinchado a otro encogido con la temperatura. Esta transición de fase hace muy interesante la síntesis de microgeles termosensibles (partículas poliméricas reticuladas de tamaño micrométrico). Sin embargo, hay que tener en cuenta que tanto los geles como los microgeles son sensibles a otras condiciones ambientales (como el pH y la fuerza iónica). Como su propio nombre indica, un microgel es una especie de "gel pequeño", es decir, una red polimérica con entidad de partícula. En concreto, se trata de partículas en el rango coloidal de 10 a 1000 nm. Suelen denominarse nanogeles si su diámetro equivalente es inferior a 100 nm.

Por ello, ha surgido un gran interés en torno a los microgeles y nanogeles como materia blanda inteligente. Podrían utilizarse en diversas aplicaciones, como superabsorbentes, o nanorreactores que responden a estímulos de catálisis controlada. De hecho, estas partículas pueden ser fácilmente penetradas por moléculas de disolvente, iones y otros tipos de pequeños reactivos. Esto abre la puerta a su uso como transportadores de fármacos, biosensores, en separación química y catálisis, entre otros.

Aunque se han realizado muchos estudios sobre la síntesis y la caracterización de dispersiones de microgeles y de nanogeles, el número de artículos relacionados directamente con las interacciones efectivas entre las partículas constituyentes es relativamente pequeño. La simulación por ordenador puede ser muy útil para aclarar estos problemas. Además, pueden utilizarse para poner a prueba las teorías y mejorar la comprensión de los procesos implicados. Más concretamente, las simulaciones de grano grueso pueden proporcionar una valiosa información sobre los efectos estéricos y electrostáticos en las diferentes propiedades de las partículas individuales sin necesidad de disponer de información detallada sobre la naturaleza química.

En la presente tesis se estudian diferentes aspectos de los micro y nanogeles mediante simulaciones de grano grueso, que permitirán entender su comportamiento para ser utilizados como transportadores de fármacos. Para ello, se ha estudiado la absorción en equilibrio de cosolutos nanométricos (que podrían representar fármacos, reactivos, pequeñas proteínas globulares y otro tipo de biomacromoléculas) dentro de hidrogeles neutros. Hemos explorado, para diferentes estados de hinchamiento, la competencia entre la exclusión estérica inducida por la red polimérica reticulada que constituye el hidrogel, y la atracción hidrofóbica de corto alcance inducida por el disolvente entre las cadenas poliméricas y la partícula de cosoluto. Para ello, se calcula el coeficiente de partición del cosoluto mediante simulaciones, y los resultados se comparan con las predicciones teóricas basadas en el cálculo del volumen excluido y de unión alrededor de las cadenas poliméricas. La interacción entre la adhesión hidrofóbica y la exclusión estérica conduce a diferentes comportamientos dependiendo de la atracción hidrofóbica o del tamaño de los cosolutos.

También se han realizado simulaciones con nanogeles cargados donde se explora su capacidad para absorber diferentes electrolitos o polielectrolitos. Por un lado, se realizaron simulaciones de grano grueso de nanogeles en presencia de tres electrolitos diferentes. Con el objetivo de evaluar el efecto de las fuerzas de dispersión sobre diferentes propiedades de los nanogeles, como el tamaño, la carga neta y el potencial electrostático superficial. Este modelo nos permitió considerar explícitamente las interacciones de dispersión entre los iones dentro de las unidades de nanogel y monómero en lugar de las interacciones entre los iones y la nanopartícula como un todo. Por otro lado, se llevaron a cabo simulaciones de grano grueso de complejos nanogel-polielectrolito, donde nuestros resultados de simulación capturan dos fenómenos reportados en experimentos con complejos reales: la inversión de carga detectada a través de datos de movilidad electroforética, que nuestras simulaciones solo muestran si la carga de polielectrolito es suficientemente grande; y la reducción de tamaño tras absorber unas pocas cadenas. Estos resultados nos permiten profundizar en la aplicación de nanogeles como dispositivos de tamaño nanométrico para la administración de fármacos.

1. Introduction

1.1. Gels, microgels and nanogels

Polymer science is a multidisciplinary scientific field that brings together researchers from diverse academic fields. To explore the nature of matter, scientific methods and theories have been applied since early times to extract information from the world around us.

It is well known that certain polymers and polyelectrolytes can be synthesized forming cross-linked networks (commonly referred to as polymer/polyelectrolyte gels). These polymer chains are molecules of high relative molecular mass made of the repetition of molecules of low relative molecular mass, called monomers. Those monomers can have ionizable or ionic groups, and then, they will form polyelectrolytes. A gel made of polyelectrolytes is called ionic or charged gel. Some of these polymers are thermo-sensitive and exhibit the so-called lower critical solution temperature (LCST)[1,2]. When the temperature is lower than the LCST, the polymer chains are soluble in water, however when it rises above the LCST, the chains undergo a pronounced transition coil-to-globule shape and aggregate among themselves. This phase transition makes the synthesis of thermo-responsive microgels (micrometric -sized cross-linked polymer particles) very interesting. They are characterized by their ability to change reversibly from a swollen to a shrunken state with temperature. However, it should be noted that both gels and microgels are

sensitive to other environmental conditions (such as pH and ionic strength). As its own name implies, a microgel is a kind of "small gel", that is to say, a polymer network with the entity of particle. Specifically, particles in the colloidal range of 10 to 1000 nm[3]. If their equivalent diameter is less than 100 nm, they are often referred to as nanogels[4].

According to their size, microgels are ranged within the mesoscopic scale. At this scale, the properties of these materials are different from massive material properties. Mesoscopic objects serve as elementary building blocks of macroscopic objects. Statistical mechanics are applied, but interactions in the mesoscopic range are affected by local fluctuations in component size and properties (such as polarization, local particle concentration, or charge distribution). The size threshold at which the behavior of a material changes into the mesoscopic range is not well defined. Particles of a few microns, such as bacteria, microgels, hair, etc., could define an upper limit. Individual molecules and atoms could be the smallest objects considered at the mesoscopic scale. For objects below the mesoscopic scale, their interactions are governed by quantum mechanics rather than statistical mechanics. See Figure 1.1.

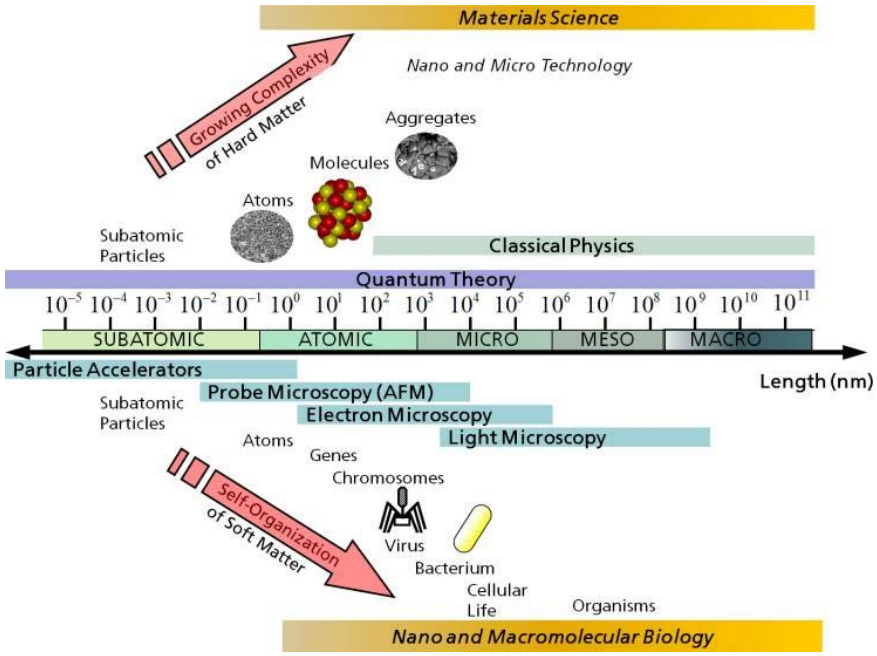

Figure 1.1 Schematic comparing the relevant length scales in materials science. Extracted from reference [5].

Their swelling capacity and their ability to respond to chemical, biochemical and physical external stimuli are precisely responsible for the technological interest in gels and microgels. Both are considered smart materials with applications such as drug delivery, health care, and microfluidic devices (in the case of microgels) or absorbent hygiene products (in the case of macroscopic gels).[6–10] The three-dimensional structures formed by polymer chain networks swell by absorbing large amounts of solvent, when the solubility conditions are suitable. When the transition occurs these polymer networks shrink expelling the solvent, keeping their identity due to chemical bonds between their chains, established in the synthesis process.

Moreover, the scientific interest is due to the complex interplay of forces that govern the swelling behavior of the gels. The chemistry of the components in the synthesis process determines the dominant interaction in the system (e.g. , hydrogen bonding, van der Waals, hydrophobic/hydrophilic, or ionic interactions) and therefore the specific swelling mechanism. These physical forces, which lead the interactions among chains within the solvent, are examples of non-covalent interactions.

As already mentioned above, microgels or nanogels form part of aqueous dispersions as colloidal particles of micro- and nanometric size, respectively. Their mechanical properties and their swelling/deswelling transition are of great importance for their use in biotechnological applications. Firstly, these particles can be to many external stimuli, such as pH, ionic strength, temperature, light, or external applied electric and magnetic fields (incorporating magnetic nanoparticles in the latter case), and therefore control their solvent-uptake ability[3]. There are some thermo-responsive microgels, like poly(*N*-isopropylacrylamide) (PNIPAM)[1] or poly(*N*-vinyl caprolactam) (PVCL)[11], whose volume phase transition usually occurs at temperatures around 32ºC-38ºC, which is very close to the temperature of the human body. Secondly, due to fact that the characteristic time of swelling/deswelling scales with the square of its typical size, a much faster response times (of the order of seconds) can be obtained than from the macroscopic gels (response times from hours to days)[12]. Thirdly, micro- and nanogels are porous and permeable structures. The total surface of polymer exposed to the solvent is maximized by the fibrous internal morphology of these particles. Hydrophobic and hydrophilic forces associated to changes in water structure close to the polymer chains may entail a very important role. Consequently, microgels are especially sensitive to the

presence of hydrophobic or hydrophilic molecules or ions in the aqueous medium. Finally, a model system of soft nanoparticles can be represented by theses gels, as the degree of softness and the total volume fraction occupied by the particles can be externally controlled.

Although the elasticity of the polymer allows the particles to be compressed and deformed, two microgels cannot fully overlap due to the repulsion of the excluded volume exerted by the polymer chains. Therefore, they are always distinguishable particles[13]. A picture of microgels at different length scales can be observed in Figure l.2.

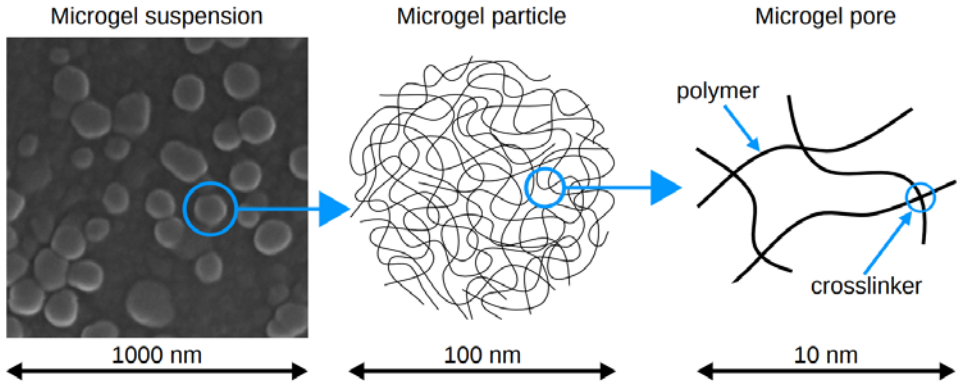

Figure 1.2 Microgels observed at different length scales. Left picture is a Scanning Electron Microscopy micrograph of a Poly-(N-vinylcaprolactam) microgels. Extracted with permission of the author from reference [14].

Accordingly, microgels and nanogels have prompted great interest as soft active materials in a variety of applications such as super-absorbers, as stimuli-responsive nanoreactors for controlled catalysis, or as transport and time-controlled delivery of therapeutic molecules [3,10,15–18]. In fact, as these particles can be easily penetrated by solvent molecules, ions and other types of small reactants such as biomacromolecules, specific drug molecules, proteins and peptides, among others. This opens a door to being able to use them as drug administrators, biosensors, chemical separation and catalysis. Similarly, micro- and nanogels can be used as nanocarriers to incorporate and deliver host molecules or drugs in a responsive way[19].

In addition, these gel nanoparticles have shown to be suitable for gene therapy, since they are capable of encapsulating genetic material (such as silenced RNA or DNA oligonucleotides). Its low permeability through cellular membranes and low stability against enzymatic degradation restricts the

potential therapeutic application of these molecules. Hence, specifically designed microgels allow them to surpass the intracellular barriers and deliver the therapeutic agents to the cytoplasm of the target cell. [20,21]

The interest of gels does not only rely on their applications, but also on their potential use as model systems under a theoretical point of view. In fact, within microgel suspensions, the interaction between a pair of particles can be easily tuned, leading to effective pair potentials with a distinct degree of softness. In addition, excluded-volume, hydrophobic and electrostatic interactions between the cross-linked polymer network and ions or more complex solutes, can be explored under multiple conditions. These interactions are the key to understand the physical properties involved in the encapsulation and diffusion of solutes inside the microgel or nanogel, the stability of the suspension, and the structural properties in both bulk volumes and interfaces.

1.1.1. Applications to drug delivery

It is well known that in the particular case of drug delivery, many drug candidates fail during preclinical evaluation due to poor efficacy, hampered bioavailability, and other challenges associated with effective drug delivery. Microgels and nanogels can be used in this context to improve the pharmacodynamics and pharmacokinetics of each therapeutic drug and make it possible to be delivered at the right time, in the right place, and in the right dose. After encapsulation, the micro- or nanogel may facilitate the transport, for example through biological environments, acting as a protective covering for the adsorbed molecule.[10] Moreover, nanogels specifically designed for this purpose offers many other advantages, which includes conformational stabilization and retained biological activity, gradual drug release, reduction of toxicity, protection from chemical and enzymatic degradation, biocompatibility, immunity and biodegradability.

In the last decades, numerous experimental studies have been done on nanogels as carriers and drug delivery systems. In fact, a new area of research has risen as biomedical nanogels, with daily rapid developments. And, during the recent years, several highly cited reviews can be found mainly devoted to this biotechnological application of nanogels,[22–34]. Hence, the intense research activity in this field is quite remarkable. Among the drugs that have been studied, we can find: cytarabine and gemcitabine (anticancer drugs),[35] fluxudirine (anticancer drug),[36] aspirin,[37] caffeine,[38] doxorubicin (anticancer drug),[39–41]

ethosuximide (antiepileptic),[42] levofloxaciona (antibiotic),[43] insulin,[44] terfenadine (antihistamine), 5-fluorouracil (anticancer drug) [45] and bovine serum albumin (protein)[46].

In addition, smaller nanoparticles, in the size range of 1-10 nm, can be transported contained by micro- and nanogels, such as drugs,[27] magnetite,[47,48] metal nanoparticles,[49–53] quantum dots[49] and other inorganic nanoparticles.[54–56] Therefore, the uptake of nanoparticles into microgels and their subsequent release have become an area of growing interest in recent years. This ability plays a key role in the formulation and controlled release of pharmaceuticals and/or drugs. It is also very important in a variety of separation problems, including ultrafiltration, chromatography and other membrane processes.

There are several interactions of the solute and the polymer network that could determine the quantity of solute absorbed by the nanogel/microgel, but the simplest interaction that we can imagine between them is steric exclusion, which is always present. In any case, the prediction of partitioning coefficients of solute-gel systems involving additional forces can be estimated with the precise knowledge of size-exclusion effects. In the case of charged gels/nanogels and charged solutes, electrostatic forces must be considered as well.

Moreover, ionic micro- and nanogels can also incorporate oppositely charged polyelectrolytes, macromolecules or inorganic nanoparticles due to attractive electrostatic forces. In fact, this principle can be exploited to protect oligonucleotides and nucleic acids from enzymatic degradation, by immobilizing such polyelectrolytes in cationic nanogels. [25,57–64] Hence, these nanogels can be used to deliver genes into a cell. In addition, nanogels have been proposed as a soft and porous alternative to solid substrates. Absorption of some polyelectrolytes (such as miktoarm star polymers or peptides) into micro- or nanogels has been investigating experimentally by some research groups.[65–69]

1.2. Background

Already in 1907, Leo Baekeland invented one of the first synthetic plastics (called Bakelite). And because of the differences between natural and synthetic polymers, Hermann Staudinger studied them and published his classic paper titled "Über Polymerisation" in 1920, which proposed that polymers are macromolecules composed of many repeating units covalently bonded together to form long chains[70]. The theory of polymers as macromolecules broke with the previous theory where all chemical compounds were low molecular weight

entities that could potentially "aggregate", and polymers gradually started to become recognized as separate from colloidal systems[71]. The way of doing research took a big turn with the advent of computers in the 1940s. A new method of studying chemical phenomena became possible. It went from researching in a laboratory to being able to implement mathematical models in computer programs and simulate the laboratory environment virtually. Since then, breakthroughs in high-performance computers have combined computer simulation with theory and experimentation to become a powerful tool for promoting innovation and gaining insights into the properties of polymers, for example.

From a theoretical viewpoint, Flory and Rehner developed their classical theory concerning cross-linked polymer networks in 1943[72,73], on which mostly of researchers have been relying on to extend their theories throughout the century. This is because, despite being such a longstanding theory, it has some pretty solid strengths. Since it does not require a large number of parameters and, although it is simple, the theory covers a variety of phenomena and situations. For example, the formalism successfully demonstrated the existence of continuous and discontinuous volume changes. In fact, Dusek and Patterson[74] predicted the phase transition of the gel (theoretically) before it was discovered experimentally. Moreover, it is adaptive and suitable for different situations and/or stimuli. This theory can explain why some gels collapse with increasing temperature, while others swell. In addition, the classical swelling theory can be used to discuss the influence of other parameters (solvent composition, loading, pH, salt concentration, etc.). For example, in other pioneering works, this formalism was used to predict how swelling depends on salt concentration and pH[75,76]. More specifically, Brannon-Peppas and Peppas reported that gels swell as pH increases, but shrink as salt is added[76].

On the other hand, this theory has some weaknesses and limitations. For example, it is based on some dubious assumptions. The theory assumes the separability of ionic, polymer/solvent mixing and elasticity contributions. In addition, an ideal polymer network is also assumed. This means that the basic model does not consider the effects of entanglements, free branches, loops, finite chain lengths or their polydispersity[77]. Furthermore, in the case of ionized polyelectrolyte gels, the influence of electrostatic interaction is also simplified. The electrostatic force between charges is completely ignored. Moreover, it uses phenomenological parameters. In other words, for special situations, theoretical considerations can hardly be predictive. Therefore, empirical (or

adjustable) parameters estimated from the swelling data have to be considered. Unfortunately, the values obtained in this way may differ from the value of non-crosslinked polymer by two or even three orders of magnitude[78]. In many cases, the cross-link density is also considered an effective parameter and is a controversial property. In summary, the predictability of this theory for specific cases is very limited.

1.3. Simulation of gels and nanogels

Under this scenario, computer simulation (used on their own or in combination with theoretical methods) appear as a helpful tool to improve the capability of prediction of the gel models. The nanogel simulations carried out over the last decade are largely inspired by earlier gel simulation computers. The first gel simulations were based on an infinite polymer/polyelectrolyte network, which was originally realized by Soviet scientists in the 1970s and 1980s[79,80]. These initial simulations sought to understand the various properties of polymer networks, but they encountered two notable problems. One of them, that due to the great absorption of the polyelectrolyte gels, the number of particles to simulate counting with the solute became prohibitive. For swollen charged gels, the solute was up to three orders of magnitude greater than the number of particles in its network. Additionally, by having to simulate electrical interactions, and being these long-range, the calculations of charged gels were further increased[81]. To solve these two problems, a coarse-grained representation was used, where the monomer units of the gel and the ions were grouped each into spheres, and the solvent was considered as a continuous dielectric medium (Primitive model)[5]. The gel spheres could be charged or neutral. Allowing to simplify both the number of solvent particles and the number of electrical interactions.

This coarse-grained representation of polymer systems has been extensively used in the study of adsorption and collapse of charged polyelectrolytes[82,83]. Since it does not contain as many particles as atomistic simulations, the times that the simulation system walks can be longer. Approaching what would be seen experimentally and facilitating the comparison with the experiments. At the beginning of the 2000's, Schneider and Linse performed the first simulations in which charged groups, counterions and Coulomb interactions were explicitly considered within a coarse-grained model of polyelectrolyte network[84]. They studied the effect of different parameters (chain flexibility, chain length, charge density and counterion valence) on the swelling of gels in

salt-free solutions. The network had the diamond-like topology previously used by Escobedo and de Pablo for uncharged gels[85]: each crosslinker connects four polyelectrolyte chains with the same amount of monomers. Some authors used the coarse-grained models to explore the swelling behavior of gels in the presence of salt, multivalent ions and charged macroions[86–90].

Unlike (macroscopic) gel simulations based on polymer/polyelectrolyte networks, explicit nanogel and microgel simulations are currently rare, mainly due to the computational resources required. By simulating the nanogel from an outside view, new data can be obtained from the system that was not seen with the inside perspective with which gels are simulated. This new aspect of the simulation allows, on the one hand, to consider that the counter ions that neutralize the nanogel can come out of it. Therefore, the nanogel could be not necessarily neutral, although the total system is. Another new consideration would be the ionic atmosphere (the electric double layer) around the nanogel, since now it makes sense to consider it. From a colloidal perspective, these properties provide important information on particle properties such as effective charge, electrostatic surface potential or size[91,92].

Opening the possibility of simulating single-nanogel particle, in 2009 a group of researchers led by C. Holm simulated a polyelectrolyte nanogel with the corresponding counterions in a periodic box, by using a molecular dynamics package for soft matter simulations called ESPResSo (Extensible Simulation Package for Research on Soft Matter)[93]. Coming to conclude that nanogels do not confine their counterions completely. In addition, Claudio et al. also compared molecular dynamics simulations with the predictions of a Poisson–Boltzmann cell model for the case of good solvent conditions and monovalent ions. Concluding that the ion distributions predicted by the model and those obtained from simulations agree quite well[94]. Others authors have extended this work of Claudio et al. to collapsed nanogels in salt-free solutions[91] and in the presence of salt[95] focusing on the thermal response of temperature-sensitive nanogels. In these works[91,95], the attractive hydrophobic forces between monomers were included in the model through an empirical interaction potential, which demonstrates the experimental behavior of poly (N-isopropylacrylamide) (PNIPAM)- based gels[96]. In agreement with Claudio et al., these simulations confirmed that nanogels do not confine all their counterions.

Summarizing, although there have been many studies on the synthesis and characterization of micro- and nanogel dispersions, the number of papers that deal directly with the effective interactions between the constituent particles

is relatively low. Computer simulations can be extremely helpful to shed light on these issues. In this sense, the main goal of this thesis is to explore for different swelling states of gels, the competition between the different interactions that govern the behavior of the gel. Explicit simulations of nanogels can improved our comprehension of their electrokinetic behavior as colloidal nanoparticles or be used to test models or theories. More specifically, our simulations provide valuable information about steric and electrostatic effects on different single-particle properties (ionic distributions, mass distribution, swelling, electrostatic potential, effective charge, and degree of ionization) without requiring detailed information on the chemical nature. These results will allow us to delve into the application of nanogels as nano-sized devices for drug delivery.

References

1 H. G. Schild, Poly(N-isopropylacrylamide): experiment, theory and application, *Prog. Polym. Sci.*, 1992, **17**, 163–249.

2 T. Okano, N. Yamada, M. Okuhara, H. Sakai and Y. Sakurai, Mechanism of cell detachment from temperature-modulated, hydrophilic-hydrophobic polymer surfaces1, *Biomater. Silver Jubil. Compend.*, 1995, **16**, 109–115.

3 R. Pelton and T. Hoare, *Microgel Suspens.*, 2011, 1–32.

4 R. G. Jones, E. S. Wilks, W. V. Metanomski, J. Kahovec, M. Hess, R. Stepto and T. Kitayama, *Compendium of Polymer Terminology and Nomenclature*, The Royal Society of Chemistry, 2009.

5 M. O. Steinhauser and S. Hiermaier, *Int. J. Mol. Sci.* , 2009, 10.

6 T. Sawai, S. Yamazaki, Y. Ishigami, Y. Ikariyama and M. Aizawa, Electrical control of reversible microgel flocculation and its estimated performance as a display device, *J. Electroanal. Chem.*, 1992, **322**, 1–7.

7 M. J. Murray and M. J. Snowden, The preparation, characterisation and applications of colloidal microgels, *Adv. Colloid Interface Sci.*, 1995, **54**, 73–91.

8 N. A. Peppas, Hydrogels and drug delivery, *Curr. Opin. Colloid Interface Sci.*, 1997, **2**, 531–537.

9 R. P. U, Temperature-sensitive aqueous microgels, *Adv. Colloid Interface Sci.*, 2000, **85**, 1–33.

10 J. Ramos, A. Imaz, J. Callejas-Fernández, L. Barbosa-Barros, J. Estelrich,

M. Quesada-Pérez and J. Forcada, Soft nanoparticles (thermo-responsive nanogels and bicelles) with biotechnological applications: From synthesis to simulation through colloidal characterization, *Soft Matter*, 2011, **7**, 5067–5082.

11 S. Wu, J. Dzubiella, J. Kaiser, M. Drechsler, X. Guo, M. Ballauff and Y. Lu, Thermosensitive Au-PNIPA Yolk–Shell Nanoparticles with Tunable Selectivity for Catalysis, *Angew. Chemie Int. Ed.*, 2012, **51**, 2229–2233.

12 G. M. Eichenbaum, P. F. Kiser, S. A. Simon and D. Needham, pH and ion-triggered volume response of anionic hydrogel microspheres, *Macromolecules*, 1998, **31**, 5084–5093.

13 L. A. Lyon and M. J. Serpe, *Hydrogel Micro and Nanoparticles*, 2012.

14 I. Adroher-Benítez, *Interactions involved in the permeation and distribution of ions and biomolecules inside charged microgels*, PhD. Thesis, University of Granada, 2017.

15 A. Noro, M. Hayashi and Y. Matsushita, Design and properties of supramolecular polymer gels, *Soft Matter*, 2012, **8**, 6416–6429.

16 S. Van Vlierberghe, P. Dubruel and E. Schacht, Biopolymer-based hydrogels as scaffolds for tissue engineering applications: A review, *Biomacromolecules*, 2011, **12**, 1387–1408.

17 M. A. Ward and T. K. Georgiou, Thermoresponsive polymers for biomedical applications, *Polymers (Basel).*, 2011, **3**, 1215–1242.

18 J. Basso, A. Miranda, S. Nunes, T. Cova, J. Sousa, C. Vitorino and A. Pais, Hydrogel-Based Drug Delivery Nanosystems for the Treatment of Brain Tumors, *Gels*, 2018, **4**, 62.

19 S. Kennedy, J. Hu, C. Kearney, H. Skaat, L. Gu, M. Gentili, H. Vandenburgh and D. Mooney, Sequential release of nanoparticle payloads from ultrasonically burstable capsules., *Biomaterials*, 2016, **75**, 91–101.

20 J. Ramos, J. Forcada and R. Hidalgo-Alvarez, Cationic polymer nanoparticles and nanogels: From synthesis to biotechnological applications, *Chem. Rev.*, 2014, **114**, 367–428.

21 S. V Vinogradov and T. Senanayake, Nanogel–drug conjugates: a step towards increasing the chemotherapeutic efficacy, *Nanomedicine*, 2013, **8**, 1229–1232.

22 J. K. Oh, R. Drumright, D. J. Siegwart and K. Matyjaszewski, The development of microgels/nanogels for drug delivery applications, *Prog. Polym. Sci.*, 2008, **33**, 448–477.

23 K. Raemdonck, J. Demeester and S. De Smedt, Advanced nanogel

engineering for drug delivery, *Soft Matter*, 2009, **5**, 707–715.

24 T. Casalini and G. Perale, From microscale to macroscale: Nine orders of magnitude for a comprehensive modeling of hydrogels for controlled drug delivery, *Gels*, 2019, **5**, 1–42.

25 E. Mauri, G. Perale and F. Rossi, Nanogel Functionalization: A Versatile Approach to Meet the Challenges of Drug and Gene Delivery, *ACS Appl. Nano Mater.*, 2018, **1**, 6525–6541.

26 I. Neamtu, A. G. Rusu, A. Diaconu, L. E. Nita and A. P. Chiriac, Basic concepts and recent advances in nanogels as carriers for medical applications, *Drug Deliv.*, 2017, **24**, 539–557.

27 A. V. Kabanov and S. V. Vinogradov, Nanogels as pharmaceutical carriers: Finite networks of infinite capabilities, *Angew. Chemie - Int. Ed.*, 2009, **48**, 5418–5429.

28 R. T. Chacko, J. Ventura, J. Zhuang and S. Thayumanavan, Polymer nanogels: A versatile nanoscopic drug delivery platform, *Adv. Drug Deliv. Rev.*, 2012, **64**, 836–851.

29 X. Zhang, S. Malhotra, M. Molina and R. Haag, Micro- and nanogels with labile crosslinks - from synthesis to biomedical applications, *Chem. Soc. Rev.*, 2015, **44**, 1948–1973.

30 M. Molina, M. Asadian-Birjand, J. Balach, J. Bergueiro, E. Miceli and M. Calderon, Stimuli-responsive nanogel composites and their application in nanomedicine, *Chem. Soc. Rev.*, 2015, **44**, 6161–6186.

31 S. Merino, C. Martin, K. Kostarelos, M. Prato and E. Vazquez, Nanocomposite Hydrogels: 3D Polymer-Nanoparticle Synergies for On-Demand Drug Delivery, *ACS Nano*, 2015, **9**, 4686–4697.

32 M. Karimi, A. Ghasemi, P. S. Zangabad, R. Rahighi, S. M. M. Basri, H. Mirshekari, M. Amiri, Z. S. Pishabad, A. Aslani, M. Bozorgomid, D. Ghosh, A. Beyzavi, A. Vaseghi, A. R. Aref, L. Haghani, S. Bahrami and M. R. Hamblin, Smart micro/nanoparticles in stimulus-responsive drug/gene delivery systems, *Chem. Soc. Rev.*, 2016, **45**, 1457–1501.

33 R. Kandil and O. M. Merkel, Recent progress of polymeric nanogels for gene delivery, *Curr. Opin. Colloid Interface Sci.*, 2019, **39**, 11–23.

34 M. Karg, A. Pich, T. Hellweg, T. Hoare, L. A. Lyon, J. J. Crassous, D. Suzuki, R. A. Gumerov, S. Schneider, I. I. Potemkin and W. Richtering, Nanogels and Microgels: From Model Colloids to Applications, Recent Developments, and Future Trends, *Langmuir*, 2019, **35**, 6231–6255.

35 C. M. Galmarini, G. Warren, M. T. Senanayake and S. V Vinogradov, Efficient overcoming of drug resistance to anticancer nucleoside analogs by

nanodelivery of active phosphorylated drugs, *Int. J. Pharm.*, 2010, **395**, 281–289.

36 S. V Vinogradov and T. Senanayake, Nanogel–drug conjugates: a step towards increasing the chemotherapeutic efficacy, *Nanomedicine (Lond).*, 2013, **8**, 1229–1232.

37 S. Patnaik, A. K. Sharma, B. S. Garg, R. P. Gandhi and K. C. Gupta, Photoregulation of drug release in azo-dextran nanogels, *Int. J. Pharm.*, 2007, **342**, 184–193.

38 N. H. Abu Samah and C. M. Heard, Enhanced in vitro transdermal delivery of caffeine using a temperature- and pH-sensitive nanogel, poly(NIPAM-co-AAc), *Int. J. Pharm.*, 2013, **453**, 630–640.

39 N. M. Oh, K. T. Oh, H. J. Baik, B. R. Lee, A. H. Lee, Y. S. Youn and E. S. Lee, A self-organized 3-diethylaminopropyl-bearing glycol chitosan nanogel for tumor acidic pH targeting: In vitro evaluation, *COLLOIDS AND SURFACES B-BIOINTERFACES*, 2010, **78**, 120–126.

40 E. Cazares-Cortes, A. Espinosa, J.-M. Guigner, A. Michel, N. Griffete, C. Wilhelm and C. Menager, Doxorubicin Intracellular Remote Release from Biocompatible Oligo(ethylene glycol) Methyl Ether Methacrylate-Based Magnetic Nanogels Triggered by Magnetic Hyperthermia, *ACS Appl. Mater. Interfaces*, 2017, **9**, 25775–25788.

41 G. Aguirre, E. Villar-Alvarez, A. Gonzalez, J. Ramos, P. Taboada and J. Forcada, Biocompatible Stimuli-Responsive Nanogels for Controlled Antitumor Drug Delivery, *J. Polym. Sci. PART A-POLYMER Chem.*, 2016, **54**, 1694–1705.

42 M.-H. Hsiao, M. Larsson, A. Larsson, H. Evenbratt, Y.-Y. Chen, Y.-Y. Chen and D.-M. Liu, Design and characterization of a novel amphiphilic chitosan nanocapsule-based thermo-gelling biogel with sustained in vivo release of the hydrophilic anti-epilepsy drug ethosuximide, *J. Control. RELEASE*, 2012, **161**, 942–948.

43 E. Montanari, G. D'Arrigo, C. Di Meo, A. Virga, T. Coviello, C. Passariello and P. Matricardi, Chasing bacteria within the cells using levofloxacin-loaded hyaluronic acid nanohydrogels, *Eur. J. Pharm. Biopharm.*, 2014, **87**, 518–523.

44 Z. Wu, X. Zhang, H. Guo, C. Li and D. Yu, An injectable and glucose-sensitive nanogel for controlled insulin release, *J. Mater. Chem.*, 2012, **22**, 22788–22796.

45 A. Alvarez-Bautista, C. M. M. Duarte, E. Mendizabal and I. Katime, Controlled delivery of drugs through smart pH-sensitivenanohydrogels for anti-cancer therapies: synthesis, drug release and cellular studies, *Des.*

MONOMERS Polym., 2016, **19**, 319–329.

46 N. M. Matsumoto, D. C. Gonzalez-Toro, R. T. Chacko, H. D. Maynard and S. Thayumanavan, Synthesis of nanogel-protein conjugates, *Polym. Chem.*, 2013, **4**, 2464–2469.

47 A. Pich, S. Bhattacharya, Y. Lu, V. Boyko and H. A. P. Adler, Temperature-sensitive hybrid microgels with magnetic properties, *LANGMUIR*, 2004, **20**, 10706–10711.

48 M. Boularas, E. Gombart, J.-F. Tranchant, L. Billon and M. Save, Design of Smart Oligo(ethylene glycol)-Based Biocompatible Hybrid Microgels Loaded with Magnetic Nanoparticles, *Macromol. Rapid Commun.*, 2015, **36**, 79–83.

49 I. Gorelikov, L. M. Field and E. Kumacheva, Hybrid microgels photoresponsive in the near-infrared spectral range, *J. Am. Chem. Soc.*, 2004, **126**, 15938–15939.

50 M. Bradley and B. S. Garcia-Risueno, Symmetric and asymmetric adsorption of pH-responsive gold nanoparticles onto microgel particles and dispersion characterisation, *J. Colloid Interface Sci.*, 2011, **355**, 321–327.

51 P. T. Davies and B. Vincent, Uptake of anionic gold nanoparticles by cationic microgel particles in dispersion: The effect of pH, *COLLOIDS SURFACES A-PHYSICOCHEMICAL Eng. Asp.*, 2010, **354**, 99–105.

52 A. M. Lazim, M. Bradley and J. Eastoe, Controlling Gold Nanoparticle Stability with Triggerable Microgels, *LANGMUIR*, 2010, **26**, 11779–11783.

53 A. Pich, A. Karak, Y. Lu, A. K. Ghosh and H. J. P. Adler, Preparation of hybrid microgels functionalized by silver nanoparticles, *Macromol. Rapid Commun.*, 2006, **27**, 344–350.

54 M. Bradley, N. Bruno and B. Vincent, Distribution of CdSe quantum dots within swollen polystyrene microgel particles using confocal microscopy, *LANGMUIR*, 2005, **21**, 2750–2753.

55 A. Pich, J. Hain, Y. Lu, V. Boyko, Y. Prots and H. J. Adler, Hybrid microgels with ZnS inclusions, *Macromolecules*, 2005, **38**, 6610–6619.

56 M. Agrawal, A. Pich, S. Gupta, N. E. Zafeiropoulos, J. Rubio-Retama, F. Simon and M. Stamm, Temperature sensitive hybrid microgels loaded with ZnO nanoparticles, *J. Mater. Chem.*, 2008, **18**, 2581–2586.

57 A. Tamura, M. Oishi and Y. Nagasaki, Enhanced Cytoplasmic Delivery of siRNA Using a Stabilized Polyion Complex Based on PEGylated Nanogels with a Cross-Linked Polyamine Structure, *Biomacromolecules*, 2009, **10**, 1818–1827.

58 W. H. Blackburn, E. B. Dickerson, M. H. Smith, J. F. McDonald and L. A. Lyon, Peptide-Functionalized Nanogels for Targeted siRNA Delivery, *Bioconjug. Chem.*, 2009, **20**, 960–968.

59 R. Sunasee, P. Wattanaarsakit, M. Ahmed, F. B. Lollmahomed and R. Narain, Biodegradable and nontoxic nanogels as nonviral gene delivery systems, *Bioconjug. Chem.*, 2012, **23**, 1925–1933.

60 M. Ahmed, P. Wattanaarsakit and R. Narain, Cationic glyco-nanogels for epidermal growth factor receptor (EGFR) specific siRNA delivery in ovarian cancer cells, *Polym. Chem.*, 2013, **4**, 3829–3836.

61 C. Vauthier, C. Zandanel and A. L. Ramon, Chitosan-based nanoparticles for in vivo delivery of interfering agents including siRNA, *Curr. Opin. Colloid Interface Sci.*, 2013, **18**, 406–418.

62 S. L. Goh, N. Murthy, M. Xu and J. M. J. Fréchet, Cross-linked microparticles as carriers for the delivery of plasmid DNA for vaccine development, *Bioconjug. Chem.*, 2004, **15**, 467–474.

63 S. Deshpande, S. Patil and N. Singh, Enhancing Gene-Knockdown Efficiency of Poly(N-isopropylacrylamide) Nanogels, *ACS Omega*, 2018, **3**, 8042–8049.

64 D. Huang, H. Qian, H. Qiao, W. Chen, J. Feijen and Z. Zhong, Bioresponsive functional nanogels as an emerging platform for cancer therapy, *Expert Opin. Drug Deliv.*, 2018, **15**, 703–716.

65 J. Kleinen and W. Richtering, Defined complexes of negatively charged multisensitive poly(N- isopropylacrylamide-co-methacrylic acid) microgels and poly(diallydimethylammonium chloride), *Macromolecules*, 2008, **41**, 1785–1790.

66 J. Kleinen and W. Richtering, Rearrangements in and release from responsive microgel-polyelectrolyte complexes induced by temperature and time, *J. Phys. Chem. B*, 2011, **115**, 3804–3810.

67 J. Kleinen and W. Richtering, Polyelectrolyte microgels based on poly-N-isopropylacrylamide: Influence of charge density on microgel properties, binding of poly-diallyldimethylammonium chloride, and properties of polyelectrolyte complexes, *Colloid Polym. Sci.*, 2011, **289**, 739–749.

68 S. Walta, D. V. Pergushov, A. Oppermann, A. A. Steinschulte, K. Geisel, L. V. Sigolaeva, F. A. Plamper, D. Wöll and W. Richtering, Microgels enable capacious uptake and controlled release of architecturally complex macromolecular species, *Polymer (Guildf).*, 2017, **119**, 50–58.

69 H. Bysell, P. Hansson and M. Malmsten, Effect of charge density on the interaction between cationic peptides and oppositely charged

microgels, *J. Phys. Chem. B*, 2010, **114**, 7207–7215.

70 H. Staudinger, Über Polymerisation, *Berichte der Dtsch. Chem. Gesellschaft (A B Ser.*, 1920, **53**, 1073–1085.

71 R. Olby, The macromolecular concept and the origins of molecular biology., *J. Chem. Educ.*, 1970, **47**, 168–174.

72 P. J. Flory and J. Rehner, Statistical Mechanics of Cross-Linked Polymer Networks I. Rubberlike Elasticity, *J. Chem. Phys.*, 1943, **11**, 512–520.

73 P. J. Flory and J. Rehner, Statistical Mechanics of Cross-Linked Polymer Networks II. Swelling, *J. Chem. Phys.*, 1943, **11**, 521–526.

74 K. Dušek and D. Patterson, Transition in swollen polymer networks induced by intramolecular condensation, *J. Polym. Sci. Part A-2 Polym. Phys.*, 1968, **6**, 1209–1216.

75 A. R. Khokhlov, Swelling and collapse of polymer networks, *Polymer (Guildf).*, 1980, **21**, 376–380.

76 L. Brannon-Peppast, EQUILIBRIUM SWELLING HYDROGELS OF pH-SENSITIVE, *Chem. Eng.*, 1991, **46**, 715–722.

77 K. Dušek and M. Dušková-Smrčková, Network structure formation during crosslinking of organic coating systems, *Prog. Polym. Sci.*, 2000, **25**, 1215–1260.

78 S. Hirotsu, Y. Hirokawa and T. Tanaka, Volume-phase transitions of ionized N-isopropylacrylamide gels, *J. Chem. Phys.*, 1987, **87**, 1392–1395.

79 I. S. Remeyev and A. M. Yel'Yashevich, Computer simulation of deformation properties of 'phantom' networks, *Polym. Sci. U.S.S.R.*, 1985, **27**, 706–714.

80 A. M. Elyashevich, Computer simulation of network formation processes, structure and mechanical properties of polymer networks, *Polymer (Guildf).*, 1979, **20**, 1382–1388.

81 M. Quesada-Pérez, J. A. Maroto-Centeno, J. Forcada and R. Hidalgo-Alvarez, Gel swelling theories: The classical formalism and recent approaches, *Soft Matter*, 2011, **7**, 10536–10547.

82 R. G. Winkler and A. G. Cherstvy, Critical adsorption of polyelectrolytes onto charged spherical colloids, *Phys. Rev. Lett.*, 2006, **96**, 1–4.

83 S. Ulrich, M. Seijo and S. Stoll, The many facets of polyelectrolytes and oppositely charged macroions complex formation, *Curr. Opin. Colloid Interface Sci.*, 2006, **11**, 268–272.

84 S. Schneider and P. Linse, Monte Carlo simulation of defect-free cross-

linked polyelectrolyte gels, *J. Phys. Chem. B*, 2003, **107**, 8030–8040.

85 F. A. Escobedo and J. J. de Pablo, Monte Carlo simulation of branched and crosslinked polymers, *J. Chem. Phys.*, 1996, **104**, 4788–4801.

86 S. Edgecombe, S. Schneider and P. Linse, Monte Carlo simulations of defect-free cross-linked gels in the presence of salt, *Macromolecules*, 2004, **37**, 10089–10100.

87 B. A. Mann, C. Holm and K. Kremer, Swelling of polyelectrolyte networks, *J. Chem. Phys.*, , DOI:10.1063/1.1882275.

88 S. Edgecombe and P. Linse, Monte Carlo simulations of cross-linked polyelectrolyte gels with oppositely charged macroions, *Langmuir*, 2006, **22**, 3836–3843.

89 D. W. Yin, M. Olvera De La Cruz and J. J. De Pablo, Swelling and collapse of polyelectrolyte gels in equilibrium with monovalent and divalent electrolyte solutions, *J. Chem. Phys.*, , DOI:10.1063/1.3264950.

90 D. W. Yin, Q. Yan and J. J. De Pablo, Molecular dynamics simulation of discontinuous volume phase transitions in highly-charged crosslinked polyelectrolyte networks with explicit counterions in good solvent, *J. Chem. Phys.*, , DOI:10.1063/1.2102827.

91 M. Quesada-Pérez and A. Martín-Molina, Monte Carlo simulation of thermo-responsive charged nanogels in salt-free solutions, *Soft Matter*, 2013, **9**, 7086–7094.

92 P. Košovan, T. Richter and C. Holm, eds. G. Sadowski and W. Richtering, Springer International Publishing, Cham, 2013, pp. 205–221.

93 H. J. Limbach, A. Arnold, B. A. Mann and C. Holm, ESPResSo-an extensible simulation package for research on soft matter systems, *Comput. Phys. Commun.*, 2006, **174**, 704–727.

94 G. C. Claudio, K. Kremer and C. Holm, Comparison of a hydrogel model to the Poisson-Boltzmann cell model, *J. Chem. Phys.*, , DOI:10.1063/1.3207275.

95 M. Quesada-Pérez, S. Ahualli and A. Martín-Molina, Temperature-sensitive nanogels in the presence of salt: Explicit coarse-grained simulations, *J. Chem. Phys.*, , DOI:10.1063/1.4895960.

96 M. Quesada-Pérez, J. Ramos, J. Forcada and A. Martín-Molina, Computer simulations of thermo-sensitive microgels: Quantitative comparison with experimental swelling data, *J. Chem. Phys.*, , DOI:10.1063/1.4729946.

2. Objectives

In this section the goals of the thesis are listed by individual papers. Along these papers different simulation studies are proposed dealing with microgels and nanogels, and their absorption and encapsulation capacities of various electrolytes, solutes or even polyelectrolyte complexes. In any case, we should keep in mind that our main goal is the understanding of these colloidal systems and the correct interpretation of the physical mechanisms behind their behavior.

2.1. Paper I

Coarse-grained Monte Carlo simulations of the absorption of diluted spherical cosolutes inside a neutral hydrogel for different swelling states are performed. One of the goals of this paper is to understand the interplay between the excluded-volume repulsion exerted by polymer chains inside the hydrogel and the solvent-induced hydrophobic attraction between the monomeric units and the cosolute particle. To do this, a hydrogel with different swelling rates that is permeated by a cosolute will be simulated. The variables on which the study will focus are, on the one hand, the size of the cosolute, which is expected to increase the exclusion of volume of the cosolute within the gel; and on the other hand, the depth and range of the hydrophobic attraction felt by the cosolute to the monomers of the gel. Another objective is to

compare the results from the simulations with a theoretical expression developed to predict conditions that favor a maximum absorption of the cosolute by the gel.

2.2. Paper II

Here the goal is to analyze the effects of dispersion forces suffered by nanogels. To do this, a thermosensitive nanogel in the presence of different electrolytes is studied by means of coarse-grained Monte Carlo simulation. These simulations attempt to reproduce previous experimental results in which it has been observed that low NaSCN concentrations induce charge inversion in PNIPAM microgels. Particularly, a charge reversal and/or a surface electrostatic potential reversal are expected in simulations of collapsed nanogels in the presence of NaSCN but not after the addition of other electrolytes (such as NaCl and $NaNO_3$).

In other words, our objective is to find out to what extent dispersion forces can justify certain ion specific phenomena observed in micro- or nanogels. Given that ions can permeate micro- and nanogels, our simulation explicitly consider interactions between ions and polymer chains or their monomer units (which constitutes a novelty itself) rather than interactions between the ions and the whole particle, as done in the case of hard and impenetrable colloids.

2.3. Paper III

Coarse-grained Monte Carlo simulations of complexes consisting of a nanogel and oppositely charged polyelectrolyte chains with different charges, numbers of monomers per chain and topology are carried out.

The goal is to analyze the absorption of these chains within the nanogel, and study the properties of the nanogel-polyelectrolyte complex paying special attention to size and charge effects. Our simulations also intend to capture two phenomena observed experimentally with microgel-polyelectrolyte complexes: the deswelling and charge inversion of the nanogel undergone after absorption of the electrolyte chains. It would also be interesting to observe how the chains are distributed inside the nanogel, and if they have a preferential location. Finally, a comparison between ring and linear polyelectrolytes is performed to discover if the distribution of the chain charge has important effects.

3. Methodology

3.1. Monte Carlo simulations

The Monte Carlo (MC) simulation is a very valuable alternative for the study of the properties in the equilibrium of simple and colloidal fluids. It is a statistical method based on probability theory that allows characterizing a system made up of a number of particles on the order of N_A, using a much smaller number of them. Through MC simulation, the system does not evolve according to the real trajectories that the particles follow over time, but rather it does so through fictitious trajectories governed by statistical laws and that, on average, also lead to the values of the macroscopic variables that characterize the state of balance of said system. Thus, the MC method is specially designed for the study of systems in equilibrium where time does not play a fundamental role.

In particular, this allows us to study the behavior or interactions of different systems, such as gels or nanogels. Either seeing the absorption of different cosolutes within these gels, their own characteristics such as their temperature-sensitive volume variation; or from an outside view, look for the forces that mediate the approach to external objects of a nanogel, or even another nanogel. All these situations are feasible to study with MC because they are systems in equilibrium.

In order to explain the Metropolis algorithm, used in MC simulations, let us consider, theoretically, the mean value at equilibrium of a generic function $G(\boldsymbol{r}_1, \boldsymbol{r}_2, \dots, \boldsymbol{r}_N) = G(\boldsymbol{r}_i)$ with $i = 1,2, \dots, N$, which depends on the configuration of a system of N particles, is given through a configurational distribution function as follows:

$$\langle G(\boldsymbol{r}_i) \rangle = \int G(\boldsymbol{r}_i) P(\boldsymbol{r}_i)\, d^3 r_1 \cdots d^3 r_N \tag{3.1}$$

where $P(\boldsymbol{r}_i)$ is the probability density function. Any ensemble average must be calculated by analyzing the entire region of the phasic space accessible by the system. However, there are a large number of configurations that contribute very little to the average value. Precisely what is achieved with the MC method is to calculate a distribution function in pairs, from a finite number of configurations without knowing the probability function explicitly. To this end, what is done is to sample the states with a more significant contribution more times (significant sampling). Thus, the previous average can be rewritten in terms of a sum of a finite number S of configurations:

$$\langle G(\boldsymbol{r}_1, \dots, \boldsymbol{r}_N) \rangle = \frac{1}{S} \sum_{m=1}^{S} G\left(\boldsymbol{r}_1{}^{(m)}, \dots, \boldsymbol{r}_N{}^{(m)}\right) = \frac{1}{S} \sum_{m=1}^{S} G\left(\boldsymbol{r}_i{}^{(m)}\right) \tag{3.2}$$

where $G\left(\boldsymbol{r}_i{}^{(m)}\right)$ represents the value that the function takes in the configuration m, being the case $m = 1$ the one corresponding to the initial configuration. In principle, the validity of equation (3.2) will depend on the statistical quality. Consequently, the greater the number of configurations, the better the results. As has been said before, the trajectories that the particles follow are not real but respond to a sequence of states that are reached by statistical criteria. One way to generate these states is based on the concept of a Markov chain: a finite sequence of states, each of which is related only to the one that precedes it. Accordingly, Markov's master equation relates the probability per unit time that the system evolves from state k to state j, $W_{k \to j}$, with the probability of finding the system in state k, $P\left(\boldsymbol{r}_i{}^{(k)}\right)$:[1]

$$\frac{P(\boldsymbol{r}_i{}^{(k)})}{dt} = \sum_{\mathrm{j}} \left[-W_{k\to j} P(\boldsymbol{r}_i{}^{(k)}) + W_{j\to k} P(\boldsymbol{r}_i{}^{(j)}) \right] \tag{3.3}$$

If in equilibrium the function P does not vary with time and assuming that these probability functions are given by a Boltzmann statistic, it follows that:

$$\frac{W_{k\to j}}{W_{j\to k}} = \frac{P(\boldsymbol{r}_i{}^{(k)})}{P(\boldsymbol{r}_i{}^{(j)})} = exp\left\{ -\left[\frac{U(\boldsymbol{r}_i{}^{(j)})}{k_B T} - \frac{U(\boldsymbol{r}_i{}^{(k)})}{k_B T} \right] \right\} \tag{3.4}$$

where k_B is Boltzmann's constant and T the absolute temperature. And therefore:

$$\frac{W_{k\to j}}{W_{j\to k}} = exp\left(-\frac{\Delta U_{k\to j}}{k_B T} \right) \tag{3.5}$$

In accordance with this result, the Metropolis algorithm proposes to generate particle configurations as follows:[1,2]

$$W_{k\to j} \propto \begin{cases} 1 & if \quad \Delta U_{k\to j} \leq 0 \\ exp\left(-\frac{\Delta U_{k\to j}}{k_B T} \right) & if \quad \Delta U_{k\to j} > 0 \end{cases} \tag{3.6}$$

That is, given a state k, a test state j is randomly generated and then $\Delta U_{k\to j}$ is calculated. If this difference in energy is negative, state j is accepted. Otherwise, a random number between 0 and 1 is generated so that if $exp(-\Delta U_{k\to j}/k_B T)$ is less than that number, the test state is rejected. Instead, the new configuration is accepted if the number is less than the exponential.

The reason why the statistical evolution according to the Metropolis algorithm is linked to the search for a region of the configurational space where the potential energy of the system is minimal, is related to the fact that within the formalism of the canonical ensemble this condition it is equivalent to the search for a minimum in Helmholtz free energy, which characterizes from a thermodynamic point of view the equilibrium state of a system where the volume and the temperature are constant.

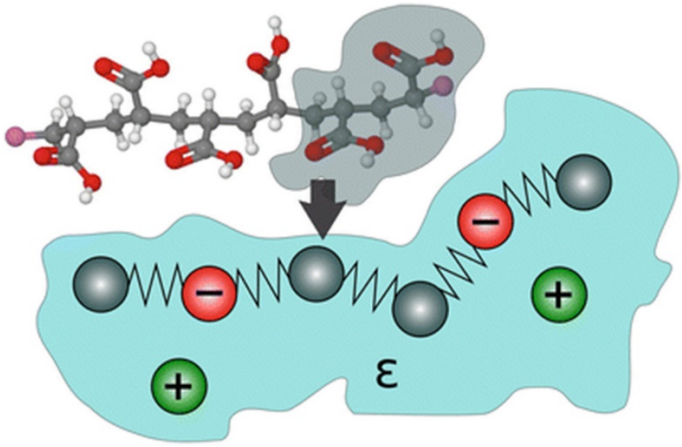

Figure 3.1 Schematic illustration of the coarse-grained model of a polyelectrolyte chain. The atomic groups of each monomer unit are grouped into one coarse-grained particle. These particles are connected by springs to form the chain (bead-spring model). The grey and red beads represent neutral and charged monomer units, respectively. In many cases, ions are explicitly treated, but the solvent is considered a dielectric continuum. Figure reproduced from reference[3] with permission of Springer International Publishing.

3.1.1. Model of simulations

The simulation scheme implemented in the present thesis consist of the combination of two models. On the one hand, the polyelectrolyte gel is described within a bead-spring model, where instead of simulating all the molecules of the gel, the closes ones are grouped together as a simulation element. This reduces the number of system components and interactions, and considerably the simulation time. The usual model for microgels and nanogels consists of an idealized representation of a polymer network in which monomer units and cross-linkers are modelled as spheres of a fixed diameter. Each polymer chain is modelled as a sequence of a given number of spherical monomer units (beads), named as N_{bead}. The number of fixed charged beads per chain and the corresponding fraction are designated by $N_{charged}$ and f ($= N_{charged}/N_{bead}$), respectively. The charge of the chain is uniformly distributed, and these monomers are charged with the positive or negative elementary charge (e), if a cationic or anionic gel is simulated, respectively. On the other hand, the molecules of the solvent, like water, are despised because of their small size. Therefore, the solvent is modelled as a continuum with a constant dielectric permittivity. In addition, the cosolute molecules are also grouped and modelled as spheres of a fixed diameter. These spheres are also charged based on their electric charge, like charged monomers. Figure 3.1

shows the combination of models: a polyelectrolyte chain with bead-spring model and the solvent with the primitive model.

Steric Interaction. There are two usual ways that we can model the short-range repulsion between any pair of these particles due to excluded volume effects. Depending on whether we want to compare the simulations with theory or experimental results, but not necessarily, we have used one or the other. For a closer match with a theory model, we have used the exclude volume effects, that can be modelled by means of the hard sphere potential:

$$u_{HS}(r) = \begin{cases} \infty & r \leq \sigma \\ 0 & r > \sigma \end{cases} \tag{3.7}$$

where r is the center-to-center distance between a given pair of particles, and since we want to put an infinite potential avoiding the overlapping of the spheres, the minimum approach distance will be the sum of the radii of these, $\sigma = R_i + R_j$, where R_i stands for the radius of species i. On the other hand, when we preferred a experimental approach with our simulations, where the spheres have a smooth approach rather than an abrupt jump, we have used the exclude volume effects, that can be modelled means of a truncated Weeks–Chandler–Andersen potential:[4–7]

$$u_{LJ}(r) = \begin{cases} 4\varepsilon_{LJ}\left(\frac{\sigma^{12}}{r^{12}} - \frac{\sigma^{6}}{r^{6}} - c\right) & r \leq r_c \\ 0 & r > r_c \end{cases} \tag{3.8}$$

where $\varepsilon_{LJ} = 4.11 \times 10^{-21}\ J$ denote the characteristic Lennard-Jones repulsion energy, r_c is the cutoff distance and c is a constant chosen so that $u_{LJ}(r) = 0$. There is a condition for the interaction potential to be purely repulsive, and it is when $r_c = \sigma\sqrt[6]{2}$. We can apply this condition to equation (3.8), which allows us to obtain the previous constant as $c = -\frac{1}{4}$.

Elastic interaction. Consecutive beads of a chain are connected by harmonic bonds. These bonds can be simulated as spring-type links, whose interaction potential is:

$$u_{bond}(r) = \frac{k_{bond}}{2}(r - r_0)^2 \tag{3.9}$$

where k_{bond} is the elastic force constant and r_0 is the equilibrium bond length corresponding to this harmonic potential (0.65 nm in our case). Taking as reference Schneider and Edgecombe *et al.*[8–10] in pioneering coarse-grained simulations of polyelectrolyte gels, the value of elastic force constant could be $k_{bond} = 0.4\ N/m$. Other authors proposed elastic constants much greater than $k_B T/\sigma^2$.[5,11] This ensures that thermal fluctuations undergone by monomers are much smaller than their diameter. The elastic constant proposed by Schneider and Edgecombe and employed in our simulations satisfies this condition.

Electric interaction. The charged species (charged monomers and ions) will interact electrostatically through the Coulomb potential:

$$u_{elec}(r) = \frac{Z_i Z_j e^2}{4\pi\varepsilon_0\varepsilon_r r} \tag{3.10}$$

where Z_i is the valence of species i, ε_0 and ε_r are the vacuum permittivity and relative vacuum permittivity of the solvent, respectively.

It should be considered that if we are using periodic conditions in the simulation, and because the electrical interaction is long-range, a charged particle will interact with all the rest particles of the cell, and all the particles of all the imaginary nearby cells until their interaction is negligible by their distance. This could entail a considerable computational cost. Thereby, the Ewald summation method is a technique used to efficiently sum the interactions between charged particles and all their periodic images. This method has been used to account for long-range contributions of potential energy without having to account directly for all those contributions. Ewald summations truly consider the periodicity of the replicated system, substituting the interaction energies in real space with a tantamount summation in Fourier space. The advantages of the Ewald summations are the fast convergence of the summation in the Fourier space in contrast with its real space equivalent.

Using this method, the final Coulomb energy will have a short-range contribution E^S (from the particle to a distance α_c) in real space due to the

unshielded charges, another long-range contribution E^L (from α_c to ∞) in Fourier space, where the calculations are more immediate, and a spurious term of self-interaction E^{self}, that is subtracted, to compensate for the interaction of the particle with its images in the reciprocal plane. The total Coulomb interaction energy of the system can be written as:[12]

$$E^{total} = E^S + E^L - E^{self} \tag{3.11}$$

$$E^S = \frac{e^2}{4\pi\varepsilon_0\varepsilon_r}\frac{1}{2}\sum_{i<j}\sum_{m\in Z^3}\frac{Z_i Z_j}{\left|\boldsymbol{r}_{ij}+\boldsymbol{m}L\right|}erfc\left(\alpha_c\left|\boldsymbol{r}_{ij}+\boldsymbol{m}L\right|\right) \tag{3.12}$$

$$E^L = \frac{e^2}{2L^3\varepsilon_0\varepsilon_r}\sum_{k\neq 0}\frac{exp[-k^2/4{\alpha_c}^2]}{k^2}|S(\boldsymbol{k})|^2 \tag{3.13}$$

$$E^{self} = \frac{e^2\alpha_c}{4\pi\varepsilon_0\varepsilon_r\sqrt{\pi}}\sum_i {Z_i}^2 \tag{3.14}$$

where α_c is the parameter that controls the convergence of the Ewald sums, $\boldsymbol{r}_{ij}$ is the vector that marks the distance from two charged particles, L is the length of the simulation cell, and $S(\boldsymbol{k})$ is the structure factor used to calculate the electrostatic potential from which its contribution in Fourier space has been determined. Several test simulations must be done to choose an appropriate α_c, which could consume too many resources if too many interactions are considered in the real space.

Hydrophobic interaction. The interaction energy between nonbonded monomeric units is also considered in our model to capture the thermo-shrinking behavior. It is well known that it is caused by the shift from entropy-ruled to enthalpy-ruled forces, where water degrees of freedom and hydrogen bonds play a fundamental role.[13]

Therefore, this effect results in an increase of the attractive hydrophobic interaction between the monomeric units when the temperature is increased.[14] This hydrophobic force is modelled through an interaction potential[15] ($u_{hyd}(r)$) which consists of a smooth approach of the square-well potential (previously used by other authors)[16–18] whose depth increases with temperature. This potential and its depth (ε_h) are described by the following functional forms:

$$u_{hyd}(r) = -\frac{\varepsilon_h}{2}\Big(1 - tanh\big(k_h(r - r_h)\big)\Big) \tag{3.15}$$

$$\varepsilon_h(T) = \frac{\varepsilon_{max}}{2}\Big(1 + tanh\Big(k_{\varepsilon/2}\big(T - T_{\varepsilon/2}\big)\Big)\Big) \tag{3.16}$$

where r_h is the range of the potential, k_h is related to the slope ofthe sigmoid, ε_{max} is the maximum depth of the hydrophobic potential (reached at high temperatures), $T_{\varepsilon/2}$ is the temperature for which $\varepsilon_h = \varepsilon_{max}/2$ and $k_{\varepsilon/2}$ is proportional to the slope of the function at that point. For the particular case of (NIPAM)-based microgels, the potential parameters can be adopted as the following values: $r_h = 0.9\ nm$, $k_h = 12.2\ nm^{-1}$, $T_{\varepsilon/2} = 307.5\ K$, $k_{\varepsilon/2} = 0.0667\ K^{-1}$ and $\varepsilon_{max} = 7.5 \times 10^{-21}\ J$.[15] The hydrophobic interaction is quite relevant compared to the other interactions used. Since while the ones described above have been used easily for at least a century, the latter began to be used around a decade ago. And this is because it opened a path that until then had not been considered. This step that was taken consists of studying, through simulations, the thermosensitive behavior of polymers, such as gels. Behavior that has been studied experimentally for a long time, in which this change in volume with temperature was observed. Additionally, theoretical studies were also carried out based on the Flory-Rehner theory[19], developed half a century ago. Where the Flory solvency parameter (χ) could explain this temperature-dependent volume transition. However, there was no suitable tool that could emulate the experimental data through simulations, until a scarce decade ago.

In addition, if a thermo-responsive gels is modelled, where there are charged particles in the simulation, the temperature dependence of the dielectric permittivity is needed in consideration as well, adopting the following expression:[20]

$$\varepsilon_r = \frac{5321}{T} + 233.76 - 0.9297T + 0.1417 \times 10^2 T^2 - 0.8292 \times 10^6 T^3 \tag{3.17}$$

So far, we have explained different characteristics in the simulation model, common regardless of the size of the gel. But there is a marked difference, and it is the size of the structure of these two. When simulating a nanogel, it is

computationally viable to configure it as a delimited structure, since it can be contained by our simulation space without the simulation data overflowing. This allows us to get an outside perspective on it and even see its interaction with other external components of equal or smaller size. In this type of simulations, thousands of spheres modelling nanogel monomers and solute could be handled simulating with MC methods on a computer. But these numbers would increase several orders of magnitude if one wanted to simulate a gel in all its immensity, making simulation calculations prohibitive. For this reason, when a gel or microgel has been studied, a small internal part of it has been simulated, recreating its internal structure, and extrapolating with periodic conditions on a larger scale. With these simulations, results can be obtained from systems with a significantly large size and a reduced computing cost.

3.2. Gel Simulation

In order to simulate a microgel with MC methods, we have used the grand canonical ensemble, also known as μVT ensemble, where the temperature, the simulation volume and the chemical potential are kept constant. In this system, the particles will move freely, seeking the global position in equilibrium. To do this, many movements are simulated, but not all movements are accepted. In addition, the number of particles is not fixed. Since the simulation represents a portion inside the total macrogel, the ions are going to diffuse freely throughout the medium, which implies that they can enter or leave our simulation space. To represent this condition, there are special movements that can insert or remove a random cosolute of the simulation cell. So, there are different type of movements, but the displacement movement is more likely to be applied at the simulation. The relative frequencies of each type of movement are of the order of those used by Valleau *et al* in a classic work on MC in the grand canonical ensemble.[21]

Displacement movement. This process consists of selecting a particle at random and trying to move it a random distance. After the translation, the energy variation of the system produced by the displacement is employed to compute an acceptance probability, and the movement is only accepted if the energy variation is negative, or positive but less than the acceptance probability:

$$P_{mov}^{acc} = min\left[1, exp\left(-\frac{\Delta U_{mov}}{k_B T}\right)\right] \quad (3.18)$$

where P_{mov}^{acc} a is the probability to move the particle and ΔU_{mov} is the change in the potential energy with that move. After each movement attempt, whether the movement is accepted or not, the final position of the selected particle is stored. And by making a statistical balance of the stored positions, the configuration of the real system in thermodynamic equilibrium can be obtained. Which allows us to delve into the behavior of nanogels, and their various qualities and behaviors. There is a consideration to take into account in this method, the statistical analysis makes sense when we are in a configuration close to the real one. But our initial configuration starts from a much more orderly one. A defect-free network with diamond-like topology where the nodes are positioned on the diamond lattice and the monomer beads in the lines connecting them (see Figure 3.2.). The topology of the network is unchanged throughout the simulations, thus representing a covalently cross-linked network. The network is assembled connecting the chain ends to the tetrafunctional cross-linkers. Figure 3.2. allows us to appreciate how the simulation is only a part inside the macrogel, and because it makes sense that the cosolutes can enter or exit freely. Periodic boundary conditions are applied.[22]

Since the initial configuration is far from looking like a real one, the program has an initial stage of thermalization, where movements are made that do not save the positions, that is, they do not have statistical weight. Thus, the simulation usually performs at least a number of 10^8 thermalization movements.

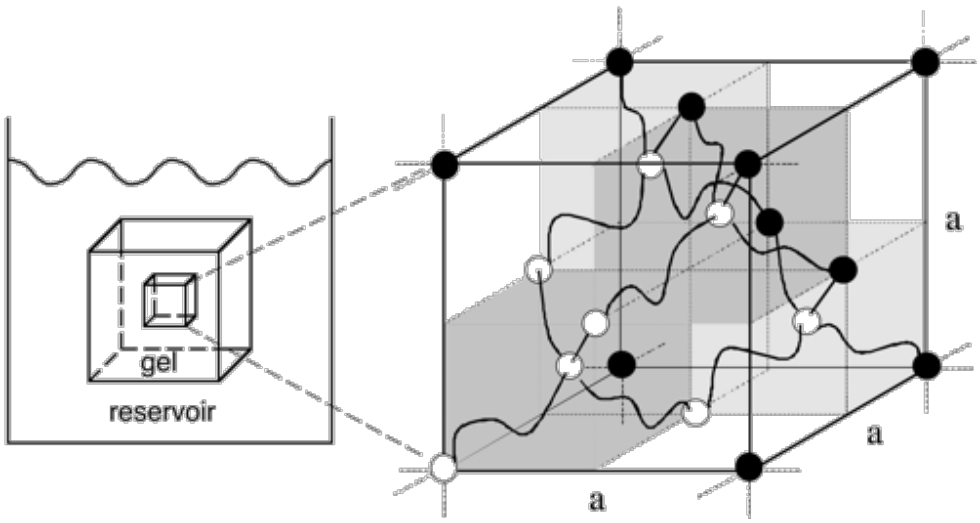

Figure 3.2. (left) Schematic illustration of a macroscopic gel in a solvent reservoir. (right) Schematic illustration of a unit cell of a defect-free network of diamond-like topology containing eight tetrafunctional nodes (open spheres) linked by uncrossed chains (wavy lines). Note that four of the eight subcubes contain chains (shaded) while the other four are empty. Reprinted with permission from[8]. Copyright 2021 American Chemical Society.

Insertion/removal movement. These two processes consist of adding or removing a random cosolute from our simulation space, respectively. Acting in an analogous way to the displacement of a particle, the energy variation of the system is calculated before and after the operation, if the energy variation is negative or less than the insertion or removal acceptance probabilities, respectively, the motion is accepted. Represented the probabilities as:[23]

$$P_{ins}^{acc} = min\left[1, exp\left(-\frac{\Delta U_i}{k_B T} + ln\left(\frac{\rho_c^{bulk} N_A L^3 \gamma}{N_c + 1}\right)\right)\right] \tag{3.19}$$

$$P_{rem}^{acc} = min\left[1, exp\left(-\frac{\Delta U_r}{k_B T} - ln\left(\frac{\rho_c^{bulk} N_A L^3 \gamma}{N_c}\right)\right)\right] \tag{3.20}$$

where ΔU_i and ΔU_r are the changes of potential energy involved in each insertion or removal, respectively, N_c is the current number of cosolute molecules before the insertion or removal attempts, ρ_c^{bulk} is the cosolute concentration (in mole m^{-3}) in the reservoir (bulk) and γ is the mean activity coefficient,

which was estimated from the Carnahan–Starling expression for hard spheres:[24]

$$ln\,\gamma = \frac{\phi_c^{bulk}\left(8 - 9\phi_c^{bulk} + 3\phi_c^{bulk}\right)}{\left(1 - \phi_c^{bulk}\right)^3} \tag{3.21}$$

where ϕ_c^{bulk} is the volume fraction of the cosolute in the reservoir. Whether the operation is accepted or rejected, the resulting position is saved to make statistics with the rest of the displacement movements, which allows us to estimate the global system in equilibrium.

By simulating the inside of a macrogel, we can obtain useful information about it. Like, for example, how permeable is the gel to a given solute. To calculate this situation, we seek to obtain the parameter that characterizes the net absorption of certain substance inside the macrogel, the partition coefficient, defined as

$$K = \frac{\rho_c}{\rho_c^{bulk}} \tag{3.22}$$

where ρ_c and ρ_c^{bulk} are the concentration of cosolute particles inside the macrogel and in the bulk suspension, respectively. Moreover, if we are in the limiting case of infinite dilution of cosolute particles, the mutual interactions between cosolute particles can be neglected. And therefore:

$$K_0 = \lim_{\rho_c^{bulk} \to 0} K \tag{3.23}$$

This condition is useful to investigate the role of the interaction between the cosolute particles and the interconnected monomers of the macrogel network without the interaction of cosolutes with other cosolutes.

Another important element of the simulation would be the swollen rate of the macrogel. This behavior could be expressed in the simulation through the polymer volume fraction:

$$\phi_m = \frac{4\pi\rho_m {R_m}^3}{3} \tag{3.24}$$

where R_m is the radius of the monomers in the gel, and $\rho_m = N_m/V$ is the density of the gel, that is, the number of monomers between the simulation space. As the number of monomers in our simulation is fixed, but the volume is adjusted depending on the desired polymer volume fraction, it can be concluded that the higher the simulation volume, the more expanded the macrogel is. Thus, an inversely proportional relationship can be obtained between the polymer volume fraction and the swelling of the gel. Moreover, the dependence of K with ϕ_m provides a description of the equilibrium cosolute absorption as a function of the swelling state of the macrogel, and so it can lead to a realistic estimate of the optimum swelling that maximizes the cosolute uptake.

3.3. Nanogel Simulation

In order to simulate a nanogel instead, the canonical ensemble, also known as NVT ensemble, can be used, where the temperature, the volume of the simulation cell and the number of particles in the system are kept constant. This ensemble is used instead of the grand canonical one because the nanogel is simulated from an outside view. Instead of simulating the inside of the gel, where it made sense for the cosolute to diffuse into or out of the simulation space, since the solute does not leave the macrogel as such, it just flows through it. However, with a nanogel, we generate a fixed simulation space large enough to house the nanogel itself. Therefore, the particles will move freely, but their total number is fixed. Thus, there is no insertion/removal movement in the nanogel simulation. Only displacement movement are applied (as explained in the previous section) in the simulation. Periodic boundary conditions are applied, although there is some distance between the nanogel and the boundaries.

Similarly, our initial configuration is also a diamond-like topology, however not all crosslinkers are linked to four chains as with the macrogel. Since the nanogel is a finite entity, there must be crosslinkers with three and even two neighbors. Figure 3.3. (left) shows what an initial configuration could look like before thermalization. Figure 3.3. (right) shows how once the particles are allowed to move, the shape becomes more spherical. As we have an outside perspective of the nanogel, a special displacement movement can be

performed in which all the nanogel particles expand or contract with respect to the mass center of the nanogel. This movement is preferably carried out in the thermalization phase, which allows accelerating that phase. This movement consists of varying the size of the nanogel multiplying the position vector of each nanogel particle (with respect to the mass center) by a factor (α) close to 1 keeping the simulation cell constant. Analogously to the displacement of a particle, the energy variation of the system before and after is computed with a probability of acceptance of volume change. If this is negative, or positive but less than the probability of acceptance, the volume change is accepted. The probability of accepting the volume change would be:[25]

$$P_{\alpha}^{acc} = min\left[1, \alpha^{3N_{par}} exp\left(-\frac{\Delta U_{\alpha}}{k_B T}\right)\right] \tag{3.25}$$

where P_{α}^{acc} a is the probability that the coordinates of all particles are multiplied by α, ΔU is the change in the potential energy after the displacement and N_{par} is the number of particles in the nanogel network.

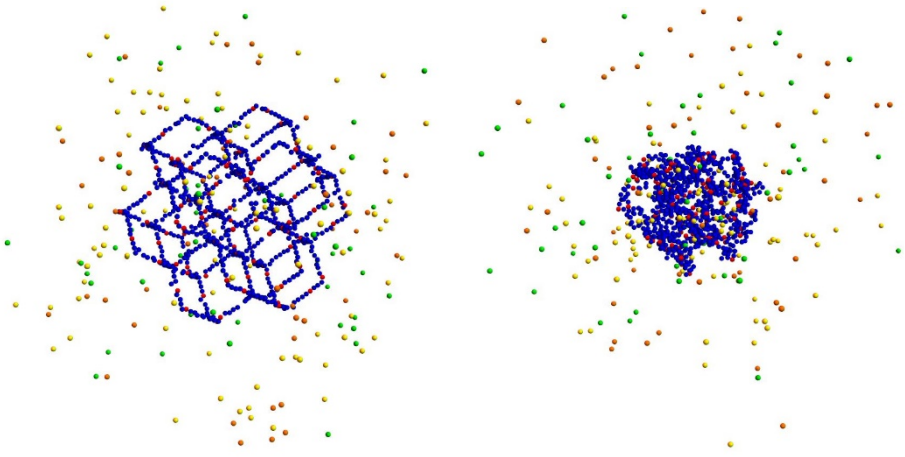

Figure 3.3. Snapshots of the initial diamond-like configuration studied in Paper II to generate a nanogel (left) and a representative configuration of the nanogel after equilibration (right).

By simulating an exterior view of the nanogel, we can obtain results that from an interior perspective would be impossible to achieve. For example, when treating it as a particle, it is ideal to get the radius of the nanogel. Which

helps us to see how its size varies under different conditions. Like simulating a nanogel at different temperatures and obtaining its swelling curve that depends on temperature.

In order to determine the radius of the nanogel (R_{NG}), we are going to calculate its relationship with the radius of gyration (R_g), considering what would be the R_g^2 of a rigid sphere with a geometric radius R_{sph} and volume V_{sph}:

$$R_g^2 = \frac{\int r_{sph}^2 dV_{sph}}{V_{sph}} = \frac{\iiint r_{sph}^4 sin(\theta) dr_{sph} d\theta d\varphi}{\frac{4}{3}\pi R_{sph}^3} = \frac{3}{5} R_{sph}^2 \qquad (3.26)$$

where r_{sph}, θ and φ are the spherical coordinates of the volume integral. Therefore, considering the nanogel as a rigid sphere we can consider that $R_{NG} \equiv R_{sph}$, and therefore:

$$R_{NG} = \sqrt{\frac{5}{3}} R_g \qquad (3.27)$$

The radius of gyration of a particular molecule at a given time is defined as:

$$R_g^2 = \frac{\sum r_{par}^2}{N_{par}} \qquad (3.28)$$

where r_{par} is the distance of each particle of the nanogel to the nanogel mass center. As the simulation is using MC methods, where the state being simulated does not have to be real, but the statistical average does. We can calculate the R_g^2 of each simulation, using formula (3.28), from averaging all the R_g^2 of each iteration once the thermalization process has passed. And from here, it is immediate to obtain the R_{NG} using equation (3.27).

One of the most interesting properties of nanogels is the electrical potential that they generate around them. Since this is what mediates the interaction with other elements of its environment sensitive to electrical charges, even with other nearby charged nanogels. By simulating a nanogel as a finite particle, the simulation allows us to account for the total charge contained within

the nanogel, and even its spatial distribution. We could calculate the net charge enclosed by a sphere of radius r as:

$$Q(r) = \int_0^r \rho(r) 4\pi r^2 dr \tag{3.29}$$

where ρ is the concentration of charged particles from the simulation. In addition, if we calculated previously the R_{NG} with equation (3.27), the effective net charge of the nanogel can be obtain as $Q(R_{NG})$. Applying Gauss's law to equation (3.29), the electric field at a distance r is:

$$E(r) = \frac{Q(r)}{4\pi\varepsilon_0\varepsilon_r r^2} \tag{3.30}$$

Finally, the electrostatic potential is calculated integrating the electric field of the nanogel:

$$\psi(r) = \int_0^r E(r) dr \tag{3.31}$$

With $\psi(r)$ and R_{NG}, we can obtain the electrostatic potential at the surface of the nanogel $\psi_s = \psi(R_{NG})$, which indicates the maximum approach potential that a charged particle approaching the nanogel will suffer. This surface potential can give us some information about the electrokinetic behavior of these soft nanoparticles as the zeta potential does in the case of hard particles. The zeta potential is the electrical potential at the plane which separates mobile fluid from fluid that remains attached to the surface. Zeta potential is not measurable directly, but it can be calculated using theoretical models and an experimentally-determined dynamic electrophoretic mobility or electrophoretic mobility. Therefore, the simulation data obtained can be compared qualitatively with its experimental analogue data.

References

1 D. Chandler, *Introduction to Modern Statistical Mechanics*, 1987.

2 J.-P. Hansen and I. R. McDonald, Theory of simple liquids.

3 P. Košovan, T. Richter and C. Holm, eds. G. Sadowski and W. Richtering, Springer International Publishing, Cham, 2013, pp. 205–221.

4 B. A. Mann, R. Everaers, C. Holm and K. Kremer, Scaling in polyelectrolyte networks, *Europhys. Lett.*, 2004, **67**, 786–792.

5 B. A. Mann, C. Holm and K. Kremer, Swelling of polyelectrolyte networks, *J. Chem. Phys.*, , DOI:10.1063/1.1882275.

6 D. W. Yin, Q. Yan and J. J. De Pablo, Molecular dynamics simulation of discontinuous volume phase transitions in highly-charged crosslinked polyelectrolyte networks with explicit counterions in good solvent, *J. Chem. Phys.*, , DOI:10.1063/1.2102827.

7 D. W. Yin, M. Olvera De La Cruz and J. J. De Pablo, Swelling and collapse of polyelectrolyte gels in equilibrium with monovalent and divalent electrolyte solutions, *J. Chem. Phys.*, , DOI:10.1063/1.3264950.

8 S. Schneider and P. Linse, Monte Carlo simulation of defect-free cross-linked polyelectrolyte gels, *J. Phys. Chem. B*, 2003, **107**, 8030–8040.

9 S. Edgecombe, S. Schneider and P. Linse, Monte Carlo simulations of defect-free cross-linked gels in the presence of salt, *Macromolecules*, 2004, **37**, 10089–10100.

10 S. Schneider and P. Linse, Discontinuous volume transitions in cross-linked polyelectrolyte gels induced by short-range attractions and strong electrostatic coupling, *Macromolecules*, 2004, **37**, 3850–3856.

11 G. C. Claudio, K. Kremer and C. Holm, Comparison of a hydrogel model to the Poisson-Boltzmann cell model, *J. Chem. Phys.*, , DOI:10.1063/1.3207275.

12 H. Lee and W. Cai, Ewald summation for Coulomb interactions in a periodic supercell, *Lect. Notes, Stanford Univ.*, 2009, **3**, 1–12.

13 I. Adroher-Benítez, A. Martín-Molina, S. Ahualli, M. Quesada-Pérez, G. Odriozola and A. Moncho-Jordá, Competition between excluded-volume and electrostatic interactions for nanogel swelling: Effects of the counterion valence and nanogel charge, *Phys. Chem. Chem. Phys.*, 2017, **19**, 6838–6848.

14 J. Estelrich, M. Quesada-Perez, J. Forcada and J. Callejas-Fernandez, in *Soft Nanoparticles for Biomedical Applications*, The Royal Society of Chemistry, 2014, pp. 1–18.

15 M. Quesada-Pérez, J. Ramos, J. Forcada and A. Martín-Molina, Computer simulations of thermo-sensitive microgels: Quantitative comparison with experimental swelling data, *J. Chem. Phys.*, , DOI:10.1063/1.4729946.

16 M. O. Khan, S. M. Mel'nikov and B. Jonsson, Anomalous salt effects on DNA conformation: Experiment and theory, *Macromolecules*, 1999, **32**, 8836–8840.

17 F. A. Escobedo and J. J. de Pablo, Monte Carlo simulation of branched and crosslinked polymers, *J. Chem. Phys.*, 1996, **104**, 4788–4801.

18 M. Quesada-Pérez, J. A. Maroto-Centeno, J. Forcada and R. Hidalgo-Alvarez, Gel swelling theories: The classical formalism and recent approaches, *Soft Matter*, 2011, **7**, 10536–10547.

19 P. J. Flory and J. Rehner, Statistical Mechanics of Cross-Linked Polymer Networks II. Swelling, *J. Chem. Phys.*, 1943, **11**, 521–526.

20 A. H. Johnstone, CRC Handbook of Chemistry and Physics—69th Edition Editor in Chief R. C. Weast, CRC Press Inc., Boca Raton, Florida, 1988, pp. 2400, price £57.50. ISBN 0–8493–0369–5, *J. Chem. Technol. Biotechnol.*, 1991, **50**, 294–295.

21 J. P. Valleau and L. K. Cohen, Primitive model electrolytes. I. Grand canonical Monte Carlo computations, *J. Chem. Phys.*, 1980, **72**, 5935–5941.

22 M. Quesada-Pérez, J. Guadalupe Ibarra-Armenta and A. Martn-Molina, Computer simulations of thermo-shrinking polyelectrolyte gels, *J. Chem. Phys.*, , DOI:10.1063/1.3632051.

23 S. Lamperski, The individual and mean activity coefficients of an electrolyte from the inverse GCMC simulation, *Mol. Simul.*, 2007, **33**, 1193–1198.

24 N. F. Carnahan and K. E. Starling, Equation of State for Nonattracting Rigid Spheres, *J. Chem. Phys.*, 1969, **51**, 635–636.

25 D. Frenkel and B. Smit, Understanding molecular simulation: From algorithms to applications, *Underst. Mol. Simul. From algorithms to Appl.*, , DOI:10.1063/1.881812.

4. Paper I: Maximizing the absorption of small cosolutes inside neutral hydrogels: steric exclusion versus hydrophobic adhesion

L. Pérez-Mas, A. Martín-Molina, M. Quesada-Pérez and A. Moncho-Jordá

The content of this chapter is published in: *Physical Chemistry Chemical Physics*, **2018**, *20*, 2814.

https://doi.org/10.1039/C7CP07679G

Abstract

In this work the equilibrium absorption of nanometric cosolutes (which could represent drugs, reactants, small globular proteins and other kind of biomacromolecules) inside neutral hydrogels is studied. We specially focus on exploring, for different swelling states, the competition between the steric exclusion induced by the cross-linked polymer network constituting the hydrogel, and the solvent-induced short range hydrophobic attraction between the polymer chains and the cosolute particle. For this purpose, the cosolute partition coefficient is calculated by means of coarse-grained grand canonical Monte Carlo simulations, and the results are compared to theoretical predictions based on the calculation of the excluded and binding volume around the polymer chains. For small hydrophobic attractions or large cosolute sizes, the steric repulsion dominates, and the partition coefficient decreases monotonically with the polymer volume fraction, ϕ_m. However, for large enough hydrophobic attraction strength, the interplay between hydrophobic adhesion and the steric exclusion leads to a maximum in the partition coefficient at certain intermediate polymer density. Good qualitative and quantitative agreement is achieved between simulation results and theoretical predictions in the limit of small ϕ_m, pointing out the importance of geometrical aspects of the cross-linked polymer network, even for hydrogels in the swollen state. In addition, the theory is able to predict analytically the onset of the maximum formation in terms of the details of the cosolute-monomer pair interaction, in good agreement with simulations too. Finally, the effect of the many-body attractions between the cosolute and multiple polymer chains is quantified. The results clearly show that these many-body attractions play a very relevant role determining the cosolute binding, enhancing its absorption in more than one order of magnitude.

4.1. Introduction

Hydrogels are soft particles formed by a cross-linked polymer network dispersed in water that can be synthesized with nanoscopic dimensions. These nanoparticles have gained consider-able attention during the last decades due to their unique physicochemical properties. First of all, hydrogel particles experience a volume phase transition between swollen and shrunken states, in response to many external stimuli such as pH, ionic strength, temperature, light, or external applied electric and magnetic fields.[1–4] The characteristic time of swelling/deswelling scales with the square of its typical size, leading to much faster response times to reach equilibrium (of the order of seconds) than

the so-called macroscopic gels (response times from hours to days).[5] Due to their porous morphology, hydro-gels are able to absorb large amounts of small biomacromolecules (such as proteins, peptides or DNA), drugs or chemical reactants. Moreover, the fibrous internal morphology of these particles maximizes the total exposed surface of polymer to the solvent, which can be exploited to enhance the attachment of the substance to the polymeric matrix of the microgel. Finally, due to their large water content, the uploading of biomacromolecules can be achieved maintaining their biological activity and conformational state.[6–10] Hydrogels are specially interesting for applications that involve the uptake of hydrophobic cosolutes. Indeed, the poor solubility of many newly designed hydrophobic therapeutic drugs has resulted in numerous problems for their transport and release.[11,12] The combination of all these important features make hydrogels excellent candidates for different biomedical and industrial applications, such as transport and time-controlled delivery of therapeutic molecules,[13–17] or as stimuli-responsive nanoreactors for controlled catalysis.[18–21] The diffusion, encapsulation and attachment of a certain cosolute inside a neutral hydrogel are mainly determined by two interactions, namely the excluded-volume repulsion exerted by the polymer chains, and the hydrophobic (hydrophilic) cosolute–polymer attraction (repulsion) caused by changes in water structure around the cosolute and the polymer chain.[22–25] These interactions represent in fact effective potentials that gather chemistry-specific information from the detailed atomistic level, in which the solvent degrees of freedom, hydrogen-bonding effects and the conformational flexibility of the polymer have been coarse-grained using certain statistical averaging procedure.[26,27] Therefore, entropic and enthalpic contributions are usually implied in this kind of interactions. The strength of this interaction can be significantly large, giving rise to a noteworthy accumulation or depletion of cosolute inside the hydrogel. The steric exclusion controls the in-diffusion of the cosolute inside the particle, whereas the hydrophobic attraction determines the binding energy of the substance inside the polymer matrix. Indeed, large-sized solutes are less likely to diffuse inside the polymeric matrix compared to small ones, since the average pore size (or interchain spacing) establishes a threshold to the size of cosolutes that can permeate inside the polymer matrix.[28] On the other hand, the specific nature of the polymer chains can also contribute to amplify the hydrophobic adhesion. In this sense, experimental observations clearly show that protein sorption can be enhanced in hydrogel particles containing a larger amount of hydrophobic comonomer.[29] The adhesive properties of the hydrogel can also be switched by changing its swelling state.[30] For

instance, the swollen con-figuration is achieved because the polymer chains are hydrophilic and so more likely to be surrounded by water molecules. Conversely, the shrunken state is the consequence of hydrophobic polymer–water repulsions that induce the collapse of the particle, although other effects as hydrogen bonding or van der Waals interactions may also be involved.[1] Consequently, in the swollen conformation, the polymer packing fraction inside the particle decreases, leading to a reduced excluded-volume repulsion. However, in this state the hydrogel becomes predominantly hydrophilic, so the cosolute binding is also smaller. In the shrunken (hydrophobic) state, the steric exclusion is greatly enhanced, but at the same time the hydro-phobic affinity of the cosolute becomes very important too. This interplay between both effects has been observed in many experiments of protein sorption into neutral hydrogels and grafted coatings.[31–34] As a result of this competition, the internal permeation of the protein is favored for swollen hydrogels, whereas a strong hydrophobic binding adsorption onto the hydrogel surface is promoted in the shrunken state.[35–37] Analogously, it has been shown experimentally that the uptake of water–solute drugs (or ions) induced by shrunken hydrogels can be substantially increased due to the hydrophobic character of the drug molecules.[38–40] In concrete, Punjabi *et al.* have recently observed that significantly more drug is taken up by each of the hydrogels (MAA-NIPAM) at 70 ºC (condensed state) compared to 25 ºC (swollen state). This result was attributable to the increased hydrophobicity of the microgel at higher temperatures. This maintained swelling at high temperatures is important in facilitating the higher observed drug loading at 70 ºC, allowing hydrophobic partitioning to control the drug uptake behavior as opposed to mass transfer.[40]

As mentioned above, the partitioning inside a neutral hydrogel is the result of a complex interplay between excluded-volume and hydrophobic binding effects. Given the large number of applications of these systems, this work intends to explore under a theoretical point of view different strategies to maximize the internal uptake of cosolutes (such as globular proteins or therapeutic drugs), inside a neutral hydrogel polymer network. In addition, it would be interesting to find out if the morphological details of the cross-linked polymer network and the many-body attractions between the cosolute particle and multiple polymer chains play a significant role on the cosolute partitioning. To address these fundamental questions, we perform Monte Carlo (MC) coarse-grained simulations of a neutral hydrogel in the presence of hydrophobic cosolutes. The hydrophobic inter-action between the cosolute and the polymer

chain is taken into account by assuming an attractive short-range interaction. Accordingly, characteristic parameters of this interaction (as its strength and range) are tuned in order to discover the optimal conditions at which a maximum of internal sorption is reached. Moreover, the influence of the size of the cosolute is also analyzed. In addition to the simulations, a simple theoretical model based on the calculation of the excluded and binding volumes around the polymer is developed to predict the onset of maximum formation. The paper is organized as follows. In Section 1.2 the theoretical models for the partition coefficient in the regime of infinite dilution of cosolute particles are presented. The MC computer simulations to tackle the cosolute absorption inside a cross-linked polymer network are described in Section 1.3. The results obtained from these simulations and the comparison with the theoretical predictions are shown in Section 1.4, and the most relevant conclusions summarized in Section 1.5. Finally, some details of the theoretical calculations are described in the Appendixes.

4.2. Theory: partition coefficient of attractive spherical cosolutes inside cross-linked polymer networks

In this section, a theory to predict the absorption of spherical cosolutes (representing small globular proteins, drugs, reactants,…) inside neutral hydrogels is developed. We define V as the total volume of the hydrogel network, with N_{cross} cross-linkers and N_{beads} beads. Hence, the total number of monomers is $N_m = N_{cross} + N_{beads}$. The most important parameter that characterizes the net absorption of certain substance inside the hydrogel is the so-called partition coefficient, defined as

$$K = \frac{\rho_c}{\rho_c^{bulk}} \tag{4.1}$$

where ρ_c and ρ_c^{bulk} care the concentration of cosolute particles inside the hydrogel and in the bulk suspension, respectively. K is in general a very complex quantity that depends on many parameters, such as the cosolute–cosolute and monomer–cosolute pair interaction potentials, bulk cosolute concentration, polymer packing fraction inside the hydrogel, cross-linking concentration and the particular morphology of the network. In this work, the assembly of N_m monomers are connected by means of tetrafunctional cross-linkers (each

cross-linker is connected to four chains). This kind of structure is quite general, as it represents the internal structure of many realistic hydrogel systems, such as poly(*N*-isopropylacrylamide) (PNIPAM) or poly(*N*-vinylcaprolactam) (PVCL), among others. We also consider that all chains between two cross-linkers nodes have the same length. This means that, if ν is the number of beads per chain and N_{chains} is the total number of chains, then $N_{beads} = \nu N_{chains}$. For a tetrafunctional cross-linked network, it can be shown that $N_{chains} = 2N_{cross}$. Therefore,

$$N_m = (1 + 2\nu)N_{cross} \tag{4.2}$$

The total number of bonds between two interconnected monomers can also be estimated in a similar way. For each cross-linker, there are 2 chains, and for each chain, there are $(\nu + 1)$ bonds, so

$$N_{bonds} = 2(\nu + 1)N_{cross} \tag{4.3}$$

We further assume that monomers and cosolutes are spherical particles, with radius R_m and R_c, respectively, and that two interconnected monomers are in close contact, so the distance between them is $2R_m$.

In order to investigate the role of the interaction between the cosolute particles and the interconnected monomers of the hydrogel network, we focus our study in the limiting case of infinite dilution of cosolute particles. In this regime, the mutual interactions between cosolute particles can be neglected, and the partition coefficient can be simply written in terms of the effective interaction energy that the cosolute experiences inside the hydrogel, u_{eff}:

$$K_0 = \lim_{\rho_c^{bulk} \to 0} K = e^{-\beta u_{eff}} \tag{4.4}$$

with $\beta = 1/(k_B T)$, where T is the absolute temperature. For this purpose, the pair potential between the cosolute particle and a monomer, $u_{cm}(r)$, must be known. $u_{cm}(r)$ should be regarded as an effective potential obtained after certain coarse-graining procedure, in which the degrees of freedom of the cosolute, the polymer chain and the surrounding solvent molecules have been traced out. In general, $u_{cm}(r)$ has a repulsive barrier that prevents the particle interpenetration, followed by a short-range repulsive or attractive tail that yields an additional exclusion or binding. In spite of the short-range character of this force (of a few water molecule diameters), it plays a very important role in many physico-chemical and bio-logical phenomena, such as protein stabilization and polymer coil-to-globule transitions.[41–44] In this work, we are not interested in the swelling transition of the hydrogel in the presence of finite

concentration of cosolute molecules. Instead, we especially focus on studying the cosolute partitioning inside the hydrogel in the presence of hydrophobic attractive interactions. Given the short-range character of the cosolute–monomer pair interaction potential, its specific details are not very important. Therefore, approximations can be done as soon as $u_{cm}(r)$ is chosen to fairly represent the volume exclusion repulsion effect and the existence of certain short-range hydrophobic attraction. A feasible and practical way to introduce both effects can be achieved through the square-well potential

$$u_{cm}(r) = \begin{cases} \infty & r \leq R_{exc} \\ -\varepsilon & R_{exc} < r \leq R_{bind} \\ 0 & r > R_m + R_c + \Delta \end{cases} \tag{4.5}$$

where $R_{exc} = R_m + R_c$ is the excluded radius, $R_{bind} = R_m + R_c + \Delta$ is the range of the attractive well (Δ is the thickness of the attractive region) and $\varepsilon > 0$ stands for the attraction strength. Despite its simplicity, this potential retains the most important features of the real interaction. Indeed, since the hydrophobic attraction is in general short-ranged, the effective pair potential could be characterized within a square-well form, where ε and Δ are chosen to match the second and third virial coefficients of the real interaction. In addition, this choice has the particular advantage of allowing the analytical calculation of the partition coefficient in some limits, as will be shown below.

Once the pair potential and the network structure are fixed, the partition coefficient depends exclusively on the polymer volume fraction inside the hydrogel, $K = K(\phi_m)$, with $\phi_m = 4\pi\rho_m R_m^3/3$ ($\rho_m = N_m/V$). The knowledge of $K(\phi_m)$ provides a complete description of the equilibrium cosolute absorption as a function of the swelling state of the hydrogel, and so it can lead to a realistic estimate of the optimum swelling that maximizes the cosolute uptake. In the following section, a theory to predict the value of K_0 for swollen hydrogels is presented. This is indeed the simplest situation, as many-body correlations induced by the polymer chains can be neglected. Then, in a second step, an approximate model to extend this theory for large ϕ_m is shown.

4.2.1. Calculation of K_0 for swollen hydrogels

When the hydrogel is immersed in a good solvent, the cross-linked polymer chains are extended. Under this particular case, it is very unlikely that two neighboring polymer chains approach each other. This means that the absorption of the cosolute will involve only the interaction with a single chain. Making

use of this approximation, the volume excluded by the polymers and the volume of the binding region around them (the region where the cosolute experiences an attraction to the polymers) can be calculated analytically. Then, K_0 can be expressed in terms of these excluded and binding volumes. A detailed explanation of the calculation of K_0 is shown in Appendix A. The resulting analytical expression can be written as

$$K_0(\phi_m) = 1 + \alpha\phi_m \tag{4.6}$$

where α can be split in three different additive terms

$$\alpha = a + be^{\beta\varepsilon} + ce^{2\beta\varepsilon} \tag{4.7}$$

The first term is the contribution to the partitioning coefficient arising from the volume where the interaction between the cosolute particle and the polymer chains is zero. The term proportional to $e^{\beta\varepsilon}$ accounts for the region where the cosolute is attracted to a single monomer, with a total interaction energy of $-\varepsilon$. Finally, the term proportional to $e^{2\beta\varepsilon}$ represents the contribution of the regions where the cosolute is attracted at the same time to a couple of monomers, with an energy of interaction of -2ε. Coefficients *a, b* and *c* are explicitly given by

$$a = -\lambda_{bind}^3 + \frac{(\nu+1)}{2\nu+1}(1-\lambda_{bind})^2(1+2\lambda_{bind}) \tag{4.8}$$

$$\begin{aligned} b = \lambda_{bind}^3 - \lambda_{exc}^3 \\ + \frac{(\nu+1)}{2\nu+1}\Big[(1-\lambda_{exe})^2(1+2\lambda_{exc}) \\ - (1-\lambda_{bind})^2(1+2\lambda_{bind}) - \frac{3}{8}\left(\lambda_{bind}^2 - \lambda_{exc}^2\right)^2\Big] \end{aligned} \tag{4.9}$$

$$c = \frac{3}{8}\frac{(\nu+1)}{2\nu+1}\left(\lambda_{bind}^2 - \lambda_{exc}^2\right)^2 \tag{4.10}$$

where $\lambda_{bind} = R_{bind}/R_m$ and $\lambda_{exc} = R_{exc}/R_m$. We remind that ν is the number of monomers per chain (assuming that all chains between two cross-linkers have the same length). Several comments should be mentioned at this point. First of all, the theory predicts a linear dependence of K_0 with the polymer volume fraction. This prediction represents an approximation for extended hydrogels, where the polymer packing fraction is small. By increasing

ϕ_m, more entangled overlaps between the excluded and binding volumes around the monomers entail additional non-linear terms.

Secondly, it is interesting to remark that the contribution proportional to $e^{2\beta\varepsilon}$ becomes very significant when the depth of the potential well is large enough ($\beta\varepsilon > 1$). This means that the 3-body contribution due to the simultaneous attraction between a cosolute particle with two interconnected monomer cannot be neglected, even in the limit of very small polymer packing fractions. In fact, the partition coefficient obtained assuming that the cosolute is only attracted to the closest monomer is always smaller than the one obtained from eqn (4.6) – (4.10). The explicit expression of α for this particular case is

$$\begin{aligned}\alpha_{2-body} = -\lambda_{bind}^3 + \frac{(\nu+1)}{2\nu+1}(1-\lambda_{bind})^2(1+2\lambda_{bind}) \\ + e^{\beta\varepsilon}\left\{\{\lambda_{bind}^3 - \lambda_{exc}^3 + \frac{(\nu+1)}{2\nu+1}[(1-\lambda_{exc})^2(1\right. \\ \left. + 2\lambda_{exc}) - (1-\lambda_{bind})^2(1+2\lambda_{bind})]\right\}\end{aligned} \tag{4.11}$$

Finally, it is important to emphasize that the geometrical aspects are also relevant in determining the correct expression of the partition coefficient. In other words, the fact that monomers are not free individual particles, but instead are structured forming an interconnected and cross-linked network, has significant implications even in the limit of very small ϕ_m. In order to demonstrate this, a simple thermo-dynamic calculation of K_0 has been performed using a naïve second order virial expansion in terms of the monomer and cosolute number densities, ρ_m and ρ_c, respectively (see Appendix B). In the limit of small cosolute concentration, K_0 is given by

$$K_0^{virial} = 1 + \left[-\lambda_{bind}^3 + e^{\beta\varepsilon}\left(\lambda_{bind}^3 - \lambda_{exc}^3\right)\right]\phi_m \tag{4.12}$$

However, this thermodynamic approach completely neglects the overlapping volumes between the excluded and attractive regions around interconnected monomers, and so it is expected to lead to wrong predictions.

4.2.2. Estimating K_0 for any swelling state of the hydrogel

For swollen hydrogels, the previous section showed that the network structure can be modeled by an assembly of interconnected monomers forming independent chains. However, as the polymer volume fraction increases due to hydrogel collapsing, this picture completely breaks down, since monomers

belonging to different chains (and even unconnected monomer sin the same chain) approach each other to very close distances, causing multiple overlaps of the excluded and binding volumes. This many-body effect leads to a non-linear structure-dependent behavior of $K_0(\phi_m)$. Moreover, K_0 also become dependent of other parameters, such as the persistence length of the polymer chains.

In spite of the enormous complexity of this problem, it is still possible to give a qualitative description of the expected behavior. For small attractions (small ε), the excluded-volume repulsion exerted by the polymer chains always increase with ϕ_m. Consequently, $K_0(\phi_m)$ decreases monotonically to zero as ϕ_m tends to 1 (in this limit, there is no free space for the incoming cosolute). However, as ϕ_m increases, the volume of the attractive region grows for small ϕ_m, and then decreases for large ϕ_m. If the depth of the attractive well is sufficiently large, this effect leads to the appearance of a maximum of $K_0(\phi_m)$, which is the result of the competition between the hydrophobic short-range attraction and the steric repulsion. Eventually, K_0 decays when ϕ_m is further increased, as the steric effect becomes dominant in this limit.

An exact analytical expression for the partition coefficient can be deduced for any polymer concentration if the structure of the polymer network is approximated by means of simple geometrical models. One option is to assume that the cross-linked polymers are modeled by an assembly of randomly oriented cylindrical fibers, and that the cosolute only inter-acts with the closest fiber (many-body effects neglected).[45,46] Under these grounds, the total volume fraction available for the cosolute with a distance from the closest chain larger than r is given by $\phi(r) = (1-\phi_m)^{(r/R_f)^2}$, where $R_f = \sqrt{2/3}R_m$ is the effective radius of the rod that matches the volume of an straight array of spherical monomers of radius R_m.[47] The partition coefficient is $K_0 = e^{\beta\varepsilon}\left[\phi\left(R_f + R_c\right) - \phi\left(R_f + R_c + \Delta\right)\right] + \phi\left(R_f + R_c + \Delta\right)$,which leads to

$$\mathrm{K}_0^{rods} = e^{\beta\varepsilon}[(1-\phi_m)^{\left(1+R_c/R_f\right)^2} - (1-\phi_m)^{(1+(R_c+\Delta)/\mathrm{R_f})^2} + (1-\phi_m)^{(1+(R_c+\Delta)/\mathrm{R_f})^2} \quad (4.13)$$

Another simple analytical model can be deduced considering the network as an assembly of randomly located spherical monomers of radius R_m. In this case

$$\mathrm{K}_0^{spheres} = e^{\beta\varepsilon}[(1-\phi_m)^{(1+R_c/R_m)^3} - (1-\phi_m)^{(1+(R_c+\Delta)/\mathrm{R_m})^3} + (1-\phi_m)^{(1+(R_c+\Delta)/\mathrm{R_m})^3} \quad (4.14)$$

In spite of the strong assumptions on the internal morphology of the hydrogel, both models predict the existence of a maximum of K_0, providing a qualitative explanation to the interplay between steric repulsion and hydrophobic attraction.[24] Although a quantitative description of the position and height of the maximum is still remaining, the theory previously presented for swollen hydrogels still provides an excellent way to find out whether this maximum will arise or not, by simply analyzing the partition coefficient in the limit of small ϕ_m. Indeed, for $\alpha > 0$, a maximum develops at certain intermediate polymer maxing fraction. This condition of maximum is satisfied when

$$\beta\varepsilon > \ln\left[\frac{-b+\sqrt{b^2-4ac}}{2c}\right] \quad (4.15)$$

where coefficients *a, b* and *c* are given in eqn (4.8) – (4.10).

4.3. Monte Carlo simulations

According to the model described in the introduction, monomers, cross-linkers and cosolute molecules are explicitly considered as hard spheres. The short-range repulsion between monomers and crosslinkers due to excluded volume effects is modeled by means of the usual potential for hard spheres:

$$u_{mm}(r) = \begin{cases} \infty & r \le R_i + R_j \\ 0 & r > R_i + R_j \end{cases} \quad (4.16)$$

where r is the center-to-center distance between a given pair of particles and i stands for the species. This short-range repulsion is also employed for the cosolute–cosolute excluded-volume interaction and is also considered in the square-well potential characterizing the monomer–cosolute interaction (see eqn (4.5)).It should be also mentioned that the beads forming a given chain are connected by harmonic bonds, whose interaction potential is:

$$u_{bond}(r) = \frac{k_{bond}}{2}(r-r_0)^2 \quad (4.17)$$

where k_{bond} is the elastic constant ($k_{bond} = 0.4$ N m^{-1}) and r_0 is the equilibrium bond length (in this work $r_0 = 2R_m$). The network was assembled connecting the chain ends to the tetra-functional cross-linkers (through the same harmonic bonds). For simplicity, a defect-free network with diamond-like

topology and chains of equal length was assumed. In this work, networks with 20 beads per chain were simulated. The simulation cell contains 8 nodes and 16 chains (as in previous similar works).[48–51] Two typical snapshots of the simulations for two different polymer volume fractions are depicted in Figure 4.1.

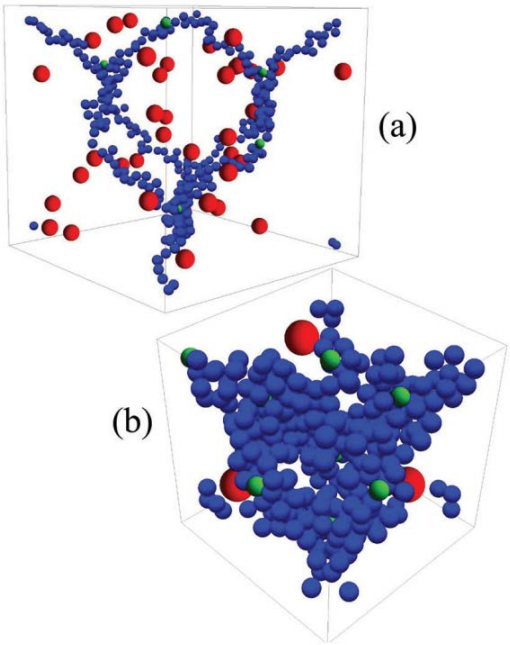

Figure 4.1: Two snapshots of the simulations for (a) $\phi_m = 0.01$ and (b) $\phi_m = 0.1$. Blue, green, and red spheres represent interconnected beads of the chains, cross-linker nodes, and cosolute particles, respectively.

The configurations of the polymer network for different polymer volume fractions were simulated here just changing the cell dimensions while the number of particles of the network remains constant. In other words, the network was simulated in the canonical ensemble. A cubic simulation box contained the particles of the polymer network and the solute. The conventional Metropolis Monte Carlo (MC) protocol was used to generate Boltzmann-weighted gel configurations. The maximum displacements corresponding to solute particles and network beads were adjusted so that their respective acceptance ratios were close to 50%. Periodic boundary conditions were applied. The nodes were initially positioned on a diamond lattice and the monomer beads in the lines connecting them.[48–51]

The equilibrium between cosolute molecules in the gel and in a reservoir at the desired concentration was simulated in the grand canonical (GC) ensemble. Thus, simulations also consider insertion and removal of one cosolute particle together with the translational MC moves. The probability of acceptance of insertion and removal are given, respectively, by:[52]

$$\text{acc(insertion)} = \min\left[1, exp\left(-\frac{\Delta u_i}{k_B T} + ln\left(\frac{\rho_c^{bulk} N_A V \gamma}{N_c + 1}\right)\right)\right] \qquad (4.18)$$

$$\text{acc(removal)} = \min\left[1, exp\left(-\frac{\Delta u_r}{k_B T} - ln\left(\frac{\rho_c^{bulk} N_A V \gamma}{N_c}\right)\right)\right] \qquad (4.19)$$

where V is the volume of the simulation cell, T is the absolute temperature, Δu_i and Δu_r are the changes of potential energy involved in a given insertion or removal, respectively, N_c is the current number of cosolute molecules before the insertion or removal attempts, ρ_c^{bulk} is the cosolute concentration (in mole m^{-3}) in the reservoir (bulk) and γ is the mean activity coefficient, which was estimated from the Carnahan–Starling expression for hardspheres:[53]

$$\ln \gamma = \frac{\phi_c^{bulk}\left(8 - 9\phi_c^{bulk} + 3\phi_c^{bulk^2}\right)}{\left(1 - \phi_c^{bulk}\right)^3} \qquad (4.20)$$

where ϕ_c^{bulk} is the volume fraction of the cosolute in the reservoir. The solvent both in the gel and the solute reservoir was modelled as a continuum at room temperature (T= 298 K).

4.4. Results and discussion

In order to investigate the interplay between steric exclusion and hydrophobic adhesion, the details of the polymer network and the cosolute particle must be specified. In this work, the neutral hydrogel is modeled by a tetrafunctional cross-linked network, considering a total number of monomers per chain given by $\nu = 20$. The radius of all monomeric units and cross-linkers is $R_m = 0.4$ nm. The cosolute–monomer pair interaction is controlled by three additional parameters (see eqn (4.5)), namely the cosolute radius, the depth and the range of the attractive well (R_c, ε and Δ, respectively). Here, we intend to provide a general description of the equilibrium partitioning of spherical cosolutes, featuring a large variety of substances. For this purpose, the values of these three

parameters are varied to cover the typical hydrophobic interaction of cosolutes sizes involved in the applications. In particular, the cosolute radius is varied from $R_c = 0.2$–0.8 nm. This range of sizes comprises the radii of many hydrophobic drugs involved in different therapeutic treatments, such as hydrocortisone, budesonide, dexamethasone, paclitaxel, tamoxifen or β-lapachone,[14,17,54,55] and chemical reactants in catalytic reactions, such as nitrobenzene or 4-nitrophenol.[19] Analogously, in order to cover different degrees of hydrophobicity, the attraction strength goes from $\varepsilon = 0$ (no attraction) to $4k_BT$ (strong attraction), and the range of the attraction varies from $\Delta = 0.05$ nm to $\Delta = 0.2$ nm. The bulk concentration of cosolute is $\rho_c^{bulk} = 10$ mM ≈ 0.006 part per nm^3, which is sufficiently small to neglect the cosolute–cosolute interactions.

4.4.1. Dependence of K_0 with the attraction strength, ε. Role of the multiple attractive bonds

For each combination of the interaction parameters, the partition coefficient as a function of the polymer packing fraction of the microgel was explored. Figure 4.2 (a) and (b) show $K_0(\phi_m)$ for different values of ε, fixing $R_c = 0.4$ nm and $\Delta = 0.05$nm. As expected, for $\varepsilon = 0$, the cosolute partitioning is completely controlled by the volume exclusion exerted by the polymer chains. When ϕ_m increases, the average size of the pores between polymer chains, l, decreases as $l \sim \phi_m^{-1/3}$, which precludes the cosolute particles from diffusing inside the microgel. This leads to a monotonous decrease of K_0 from 1 to 0 as ϕ_m increases.

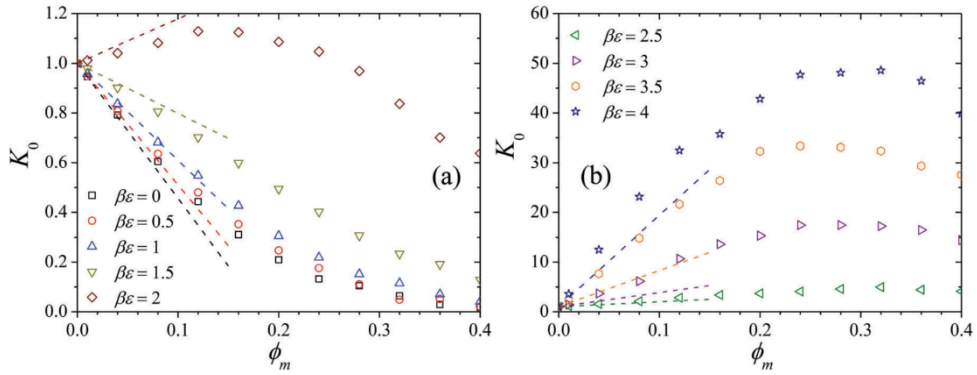

Figure 4.2: Cosolute partition coefficient as a function of the polymer packing fraction inside the hydrogel. Open symbols are the simulation data for different values of the attractive well ε, for a fixed cosolute radius $R_c = R_m = 0.4$ nm and fixed attraction range, $\Delta = 0.05$ nm. Straight dashed lines show the linear theoretical predictions obtained from eqn (4.6) – (4.10) for small ϕ_m. The data are split in two graphs, (a) and (b), in order to give a clear representation of the complete set of results.

A progressive increase of the attraction strength, ε, partially reduces the steric repulsion effect. For small attractions, the cosolute particle is more likely to bind to one or more polymer chains, increasing the value of K_0. Under these conditions of weak binding, the volume exclusion is still dominating the partitioning, so K_0 again decreases monotonically to zero. However, if the attraction strength is large enough, the cosolute binding becomes so important that is able to completely compensate the steric exclusion, inducing an increase of K_0 with ϕ_m. Technically, the reason for this absorption enhancement is due to the fact that increasing the polymer packing fraction also implies a relative increase of the volume of the attraction layer around the polymer chains. This absorption enhancement is not sustained in the limit of large ϕ_m, and eventually volume exclusion becomes again more relevant. As a result of the competition between these two effects, the partition coefficient exhibits a maximum at certain intermediate polymer packing fractions. We find this result really interesting, as it shows that it is possible to find particular conditions to maximize the uploading of certain macromolecule inside the hydrogel. A similar non-monotonic behavior has been observed for charged cosolutes inside oppositely charged polymer gels.[22] In this case, however, the origin of the monomer–cosolute attraction is not hydrophobic, but electrostatic.

It is important to remark that the height of the maximum grows with the attraction strength in a non-linear fashion, leading to values K_0 of about 50 for $\varepsilon = 4k_BT$. This huge effect is a direct consequence of multiple cosolute binding to three or more monomeric units, which occurs when the polymer chains deform to wrap around the cosolute particle. This many-body effect is expected to become very significant in shrunken hydrogels. Recent simulation and theoretical results performed in Lennard-Jones cosolutes clearly show that for strong cosolute coupling, the polymer network in the collapsed state also embeds the attracted cosolutes.[56] Only for very large polymer volume fraction $\phi_m \gtrsim 0.3$ the steric repulsion is able to hinder the cosolute penetration.

In order to quantify this multiple binding effect, other batch of simulations were performed, but in this case restricting the cosolute attraction to the closest monomer of the network. The data for the partition coefficient for this idealistic situation are shown in Figure 4.3. As observed, neglecting the multiple bonds causes huge changes in K_0. Indeed, the maximum observed for large ε decreases by one order of magnitude (or even disappears for the case of moderate attractions) and shifts towards smaller values of ϕ_m. This behavior is a signature of the important reduction of the overall attraction that arises from neglecting the many-body coupling. It is interesting to note that the multiple bonds play an important role not only for shrunken hydrogels, but also for swollen, as it systematically reduces the slope of K_0 for small ϕ_m since the binding of the cosolute to two inter-connected monomers is not taken into account (region C in Figure 4.7 of Appendix A).

The behavior reported in the simulations is captured by our theoretical models. Eqn (4.6) – (4.10) were used for predicting the small-ϕ_m linear behavior of K_0 in the general case, and eqn (4.11) for the simplified model in which the cosolute exclusively interacts with the closest monomer. The results are plotted as dashed straight lines in Figure 4.2 (a), (b) and 4.3. In all cases, the agreement is excellent, as the theory provides qualitative and quantitative accordance with the simulation results in the regime of swollen hydrogels. Conversely, the model based on the virial thermodynamic approach given by eqn (4.12) leads to wrong predictions for the slope (not shown), since it systematically overestimates the exclusion and binding volumes of the interconnected monomers. This result clearly indicates that the geometrical details of the cross-linked polymer network are very important for attractive cosolutes, even in the limit of swollen hydrogel conformations.

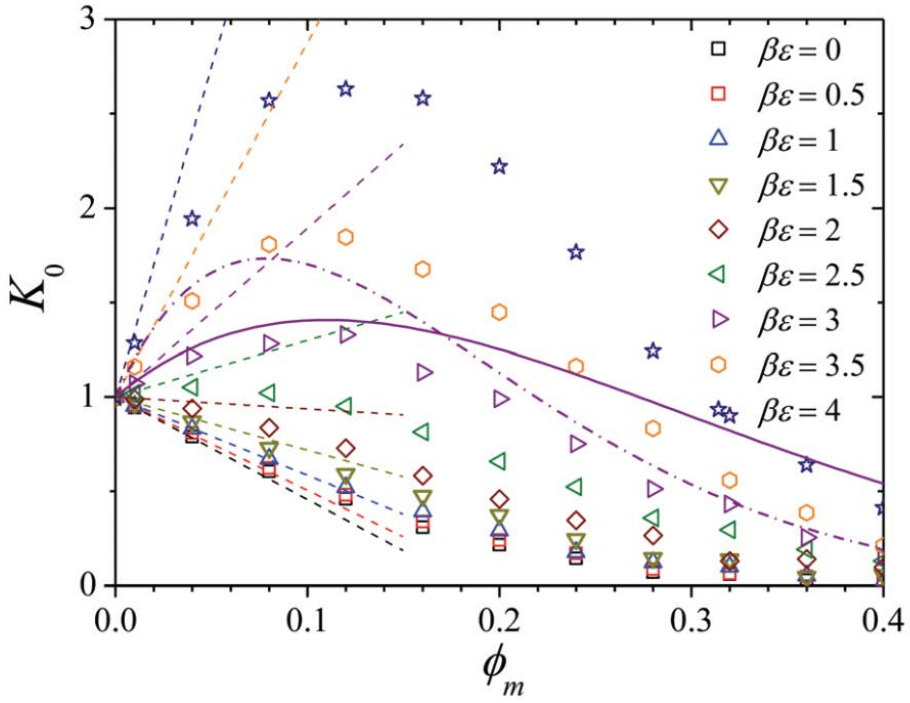

Figure 4.3: $K_0(\phi_m)$ calculated considering that the cosolute particle only interacts with the closest monomer, for $R_c = 0.4$ nm and $\Delta = 0.05$ nm. Open symbols depict the simulation results. Straight dashed lines show the linear small-ϕ theoretical prediction deduced from eqn (4.6) - (4.11). Solid and dashed-dotted lines correspond to the theoretical predictions assuming that the polymer network are made of random overlapping cylinders eqn (4.13) or random overlapping spheres eqn (4.14), respectively.

For non-diluted polymer networks, we tried to reproduce the overall curve approximating the network structure by an assembly of random located (and oriented) cylindrical chains (see eqn (4.13)) or by an assembly of random spherical monomers (eqn (4.14)). As an example, two curves for $\varepsilon = 3k_BT$ are plotted as solid and dashed-dotted lines in Figure 4.3, corresponding to both models. Both theories gather the required ingredients to give a qualitative justification of the maximum of $K_0(\phi_m)$. The model of random rods gives a better representation for swollen hydrogels, where the polymer chains are extended, whereas the model of random spheres becomes more accurate for large polymer packing fractions. However, these models completely neglect the effect of the multiple bonds, and so lead to a severe underestimate of the

location and height of the peak, when comparing with the simulation data shown in Figure 4.2 (a) and (b).

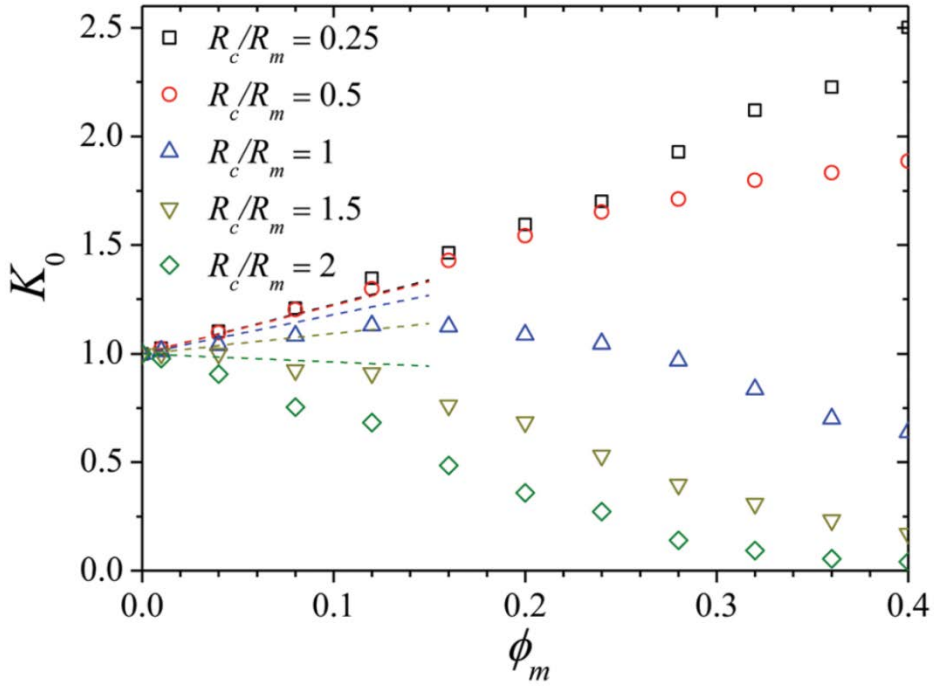

Figure 4.4: $K_0(\phi_m)$as a function of the cosolute radius, R_c, for fixed values of $\varepsilon = 2k_BT$ and $\Delta = 0.05$ nm. Open symbols represent the simulation results, and dashed lines the theoretical predictions for small ϕ_m.

4.4.2. Dependence of K_0 with the cosolute size and the range of the hydrophobic attraction (R_c and Δ)

The dependence of the partition coefficient with the cosolute size is shown in Figure 4.4 for $\varepsilon = 2k_BT$ and Δ = 0.05 nm. As expected, increasing the particle size while keeping constant the attraction always intensifies the volume exclusion effect. As a consequence, the maximum of K_0 diminishes and shifts towards smaller polymer volume fractions. If the cosolute diameter is large enough, the steric repulsion completely suppresses the peak, leading to a monotonic decay of $K_0(\phi_m)$. The theoretical predictions given by eqn (4.6) – (4.10) also reproduce the simulation data, at least for the studied cosolutes sizes. The opposite trend is found if the dependence of K_0 with the range of the attraction

Δ is examined. An example of this is shown in Figure 4.5 for $\varepsilon = 2k_BT$ and $R_c = 0.4$ nm. Indeed, increasing Δ augments the thickness of the binding region around the monomers. In addition, the overlap between the binding regions of neighboring chains also emphasizes the appearance of regions where the cosolute is attracted simultaneously to more than two monomers. The combination of both effects yields a substantial growth of the peak height. For large values of Δ, the theoretical model underestimates the values of K_0 since these many-body attractions are not totally accounted in eqn (4.6) – (4.10), even in the case of swollen states of the hydrogel.

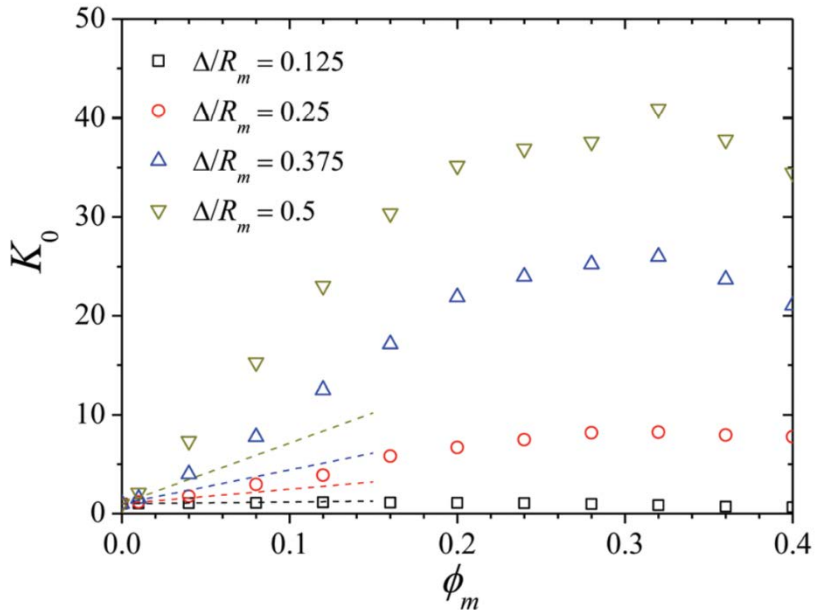

Figure 4.5: $K_0(\phi_m)$ as a function of the attraction range, Δ, for fixed values of $\varepsilon = 2k_BT$ and $R_c = 0.4$. Open symbols represent the simulation results, and dashed lines the theoretical predictions for small ϕ_m.

4.4.3. Searching for the condition of maximum

As mentioned above, the existence of a peak in the partition coefficient entails the possibility of designing a hydrogel that, for a given hydrophobic cosolute and solvent conditions, maximizes the cosolute uploading. Therefore, it would be interesting to find out the particular parameters of the cosolute-monomer interaction at which the hydrophobic attraction is strong enough to produce such a peak in K_0. For this purpose, additional MC simulations were performed to carefully search for these conditions.

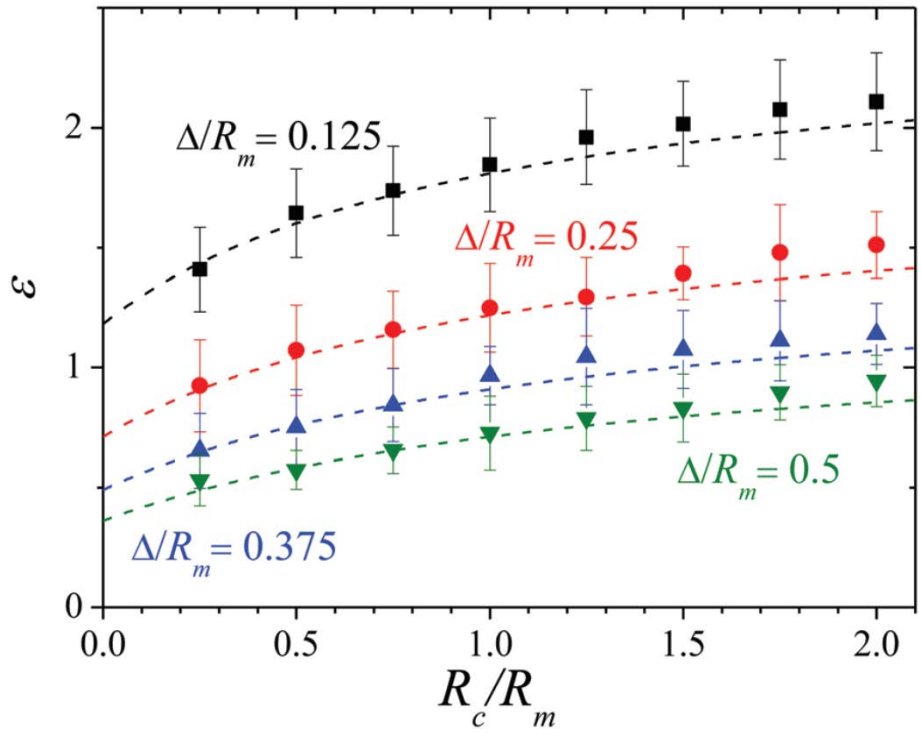

Figure 4.6: Onset of maximum formation in $K_0(\phi_m)$. Symbols depict the simulation data, and solid lines the theoretical predictions obtained with eqn (4.15).The error bars show an estimate of the fluctuations of the simulation data.

Figure 4.6 shows (in symbols) the simulation data that establishes the onset of the maximum of K_0, represented in a $\varepsilon - R_c$ diagram. The graph depicts results for several values of Δ. For points below this line, the cosolute is precluded by the steric repulsion. For points above it, the hydrophobic attraction is strong enough to induce a maximum of the partition coefficient. As expected, the attraction strength required to overcome the steric exclusion grows with the cosolute size. It is interesting to point out that, even for a point-like cosolute ($R_c = 0$), it still experiences a non-negligible volume exclusion that must be overcome to generate the maximum. Analogously, an increase of the attraction range, Δ, shifts the whole curve to smaller values of ε. The simulation results are totally corroborated by the theoretical prediction obtained from eqn (4.15), shown as solid lines. This means that, although the theory cannot provide a quantitative description of the maximum, at least itis able to predict the onset of maximum formation, in terms of the details of the cosolute–monomer

interaction. Hence, eqn (4.15) can be regarded as a simple prescription to guarantee the existence of a maximum in K_0.

4.5. Conclusions

In summary, the absorption of diluted spherical cosolutes (which could represent therapeutic drugs, reactants, globular proteins and other biomacromolecules) inside a neutral hydro-gel is studied for different swelling states. We specially focused on the interplay between the excluded-volume repulsion exerted by the polymer chains inside the hydrogel and the solvent-induced hydrophobic attraction between the cosolute particle and the monomeric units. For this purpose, MC coarse-grained simulations were performed, assuming that the cosolute-monomer interaction is given by a square well pair potential, and achieving a wide analysis in terms of different meaningful parameters, namely the cosolute radius (R_c), the depth (ε) and range (Δ) of the attraction. In spite of the simplicity of this model, it gathers the more important elements to fairly represent more realistic short-range hydrophobic attractions.

Two well-defined regimes were found depending on the value of the attraction strength. For small attractions, the steric exclusion dominates and the partition coefficient decreases monotonically with the polymer volume fraction. However, for sufficiently large hydrophobic attractions, a maximum of the partition coefficient is reached at some intermediate polymer volume fraction, which arises as a consequence of the competition between steric exclusion and hydrophobic adhesion. The location and height of the peak increase with ε and Δ, but decrease with R_c as a result of the enhancement of the volume exclusion effect. The existence of this peak in the partitioning shows that, for some specific hydrophobic cosolute, the uploading can be maximized by adjusting the swelling state, the internal morphology of the hydrogel (for instance, modifying the cross-linker density) or the nature of the polymer chains.

The results indicate that the formation of many attractive bonds between the cosolute particle and multiple monomers of the polymer network plays a very important role in determining the partitioning. The existence of these multiple attractions strongly intensifies the cosolute uptake for moderate and large polymer packing fractions. This many-body effect was quantified to show that this enhancement is also present even in the limit of small polymer concentrations (swollen hydrogels), due to the binding of the cosolute to two interconnected monomers within the same chain.

The simulation results agreed with a theoretical model based on the calculation of the volumes of the excluded and attractive regions around the polymer chains. Very good quantitative agreement between theory and simulations in the regime of swollen hydrogels was achieved. The particular choice of cosolute–monomer pair interaction potential becomes very convenient under a practical point of view, as it allows us to deduce useful analytical expressions for the partition coefficient. The theoretical predictions clearly indicate that the geometrical aspects of the cross-linked polymer network are important, even in the regime of swollen hydrogels. Moreover, the theory is able to provide the conditions that establish the onset of formation of the maximum for a hydrophobic cosolute.

An interesting extension of this work would be the study of the influence of the network topology, such as chain poly-dispersity.[57–59] According to Edgecombe and Linse,[57] as the network is made polydisperse, the microgel volume decreases, with the short chains being more stretched and the long ones less stretched as compared to a monodisperse chain length distribution. Based on this, we expect that the leading contribution of considering chain polydispersity is that swollen microgels have a lower volume, and so a corrected packing fraction ϕ_m larger than the corresponding one for monodisperse chains. In the limit of very low packing fractions (swollen hydrogel), the cosolute only interacts with the closest chain in the network and the effect of the chain polydispersity should be described by simply applying eqn (4.6) with the corrected volume fraction ϕ_m. However, for shrunken hydrogels, the chain polydispersity may have more complex effects, such as shifting and broadening/narrowing of the peak of K_0. Definitely, a more profound study of the role of chain polydispersity will be worth in future works. Another improvement of this study will also entail the investigation of cosolute partitioning in concentrated suspensions inside finite-size microgel particles. In this case, hydrophobic adhesion will enhance the internal absorption, whereas volume exclusion will promote the surface adsorption of cosolutes. In turn, the adsorbed particles may form an external layer that acts as a steric shield for further absorption.

Another interesting direction is to extend previous studies onion partitioning and microgel swelling to investigate the permeation of charged hydrophobic cosolutes inside charged hydrogels in salty suspensions.[60–69] In addition to steric and hydrophobic forces, electrostatic interactions become a very relevant contribution that completely modifies the cosolute absorption. In this regard, the partitioning not only depends on the cosolute charge, but also on how

this charged is distributed. For instance, the charged distribution of a protein is usually non-homogeneous, giving rise to an electric dipole that tends to orientate along the external field generated by the microgel. Recent studies show that the potential of mean force between the charged cosolute and the microgel can be phenomenologically separated into five different additional contributions: monopolar, dipolar, Born solvation free energy, counterion release, and osmotic.[36,70] It is important to remark here that the dipolar, Born and counterion release contributions are attractive even for like-charged hydrogels. Moreover, the theoretical predictions for this kind of systems clearly show that the combination of these attractions can be strong enough to compensate the monopolar repulsion, giving rise to a cosolute absorption even for like-charged hydrogels. All this phenomenology is very important on determining not only the equilibrium partitioning, but also the absorption and release kinetics in real applications. Therefore, the characterization of the physics behind it can help in the design of new stimuli-responsive functionalized nanomaterials.

Conflicts of interest

There are no conflicts to declare.

Appendix A: calculation of K_0 in terms of the excluded and binding volumes

In this section, the volume of the excluded and binding regions mentioned in the theory are calculated for swollen hydrogels. The network is assumed to be formed through N_{cross} tetra-functional cross-linkers, having N_{chains} chains, with ν interconnected monomers per chain. As shown in the theoretical section of this paper, the ratio between the number of bonds and the total number of monomers for this particular morphology is

$$\frac{N_{bonds}}{N_m} = \frac{2(\nu+1)}{2\nu+1} \tag{A.1}$$

The packing fraction of monomers is

$$\phi_m = \frac{4\pi}{3}\frac{N_m}{V}R_m^3 \rightarrow V = \frac{4\pi N_m R_m^3}{3\phi_m} \tag{A.2}$$

We further assume that the connected monomers inside a polymer chain are in close contact, so the distance between them is $r = 2R_m$, which is indeed a good approximation.

The position of the centers of the *N* monomeric units are specified by their coordinates $\{\overrightarrow{r_1}, \overrightarrow{r_2}, \ldots \overrightarrow{r_N}\} \equiv \{\vec{r}_i\}$. The total volume inside the hydrogel volume can be classified into four different regions. A schematic representation of the interconnected monomer units inside the network is shown in Figure 1.7. Accordingly, region A is defined as the points where the distance of the cosolute center to any monomer center is smaller than $R_{exc} = R_m + R_c$

$$A = \{\vec{r} \in V / |\vec{r} - \vec{r}_i| \leq R_{exc}\} \tag{A.3}$$

and so it corresponds to the volume of cosolute exclusion. Analogously, region B is the zone where the distance to any monomer is smaller that $R_{bind} = R_m + R_c + \Delta$

$$B = \{\vec{r} \in V / |\vec{r} - \vec{r}_i| \leq R_{bind}\} \tag{A.4}$$

Clearly, region (*B*–*A*) represents the volume where the cosolute–monomer is attractive. However, due to the proximity of the interconnected monomers, there is a belt (identified by region C) where the cosolute is attracted at the same time to a couple of monomers, with an energy of interaction of -2ε. Region C represents a 3-body cosolute–monomer–monomer correlation. In a similar way, new zones with four or higher overlaps of attractive regions can be identified, giving rise to binding energies of -3ε, -4ε and so on. However, these four and higher body contributions can be neglected for extended chains.

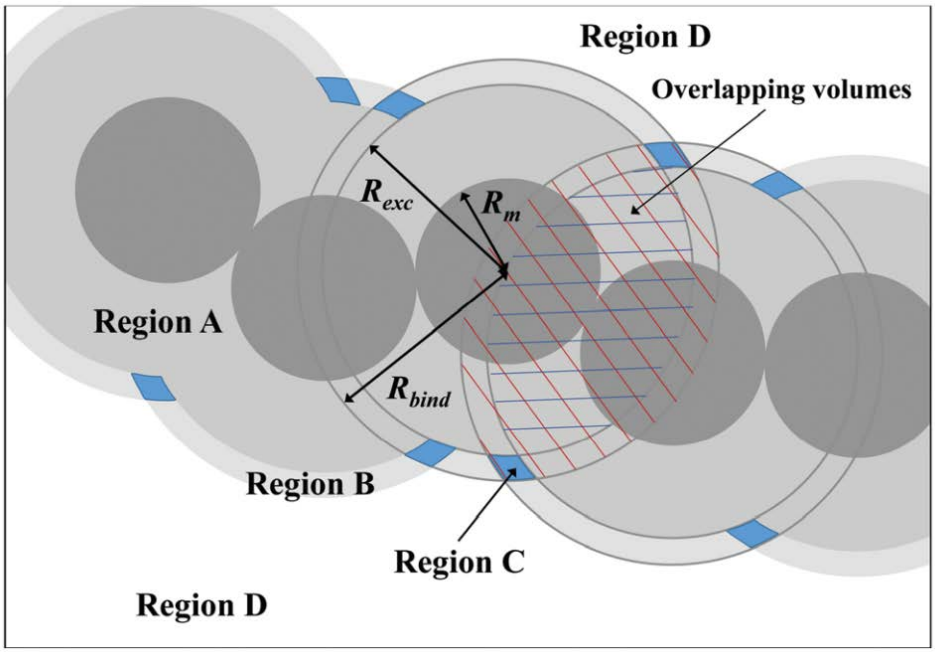

Figure 4.7: Schematic bidimensional illustration of a single chain formed by interconnected monomers. The picture depicts the four different regions (A–D) described in Appendix A. The dark blue and right hatched zones show, respectively, the overlapping volume between the excluded and attractive regions of two connected monomers.

Finally, region D corresponds to the points where the interaction with any monomer is zero

$$D = \{\vec{r} \in V / |\vec{r} - \vec{r}_i| \geq R_{bind}\} \tag{A.5}$$

Due to the simplicity of the monomer–cosolute pair potential, the partition coefficient is obtained in terms of the volume fraction of these four regions. If V_A, V_B, V_C and V_D are their volumes, and $\phi_i = V_i/V$ their volume fractions, the partition coefficient is

$$\begin{aligned} K_0 &= \frac{1}{V}(V_D + e^{\beta\varepsilon}(V_B - V_A - V_C) + e^{2\beta\varepsilon}V_C) \\ &= 1 - \phi_B + e^{\beta\varepsilon}(\phi_B - \phi_A - \phi_C) + e^{2\beta\varepsilon}\phi_C \end{aligned} \tag{A.6}$$

where we used that $V_D = 1 - V_B$.

To calculate the volume of the regions correctly, special care must be taken of removing the mutual overlapping regions between two interconnected monomers (see Figure 4.7). In general, the overlapping volume between two spheres of radius R_1 and R_2, with a center-to-center distance given by *r,* is given by

$$V'(r;R_1,R_2) = \frac{\pi(R_1+R_2-r)^2}{12r} \times [r^2 + 2r(R_1+R_2) + 6R_1R_2 - 3(R_1^2+R_2^2)] \quad \text{(A.7)}$$

for $|R_1 - R_2| \leq r \leq R_1 + R_2$. The volume of region A is obtained adding the contribution of the volume N_m spheres of radius $R_{exc} = R_m + R_c$ and then, subtracting the overlapping volumes of the N_{bonds} between them,

$$V_A = N_m \frac{4}{3}\pi R_{exc}^3 - N_{bonds}V'(2R_m; R_{exc}, R_{exc}) \quad \text{(A.8)}$$

It is convenient to define the dimensionless distances $\lambda_{exc} = R_{exc}/R_m$, so

$$V_A = R_m^3(N_m \frac{4}{3}\pi\lambda_{exc}^3 - N_{bonds}V'(2;\lambda_{exc},\lambda_{exc}) \quad \text{(A.9)}$$

The volume fraction of region A, $\phi_A = V_A/V$, is obtained using eqn (A.1), (A.2) and (A.9), which leads to

$$\phi_A = \left[\lambda_{exc}^3 - \frac{3}{4\pi}\frac{2(\nu+1)}{2\nu+1}V'(2;\lambda_{exc},\lambda_{exc})\right]\phi_m = \left[\lambda_{exc}^3 - \frac{(\nu+1)}{2\nu+1}(1-\lambda_{exc})^2(1+2\lambda_{exc})\right]\phi_m \quad \text{(A.10)}$$

Proceeding in a similar way, the volume fraction of region B is

$$\phi_B = \left[\lambda_{bind}^3 - \frac{(\nu+1)}{2\nu+1}(1-\lambda_{bind})^2(1+2\lambda_{bind})\right]\phi_m \quad \text{(A.11)}$$

where $\lambda_{bind} = R_{bind}/R_m$. Finally, the volume of region C can be written in terms off our overlapping volumes (see again Figure 4.7), so

$$\phi_C = \frac{3}{2\pi}\frac{(\nu+1)}{2\nu+1}[V'(2;\lambda_{bind},\lambda_{bind}) - 2V'(2;\lambda_{bind},\lambda_{exc}) + V'(2;\lambda_{exc},\lambda_{exc})]\phi_m = \frac{3}{8}\frac{\nu+1}{2\nu+1}\left[\lambda_{bind}^2 - \lambda_{exc}^2\right]^2\phi_m \quad \text{(A.12)}$$

The substitution of eqn (A.10), (A.11) and (A.12) into eqn (A.6) finally leads to the explicit expression of K_0 shown in eqn (4.6) – (4.10).

Appendix B: virial approximation for K_0

Within the virial expansion, the free energy per volume $f = F/V$ of the system can be written as

$$f = f_{network}(\rho_m) + \rho_c[\ln(\rho_c\Lambda_c^3) - 1] + B_2^{mm}\rho_n^2 + 2B_2^{mc}\rho_m\rho_c + B_2^{cc}\rho_c^2 \quad \text{(B.1)}$$

where Λ_c is the thermal wave length of the cosolute, and B_2^{ij} are the corresponding second virial coefficient for the mutual interactions. The cosolute chemical potential is

$$\mu_c = \frac{\partial f}{\partial \rho_c} = \ln(\rho_c\Lambda_c^3) + 2B_2^{mc}\rho_m + 2B_2^{cc}\rho_c \quad \text{(B.2)}$$

The hydrogel is in contact with a bulk reservoir of cosolutes at a concentration ρ_c^{bulk} at a common temperature, with a chemical potential given by $\mu_{c,bulk} = \ln(\rho_c^{bulk}\Lambda_c^3) + 2B_2^{cc}\rho_c^{bulk}$. The equilibrium between both phases implies the equality of the chemical potential, $\mu_c = \mu_c^{bulk}$, which leads to

$$\rho_c = \rho_c^{bulk} e^{-2B_2^{mc}\rho_m - B_2^{cc}(\rho_c - \rho_c^{bulk})} \quad \text{(B.3)}$$

In the limit of swollen hydrogels (small ρ_m) and infinite dilution of cosolutes ($\rho_c^{bulk} \to 0$), K_0 is given by

$$K_0 = \lim_{\rho_c^{bulk}\to 0} \frac{\rho_c}{\rho_c^{bulk}} \approx 1 - 2B_2^{mc}\rho_m \quad \text{(B.4)}$$

Making use the analytical expression of the second virial coefficient for the square well potential (eqn (4.5)),

$$B_2^{mc} = \frac{2\pi}{3}\left[R_{exc}^3 - \left(R_{bind}^3 - R_{exc}^3\right)\left(e^{\beta\varepsilon} - 1\right)\right], \quad \text{(B.5)}$$

the following expression for the partition coefficient is found

$$K_0 = 1 + \left[-\lambda_{bind}^3 + e^{\beta\varepsilon}\left(\lambda_{bind}^3 - \lambda_{exc}^3\right)\right]\phi_m \quad \text{(B.6)}$$

Acknowledgements

The authors thank the Spanish "Ministerio de Economía y Competitividad (MINECO), Plan Nacional de Investigación, Desarrollo e Innovación Tecnológica (I + D + i)" (Projects FIS2016-80087-C2-1-P, FIS2016-80087-C2-2-P) and the European Regional Development Fund (ERDF). Finally, the computer resources provided by PROTEUS (Instituto Carlos I de Física Teórica y Computacional, University of Granada) are gratefully acknowledged.

References

1 A. Fernández-Nieves, H. M. Wyss, J. Mattsson and D. A. Weitz, Microgel Suspensions: Fundamentals and Applications, Wiley-VCH, Weinheim, 2011.

2 M. J. Murray and M. Snowden, Adv. Colloid Interface Sci., 1995, 54, 73–91.

3 B. R. Saunders and B. Vincent, Adv. Colloid Interface Sci., 1999, 80, 1–25.

4 J. Ramos, A. Imaz, J. Callejas-Fernández, L. Barbosa-Barros, J. Estelrich, M. Quesada-Pérez and J. Forcada, Soft Matter, 2011, 7, 5067–5082.

5 G. Eichenbaum, P. Kiser, S. Simon and D. Needham, Macromolecules, 1998, 31, 5084–5093.

6 S. Frokjaer and D. E. Otzen, Nat. Rev. Drug Discovery, 2005, 4, 298–306.

7 M. Malmsten, Soft Matter, 2006, 2, 760–769.

8 S. V. Ghugare, P. Mozetic and G. Paradossi, Biomacromolecules, 2009, 10, 1589–1596.

9 S. V. Vinogradov, Nanomedicine, 2010, 5, 165–168.

10 K. H. Bae, L.-S. Wang and M. Kurisawa, J. Mater. Chem. B, 2013, 1, 5371–5388.

11 H. D. Williams, N. L. Trevaskis, S. A. Charman, R. M. Shanker, W. N. Charman, C. W. Pouton and C. J. Porter, Pharmacol. Rev., 2013, 65, 315–499.

12 G. Edwards and S. Krishna, Eur. J. Clin. Microbiol. Infect. Dis., 2004, 23, 233–242.

13 S. W. Kim, Y. H. Bae and T. Okano, Pharm. Res., 1992, 9, 283–290.

14 C. K. Kim, P. Ghosch, C. Paglioca, Z. J. Zhu, S. Menichetti and V. M. Rotello, J. Am. Chem. Soc., 2009, 131, 1360–1361.

15 S. Kennedy, J. Hu, C. Kearney, H. Skaat, L. Gu, M. Gentili, H. Vandenburgh and D. Mooney, Biomaterials, 2016, 75, 91–101.

16 S. C. Lesher-Pérez, T. Segura and C. Moraes, Integr. Biol., 2016, 8, 8–11.

17 R. Contreras-Cáceres, M. C. Leiva, R. Ortiz, A. Daz, G. Perazzoli, M. A. Casado-Rodríguez, C. Melguizo, J. M. Baeyens, J. M. López-Romero and J. Prados, Nano Res., 2017, 10, 856–875.

18 V. Lapeyre, I. Gosse, S. Chevreux and V. Ravaine, Biomacromolecules, 2006, 7, 3356–3363.
19 S. Wu, J. Dzubiella, J. Kaiser, M. Drechsler, X. Guo, M. Ballauff and Y. Lu, Angew. Chem., Int. Ed., 2012, 51, 2229–2233.
20 S. Angioletti-Uberti, Y. Lu, M. Ballauff and J. Dzubiella, J. Phys. Chem. C, 2015, 119, 15723–15730.
21 R. Roa, W. K. Kim, M. Kanduc, J. Dzubiella and S. Angioletti-Uberti, ACS Catal., 2017, 7, 5604–5611.
22 E. M. Johnson and W. M. Deen, J. Colloid Interface Sci., 1996, 178, 749–756.
23 M. J. Lazzara, D. Blankschtein and W. M. Deen, J. Colloid Interface Sci., 2000, 226, 112–122.
24 A. Moncho-Jordá and I. Adroher-Benítez, Soft Matter, 2014, 10, 5810–5823.
25 E. Calo´ and V. V. Khutoryanskiy, Eur. Polym. J., 2015, 65, 252–267.
26 A. Villa, N. F. A. van der Vegt and C. Peter, Phys. Chem. Chem. Phys., 2009, 11, 2068–2076.
27 E. Brini, C. R. Herbers, G. Deichmann and N. F. A. van der Vegt, Phys. Chem. Chem. Phys., 2012, 14, 11896–11903.
28 Q. Garrett, R. C. Chatelier, H. J. Griesser and B. K. Milthorpe, Biomaterials, 1998, 19, 2175–2186.
29 S. Lindman, I. Lynch, E. Thulin, H. Nilsson, K. A. Dawson and S. Linse, Nano Lett., 2007, 7, 914–920.
30 M. Kanduc, R. Chudoba, K. Palczynski, W. K. Kim, R. Roa and J. Dzubiella, Phys. Chem. Chem. Phys., 2017, 19, 5906–5916.
31 H. Kawaguchi, K. Fujimoto and Y. Mizuhara, Colloid Polym. Sci., 1992, 270, 53–57.
32 N. Shamim, H. Liang, K. Hidajat and M. S. Uddin, J. Colloid Interface Sci., 2008, 320, 15–21.
33 M. A. Cole, N. H. Voelcker, H. Thissen, R. G. Horn and H. J. Griesser, Soft Matter, 2010, 6, 2657–2667.
34 A. Halperin and M. Kroger, Macromolecules, 2011, 44, 6986–7005.
35 V. Grabstain and H. Bianco-Peled, Biotechnol. Prog., 2003, 19, 1728–1733.
36 I. Adroher-Benítez, A. Moncho-Jordá and J. Dzubiella, Langmuir, 2017, 33, 4567–4577.
37 C. Yigit, N. Welsch, M. Ballauff and J. Dzubiella, Langmuir, 2012, 28, 14373–14385.

38 T. Hoare and R. Pelton, Langmuir, 2008, 24, 1005–1012.

39 T. López-León, A. Alaïssari, J. L. Ortega-Vinuesa and D. Bastos-González, ChemPhysChem, 2007, 8, 148–156.

40 P. B. Punjabi, N. P. S. Chauhan, P. Juneja, N. K. Jangid and S. Kalal, Encycl. Biomed. Polym. Polym. Biomater., 2015, 4690–4700.

41 M. Sarkar, C. Li and G. J. Pielak, Biophys. Rev., 2013, 5, 187–194.

42 D. Mukherji, M. Wagner, M. D. Watson, S. Winzen, T. E. de Oliveira, C. M. Marques and K. Kremer, Soft Matter, 2016, 12, 7995–8003.

43 L. Sapir and D. Harries, Curr. Opin. Colloid Interface Sci., 2016, 22, 80–87.

44 D. Nayar, A. Folberth and N. F. A. van der Vegt, Phys. Chem. Chem. Phys., 2017, 19, 18156–18161.

45 A. G. Ogston, Trans. Faraday Soc., 1958, 54, 1754–1757.

46 J. C. Bosma and J. A. Wesselingh, J. Chromatogr. B. Biomed. Sci., 2000, 743, 169–180.

47 M. Quesada-Pérez, I. Adroher-Benítez and J. A. Maroto-Centeno, J. Chem. Phys., 2014, 140, 204901.

48 S. Schneider and P. Linse, J. Phys. Chem. B, 2003, 107, 8030–8040.

49 B. A. Mann, C. Holm and K. Kremer, J. Chem. Phys., 2005, 122, 154903.

50 M. Quesada-Pérez, J. G. Ibarra-Armenta and A. Martín-Molina, J. Chem. Phys., 2011, 135, 94109.

51 . Ahualli, A. Martín-Molina and M. Quesada-Pérez, Phys. Chem. Chem. Phys., 2014, 16, 25483–25491.

52 S. Lamperski, Mol. Simul., 2007, 33, 1193–1198.

53 N. F. Carnahan and K. E. Starling, J. Chem. Phys., 1969, 51, 635.

54 C. Wischke and S. P. Schwendeman, Int. J. Pharm., 2008, 364, 298–327.

55 T. J. Dursch, N. O. Taylor, D. E. Liu, R. Y. Wu, J. M. Prausnitz and C. J. Radke, Biomaterials, 2014, 35, 620–629.

56 W. K. Kim, A. Moncho-Jordá, R. Roa, M. Kanduc and J. Dzubiella, Macromolecules, 2017, 50, 6227–6237.

57 S. Edgecombe and P. Linse, Macromolecules, 2007, 40, 3868–3875.

58 L. G. Rizzi and Y. Levin, J. Chem. Phys., 2016, 144, 114903.

59 N. Gnan, L. Rovigatti, M. Bergman and E. Zaccarelli, Macromolecules, 2017, 50, 8777–8786.

60 A. Moncho-Jordá, J. A. Anta and J. Callejas-Fernández, J. Chem. Phys., 2013, 138, 134902.

61 A. Moncho-Jordá, J. Chem. Phys., 2013, 139, 064906.
62 T. Colla, C. N. Likos and Y. Levin, J. Chem. Phys., 2014, 141, 234902.
63 J. Heyda and J. Dzubiella, J. Phys. Chem. B, 2014, 118, 10979–10988.
64 I. Adroher-Benítez, S. Ahualli, A. Martín-Molina, M. Quesada-Pérez and A. Moncho-Jordá, Macromolecules, 2015, 48, 4645–4656.
65 A. Moncho-Jordá and J. Dzubiella, Phys. Chem. Chem. Phys., 2016, 18, 5372–5385.
66 I. Adroher-Benítez, A. Martín-Molina, S. Ahualli, M. Quesada-Pérez and A. Moncho-Jordá, Phys. Chem. Chem. Phys., 2017, 19, 6838–6848.
67 O. Rud, T. Richter, O. Borisov, C. Holm and P. Kosovan, Soft Matter, 2017, 13, 3264–3274.
68 A. R. Denton, Phys. Rev. E: Stat., Nonlinear, Soft Matter Phys., 2003, 67, 011804; A. R. Denton, Phys. Rev. E: Stat., Nonlinear, Soft Matter Phys., 2003, 68, 049904.
69 D. Gottwald, C. N. Likos, G. Kahl and H. Löwen, J. Chem. Phys., 2005, 122, 074903.
70 C. Yigit, M. Kanduc, M. Ballauff and J. Dzubiella, Langmuir, 2017, 33, 417–427.

5. Paper II: Effect of dispersion forces on the behavior of thermosensitive nano-gels: A coarse-grained simulation study.

L. Pérez-Mas, A. Martín-Molina, R. Kumar Jain and M. Quesada-Pérez

The content of this chapter is published in: *Journal of Molecular Liquids*, **2019**, *288*, 111101.

https://doi.org/10.1016/j.molliq.2019.111101

5. Paper II *Journal of Molecular Liquids*, **2019**, *288*, 111101.

Abstract

The main goal of this work is to evaluate the effect of dispersion forces on different properties of nanogels, such as the size, the net charge and the surface electrostatic potential. This task was done by means of Monte Carlo coarse-grained simulations of nanogels in the presence of three different electrolytes. This model allows us to explicitly consider the dispersion interactions between ions inside the nanogel and the monomer units rather than interactions between the ions and the nanoparticle as a whole. Our simulations reveal that dispersion forces can be responsible for the charge inversion and the surface electrostatic potential inversion that cationic nanogels undergo in the presence of NaSCN. Moreover, these phenomena only take place if the bare charge of the nanogel is small enough. Our results also suggest that dispersions forces can induce a high capacity of permeation of some ions, such as thiocyanate, even into collapsed nanogels.

5.1. Introduction

Nanogels are nanometer-sized particles that consist of a crosslinked polymer network swollen by solvent, typically water. Nanogels with sizes of hundreds of nanometers are also known as microgels. The interest in microgels has grown rapidly over the past two decades because these soft nanoparticles can undergo a volume phase transition by external stimuli (e.g. temperature, pH, ionic strength). It is this responsiveness that makes nano- and microgels smart particles in different cutting-edge technologies, such drug delivery, catalyst media, nanoreactors, sensors, photonic crystals, and so on. [1–7]

In colloid science and biochemistry, there is a wide range of phenomena showing that ions with the same valence can induce different behaviors. Such phenomena, advisably reviewed by Ninham and coworkers,[8–14] also include electrokinetic experiments with microgels. In particular, López-León and coworkers reported that the electrophoretic mobility of poly(*N*-isopropylacrlyamide) (PNIPAM) particles strongly depends on the monovalent electrolyte employed.[15] These authors also reported a puzzling finding: a concentration of 0.01 M of NaSCN was sufficient to completely reverse the electrophoretic mobility of this kind of soft particles.

The standard models of electric double layer (EDL) fail to theoretically justify these ionic specific effects (also known as Hofmeister effects) since classical approaches describe ions only by their valence. However, Ninham,

coworkers and other authors made major progress suggesting that that ionic dispersion forces should be included in the EDL theory.[8,11,24–28,16–23] In this way, ion specificity arises naturally since such forces depend on the ionic polarizability, which differs for ions with the same valence. Following this idea, Tavares *et al.*[23] and Böstrom *et al.*[24] studied the effect of van der Waals interactions on the forces between hard colloids by means of computer simulations. Their results turned out to be qualitatively consistent with specific salt effects experimentally observed by numerous researchers, which supported the idea that dispersion forces played a key role in Hofmeister effects. Other authors have also developed different theories that consider polarizability to explain the behavior of the effective charge and zeta potential of oil droplets or interfacial tensions of different electrolyte solutions.[29–31]

Inspired by the simulations carried out by Tavares *et al.* and Boström *et al.* the effect of ionic dispersion forces on the EDL of hard colloids was assessed by means of Monte Carlo (MC) simulations. According to them, ionic van der Waals interactions contribute to the ion specificity of the electrokinetic properties of these colloidal particles, but their weight strongly depends on the ion size.[26,27] In addition, it should be stressed that dispersion forces could partially justify the inversion of electrophoretic mobility reported by López-León *et al.* for latex particles at high concentrations of NaSCN.[32]

Thus, it would be interesting to find out to what extent dispersion forces can also explain some ion specific phenomena with micro- or nanogels. However, we should keep in mind that there is a key feature that distinguishes these soft colloids from hard colloidal particles: their permeability. Ions can easily enter swollen microgels. On the other hand, a recent work has concluded that the polymer volume fraction of collapsed microgels is of the order of 0.44,[33] so there is room for small ions inside the polymer network even in the case of shrunken states. Consequently, realistic simulations of nanogels in the framework of the primitive model should explicitly consider interactions between ions and polymer chains (or their monomer units) rather than interactions between the ions and the whole particle, as done in the case of hard and impenetrable colloids. In this way, the possibility of ions inside the polymer network is also accounted for.

Accordingly, the main goal of this work is to evaluate the effect of ionic dispersion forces on the electric double layer of nanogels by means of MC coarse-grained simulations. Ions and monomer units forming the polymer network will be treated on the same footing. All-atom molecular dynamics simulations

have already been employed to gain insight into conformational transitions of PNIPAM chains induced by temperature.[34–36] The effect of different electrolytes has also been investigated through this computational technique.[37,38] However, these atomistic simulations are usually restricted to small assemblies of a few polymer chains. To simulate larger spatial and time scales coarse graining is preferred. This includes the case of a whole nanogel.[39–48] Thus coarse-grained simulations of a nanogel and its electric double layer are carried out here. In such simulations the inner crosslinked structure, the topology of the nanogel and monomer-ion interactions are explicitly considered.

The rest of the paper is organized as follows. First, the model and simulation technique are described. Then results are presented and discussed. Finally, some conclusions are highlighted.

5.2. Model and simulations

5.2.1. Model

In this work, MC simulations were performed within a coarse-grained model for polyelectrolytes known as the bead-spring model, in which the monomer units of the polymer chain and ions are considered spheres whereas the solvent is not explicitly considered and instead it is treated as a dielectric continuum (primitive model). An illustrative example of the versatility of the bead-spring model is its application in viral detection. Shin *et al.* computed the mechanical tension and the contraction that a virus exerts on single-stranded DNA.[49] Such a contraction might be macroscopically detected if DNA is incorporated in a hydrogel.

In our case, each chain of the nanogel is formed by a sequence of n_{bead} spherical monomer units (beads) connected by tetrafunctional crosslinkers (also modeled by beads of the same size). A total number of 8 monomers are linked to form a single chain (n_{bead}=8). The nanogel simulated here is made of 100 chains connected by 66 crosslinkers. 39.4% of them (the innermost ones) are really connected to four polyelectrolyte chains. 24.2% and 36.4% are linked to three and two chains, respectively. There are no crosslinkers connected to only one chain. In this survey, we have explored slightly ionized nanogels. The simulation cell also contains monovalent cations and monovalent anions (in a fixed number determined by the bulk electrolyte concentration, 10 mM) as well as the excess of monovalent anions required to have an electroneutral system.

As mentioned before, we have modeled chain beads, crosslinker molecules and ions (cations and anions) as spheres, whose diameters are σ_M, σ_{CL}, σ_C and σ_A, respectively. Monomer and crosslinker molecules were assumed to have the same size ($\sigma_M = \sigma_{CL} = 0.65$ nm).[50] However, different sizes were employed for the ions of the three salts studied here: NaSCN, $NaNO_3$ and NaCl. Table 5.1 shows the diameters of hydrated and bare ions corresponding to these electrolytes. Depending of their place in the lyotropic series, these ions have been considered hydrated or dehydrated. For instance, we have considered bare diameters for SCN^- and NO_3^- because these anions are extremely chaotropic.[51] In contrast, Cl^- and Na^+ are more kosmotropic than those two, so their hydrated diameters have been used instead.

Ion	Bare ion diameter (nm)	Hydrated ion diameter (nm)
Na^+	0.19	0.72
SCN^-	0.40	0.56
NO_3^-	0.528	0.68
Cl^-	0.362	0.66

Table 5.1: Ion diameters used in our simulations

5.2.2. Interactions

The short-range repulsion between any pair of particles due to excluded volume effects is modeled by means of the hard sphere potential:

$$u_{WCA}(r) = \begin{cases} \infty & r \leq \sigma \\ 0 & r > \sigma \end{cases} \tag{5.1}$$

where r is the center-to-center distance between a given pair of particles, and $\sigma = (\sigma_i + \sigma_j)/2$ is the average diameter of both particles. The interaction of all the charged species is given by the potential of Coulomb:

$$u_C(r) = Z_i Z_j e^2 / 4\pi\varepsilon_r\varepsilon_0 r \tag{5.2}$$

where Z_i is the valence of species i, e is the elementary charge, ε_r and ε_0 are the relative permittivity and vacuum permittivity of the solvent, respectively. Being interested in thermoresponsive nanogels, the temperature dependence of the dielectric permittivity was also considered:[52]

$$\varepsilon_r = \frac{5321}{T} + 233.76 - 0.9297T + 0.1417 \times 10^{-2}T^2 - 0.8292 \times 10^{-6}T^3 \tag{5.3}$$

The interaction connecting monomer units and crosslinkers with their neighbors was modeled by harmonic bonds,[53–55]

$$u_{bond}(r) = \frac{k_{bond}}{2}(r - r_0)^2 \quad (5.4)$$

where k_{bond} is the elastic constant (k_{bond}= 0.4 N/m) and r_0 (= 0.65 nm) is the equilibrium length corresponding to this harmonic potential. The interactions due to ion polarizability between an ion and any other particle were modeled by an ionic dispersion potential:

$$u_{disp}(r) = -B_{i/j}/r^6 \quad (5.5)$$

where $B_{i/j}$ is the parameter characterizing the dispersion interaction between species *i* and *j*. More information about this parameter is provided below.

It is well known that the thermoresponsive nature of nanogels is caused by the shift from enthalpy-ruled to entropy-ruled forces, where hydrogen bonds and water degrees of freedom play a fundamental role.[56] For the particular case of PNIPAM, this effect yields an increase of the attractive hydrophobic interaction between the monomeric units upon increasing the temperature.[57] This hydrophobic force was modeled through an interaction potential[50] ($u_h(r)$) that consists in a smooth approximation of the square-well potential (previously used by other authors) [58–60] whose depth increases with temperature. The same interaction potential was employed in previous simulations of thermoresponsive nanogels.[61,62] Therein the reader can find the details concerning this potential.

5.2.3. Dispersion constants

Given that the effect of dispersion forces is studied in our work, the values of the dispersion constants $B_{i/j}$ (where *i* and *j* refers to cations, anions and monomeric units) play a key role. According to the Lifshitz theory of van der Waals forces,[51,63] the constant between two species (i and j) can be calculated as:

$$\frac{B_{i/j}}{k_B T} = 3\frac{\alpha_i(0)\alpha_j(0)}{{\varepsilon_s}^2(0)} + 6\sum_{n=1}^{\infty}\frac{\alpha_i(\nu_n)\alpha_j(\nu_n)}{{\varepsilon_s}^2(\nu_n)} \quad (5.6)$$

where k_B is the Boltzmann constant, T is the absolute temperature, $\alpha_i(\nu)$ is the effective polarizability of ion i in water and at frequency ν, $\varepsilon_s(\nu)$ is the dielectric constant of the solvent at the same frequency, and $\nu_n = 2\pi k_B T n/h$, where h is Planck's constant and n an integer. As can be seen, this theory requires the

knowledge of effective polarizabilities and dielectric constants at different frequencies, which can be estimated from the harmonic oscillator model as:

$$\alpha(\nu) = \frac{\alpha(0)}{(1 + (\nu/\nu_I)^2)} \tag{5.7}$$

$$\varepsilon_s(\nu) = 1 + \frac{(\varepsilon_s(0) - 1)}{(1 + (\nu/\nu_I)^2)} \tag{5.8}$$

where ν_I is the characteristic frequency of the harmonic oscillator, also called in this context as ionization frequency. The values of $\alpha(0)$ and ν_I employed for Na^+, NO_3^- and Cl^- are those summarized by Tavares *et al.* [23] The polarizability and the characteristic frequency used for SCN^- (6.5Å^3 and 2.4 $\times 10^{15}$ Hz) are quite similar to those reported by Kunz *et al.* [20] Given that our model considers dispersion interactions between ions and monomers, the values of $\alpha(0)$ and ν_I for monomeric units of PNIPAM are also required. The polarizability of such monomeric units was estimated from the Clausius-Mossotti relationship (turning out to be 0.033 nm^3). A characteristic frequency of 8 $\times 10^{15}$ Hz was adopted for these constituents of the polyelectrolyte nanogel. According to Mahan *et al.*, ν_I typically ranges from 1.6 $\times 10^{15}$ to 8 $\times 10^{15}$ Hz. [64] The values of the dispersion constants obtained from Lifshitz theory of van der Waals forces under the previously mentioned assumptions are summarized in Table 5.2.

Electrolyte	$\frac{B_{\text{cation/cation}}}{k_BT}(nm^6)$	$\frac{B_{\text{anion/cation}}}{k_BT}(nm^6)$	$\frac{B_{\text{anion/anion}}}{k_BT}(nm^6)$	$\frac{B_{\text{cation/m}}}{k_BT}(nm^6)$	$\frac{B_{\text{cation/m}}}{k_BT}(nm^6)$
NaSCN	1.32×10^{-5}	2.01×10^{-4}	4.81×10^{-3}	2.86×10^{-3}	4.42×10^{-2}
$NaNO_3$	1.32×10^{-5}	7.68×10^{-5}	1.13×10^{-3}	2.86×10^{-3}	1.69×10^{-2}
NaCl	1.32×10^{-5}	6.61×10^{-5}	8.19×10^{-4}	2.86×10^{-3}	1.46×10^{-2}

Table 5.2: Dispersion constants used in our simulations for different electrolytes (subindex *m* refers to monomeric units).

5.2.4. Simulations

The conventional Metropolis algorithm was applied to a cubic box of length L and periodic boundary conditions. The volume, temperature and number of particles were kept constant. In theory, the box size would be established by the nanogel concentration, being infinite for isolated nanogel particles. In practice, however, this is not achievable because, in the presence of additional electrolyte, the number of particles in the simulation box would become

prohibitive. Thereby, the simulation box must be large enough to contain the nanogel particle and a significantly developed electric double layer around it. The L-values used in our simulations are (at least) one order of magnitude larger than the Debye length. When this is the case, a considerable portion of the solution bulk is included in the simulation box.[62] Figure 5.1 shows a snapshot of the simulation cell corresponding to NaSCN at 293 K. Long-range Coulomb forces were handled through Ewald sums, which were implemented with algorithms and recommendations similar to those reported in previous papers.[61,62] Although there are efficient simulation packages for coarse-grained models of soft matter, simulations were carried out using our own computer code (in C).

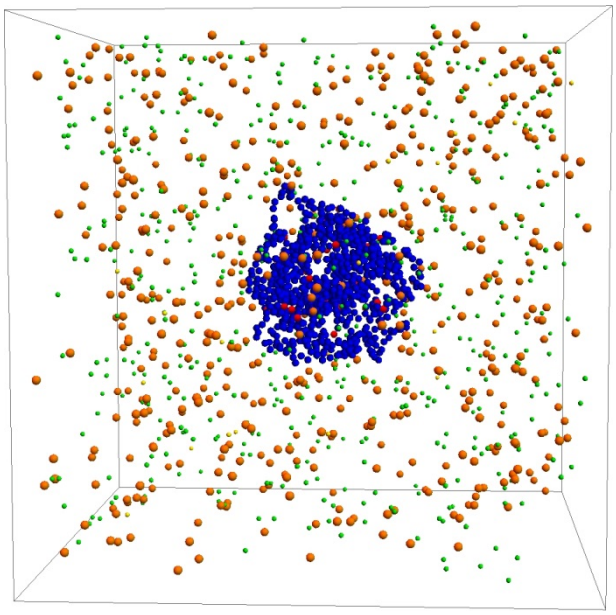

Figure 5.1: Snapshot of the simulation cell for NaSCN at 293 K. Blue and red beads represent neutral and charged monomers, respectively. Orange and green beads correspond to Na^+ and SCN^- ions, respectively.

At least 4×10^8 and 8×10^8 configurations were used for equilibration and statistics, respectively. The maximum displacements corresponding to ions and network beads were adjusted so that their respective acceptance ratios were close to 50%. To accelerate the equilibration, scaling moves of the network (in which the position of the particles are multiplied by a scaling factor α) were attempted during this process as well. The evolution of the radius of gyration of the nanogel, R_g, was monitored averaging this quantity in subsets

of 10^5 configurations to check that an equilibrium value was reached after equilibration. In addition, at least three repetitions of the simulations were done to give us an idea of its uncertainty. Simulations also provide the concentration of charged particles at a distance r from the center of mass (CM), $n_i(r)$, where i stands for charged beads and the different ionic species (excess counterions, cations and anions). From these ionic profiles, we computed the net charge and the surface electrostatic potential.

5.3. Results and discussion

Let us begin showing some results regarding the thermal response of the nanoparticles. First, we have simulated slightly charged cationic nanogels at seven different temperatures ranging from 293 to 323 K, for each electrolyte. One fifth of the chains carry only one ionized group with the positive elementary charge, $+e$ (degree of ionization: 0.025). For polymer chains or networks, our simulations can provide the so-called radius of gyration, which can also be determined from light scattering experiments. But, given that nanogels can be modeled as spheres in a first approximation, we rather employ the geometrical radius of such spheres (R_{ng}) to characterize their size. For a solid sphere, the relationship between its geometrical radius and its radius of gyration is:

$$R_{ng} = \sqrt{5/3}\, R_g \qquad (5.9)$$

Thus this expression was employed to compute the geometrical radius of the nanogel from its radius of gyration. An imaginary sphere of radius R_{ng} centered at the center of mass of the nanogel contains 90% of its monomers.[65]

5. Paper II *Journal of Molecular Liquids*, **2019**, *288*, 111101.

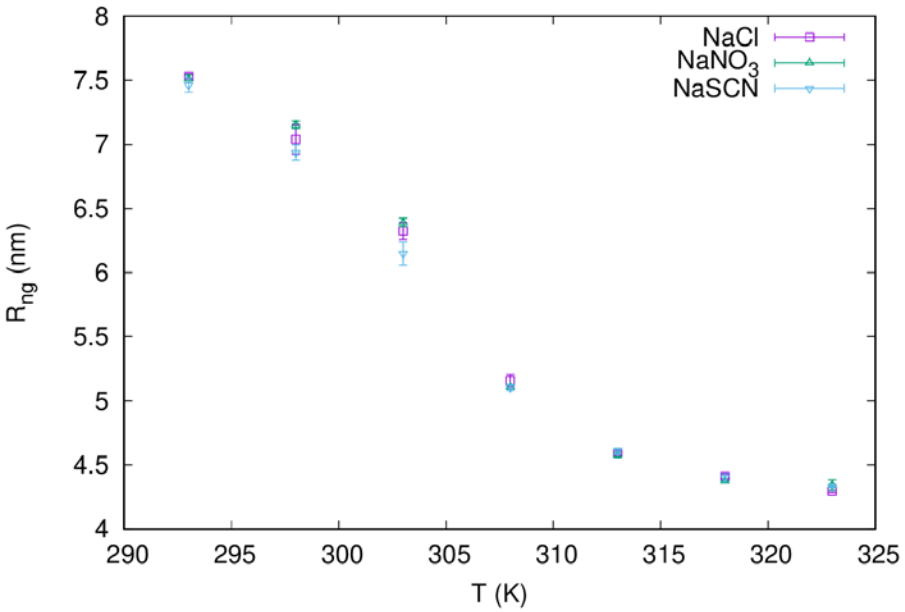

Figure 5.2: Effective radius of the nanogel (R_{ng}) as a function of temperature for different electrolytes: 10 mM NaCl (open square), 10 mM $NaNO_3$ (open up triangle), 10 mM NaSCN (open down triangle).

Figure 5.2 shows R_{ng} as a function of temperature in order to find out if the thermosensitive behavior is affected by the dispersion effects of the different salts at 10 mM. As can be seen, the nanogels go from a swollen state to a collapsed stated following a sigmoid function. The inflection point of this curve gives us the transition temperature (approximately 305 K, 33ºC), which is close to the Volume Phase Transition Temperature (VPTT) of PNIPAM. According to this figure, there are not significant differences among the three electrolytes studied. This result agrees with the behavior reported for cationic microgels with the same electrolytes at 10 mM.[15]

At this point let us turn our attention to the net charge of the nanogel. This charge includes the charge of the polymer backbone and the ions inside the nanogel (those whose distance to the CM is smaller than the radius of the nanogel). Figure 5.3 displays the net charge as a function of temperature for the three electrolytes commented previously.

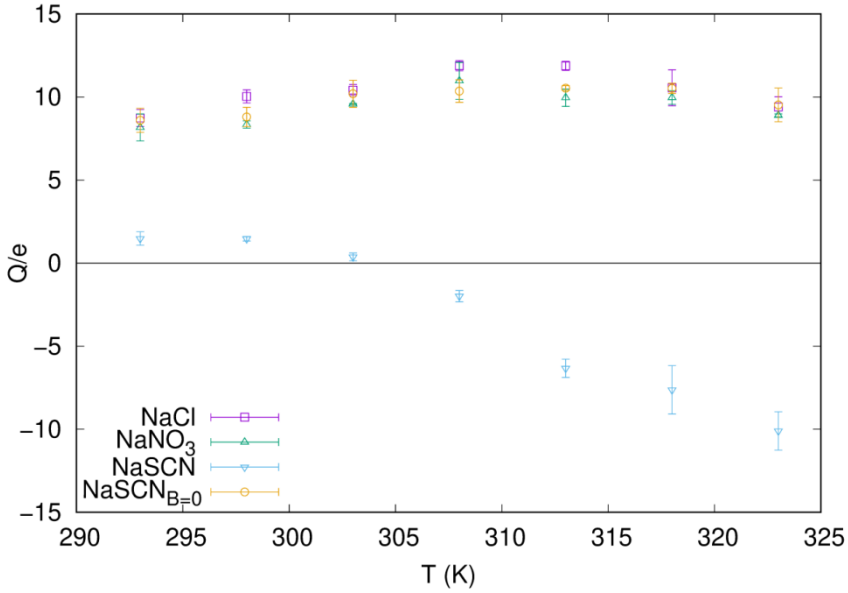

Figure 5.3: Net charge as a function of temperature for different electrolytes: 10 mM NaCl (open square), 10 mM $NaNO_3$ (open up triangle), 10 mM NaSCN (open down triangle). This figure also includes the net charge corresponding to 10 mM of NaSCN in the absence of dispersion forces (open circles).

This figure reveals two different behaviors. On the one hand, the net charges of the microgels in the presence of NaCl and $NaNO_3$ are positive and very similar (of the order of 10 elementary units in both cases). On the other hand, the net charge in the presence of NaSCN is close to zero below the VPTT and decreases above this temperature taking negatives values for a cationic nanogel. In other words, a charge reversal is observed for NaSCN. Figure 5.3 also includes the net charge corresponding to NaSCN without dispersion forces ($B_{i/j} = 0$). These values are almost identical to the net charges of NaCl and $NaNO_3$. Thus, we might conclude that dispersion forces have outstanding effects for NaSCN in the whole range of temperatures studied. In fact, they are responsible for the charge inversion found above 305 K. Although the results corresponding to NaCl and $NaNO_3$ in the absence of dispersion forces have not been shown, they are quite similar to those obtained with dispersion forces in Figure 5.1. As a consequence, dispersive effects are negligible for NaCl and $NaNO_3$.

It is also interesting to comment the behavior of the electrostatic potential at the surface of the nanogel (ψ_s). This property can provide us helpful information about the electrokinetic behaviour of these nanoparticles. Figure 2.4

shows the normalized electrostatic potential ($\Psi_s = e\psi_s/k_BT$) as a function of the temperature for the three previously shown electrolytes.

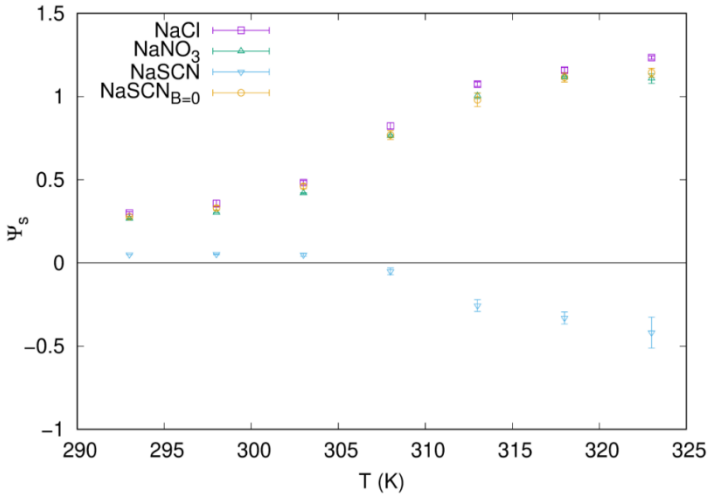

Figure 5.4: Normalized electrostatic potential as a function of temperature for different electrolytes: 10 mM NaCl (open square), 10 mM $NaNO_3$ (open up triangle), 10 mM NaSCN (open down triangle).). This figure also includes the normalized electrostatic potential corresponding to 10 mM NaSCN in the absence of dispersion forces (open circles).

Again, the behavior of electrostatic potential of NaSCN clearly differs from NaCl, $NaNO_3$ and NaSCN in the absence of dispersive forces. We might also conclude that dispersion forces induce a reversal in the electrostatic potential whereas their effects are unimportant for NaCl and $NaNO_3$. However, the behavior of the electrostatic potential and the net charge for NaCl and $NaNO_3$ are quite different. While ψ_s is small below the VPTT and grows following a sigmoid function above this temperature, the net charge in the presence of NaCl and $NaNO_3$ remains practically constant in the whole range of temperatures (Figure 5.3). This rise of ψ_s can be attributed to the reduction in size with temperature while the net charge remains constant. It is worth qualitatively comparing these results with the electrophoretic mobility (μ_e) data reported for a cationic microgel in the presence of 10 mM of the same electrolytes.[15] López-Leon *et al.* found that the magnitude of the electrophoretic mobility of cationic microgels grows near the VPTT describing a sigmoid function but exhibiting a reversal for NaSCN. These findings are in agreement with our results. According to these authors, SCN^- is a chaotropic anion that interacts with the hydrophobic moieties of PNIPAM chains enhancing their solubility and increasing

the lower critical solution temperature of the PNIPAM.[66] However, their μ_e-values for $NaNO_3$ and NaCl were quite different, which disagrees with ψ_s-values obtained by our simulations. Regarding this disagreement between experiments and simulations, we should bear in mind that our model only includes dispersion forces, and there are Hofmeister effects beyond these interactions. Just as an example related to hard colloids, a recent work has analyzed the effect of hydrophilic/hydrophobic character of the surface of different particles on the ζ-potential.[67] Regarding microgels, López-León *et al.* suggested that structural rearrangements in water induced by ions were also partially responsible for Hofmeister effects.[68] In any case, specific ionic effects attributed to NaCl and $NaNO_3$ when they interact with cationic microgels based on PNIPAM are not captured if only a generic cationic nanogel and dispersion forces are considered in the model.

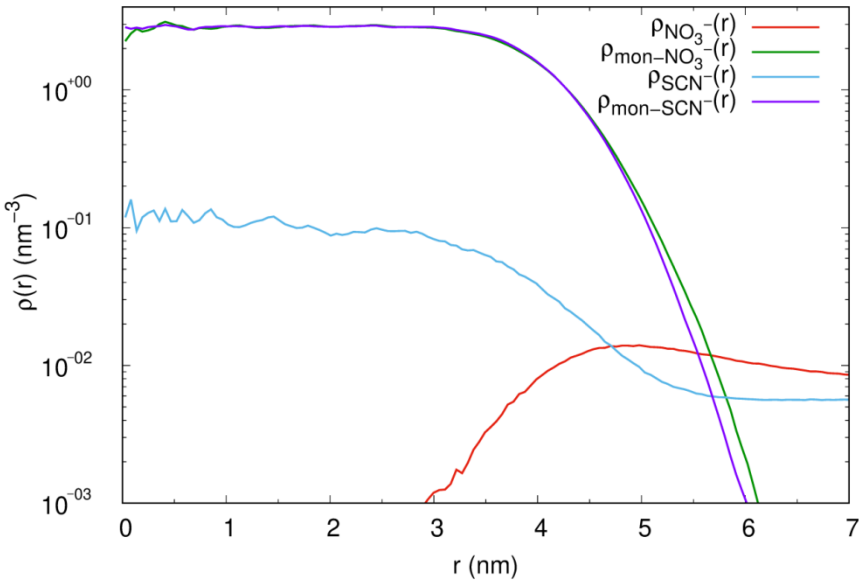

Figure 5.5: Spherically averaged local number density ($\rho(r)$) of ions SCN^- and NO_3^- and monomers in their presence as a function of the distance to the CM (r) at 323 K.

As mentioned before, simulations provide the distributions of different particles (monomers, ions, etc) around the CM of the nanogel. It would be quite illustrative to compare the distributions corresponding to SCN^-, for which dispersive effects are important, and NO_3^-. Figure 5.5 displays the spherically averaged local number density ($\rho(r)$) for these two ions and for the monomers in the presence of them at 323 K. On one hand, we might observe that the

monomers forming the nanogel for both electrolytes have a similar distribution. On the other hand, only the SCN^- appreciably permeates the nanoparticle. Its concentration inside the nanoparticle is considerably greater than outside despite the fact that the nanogel is collapsed. In contrast, the concentrations of NO_3^- and Na^+ (not shown) in the middle of the nanogel are much smaller than outside. Thus, this graph shows us how the dispersive effects are quite relevant for SCN^-, attracting these ions towards the nanogel monomers. In contrast, NO_3^- and Na^+ ions are mostly outside the nanogel since they are less attracted to the monomers.

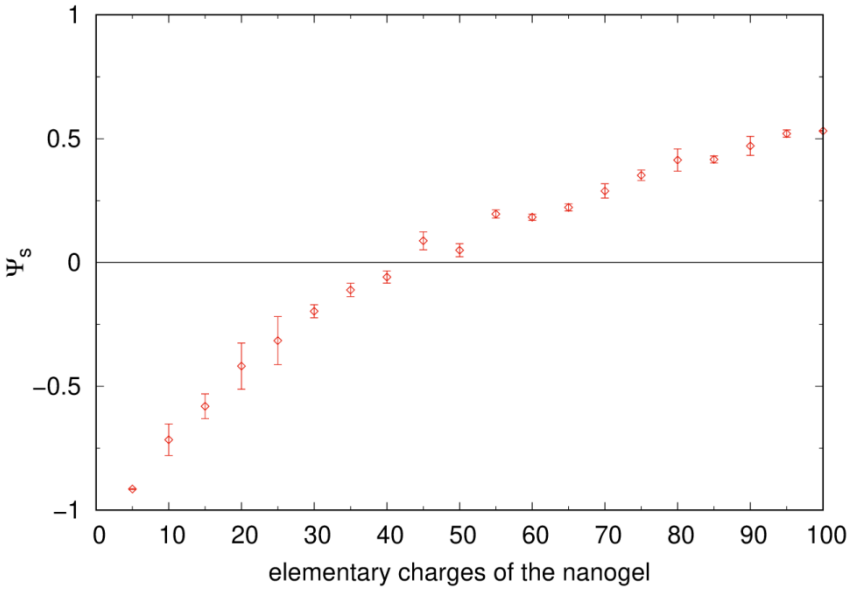

Figure 5.6: Normalized electrostatic potential as a function of the number of elementary charges of the nanogel in the presence of 10 mM of NaSCN at 323 K.

Up to this point, only 20% of the chains of the simulated nanogels carry only one charged group (2.5% of monomers). Given that these nanogels have 100 chains, this means that such nanoparticles possess 20 elementary charges. It would be appealing to analyze how the effects of dispersive forces depend on the number charge groups. Figure 5.6 shows the normalized electrostatic potential as a function of the number of elementary charges of the nanogel in the presence of NaSCN at 10 mM at 323 K. We have chosen this system because the effects of dispersion forces are stronger (Figure 5.4). As can be seen, two regions can be discerned easily. For nanogels with charges smaller than 45e (5.6% of total monomers) the normalized electrostatic potential is negative.

For greater charges this property is positive. This implies that the potential reversal only occurs bellow a threshold charge value.

5.4. Conclusion

In this work, the effects of dispersion forces have been assessed by means of coarse-grained simulation of nanogels in the presence of different electrolytes. According to our results, dispersion forces can induce charge inversion and electrostatic potential inversion for slightly charged cationic nanogels in the presence of NaSCN. This phenomenon would be straightforwardly related with the electrophoretic mobility reversal that López-Leon and coworker reported for PNIPAM microgels even at low NaSCN concentrations (such as 0.01 M).[15] These authors tried to qualitatively justify their results in terms of the dispersion potential between the ions and microgel surface, which is inversely proportional to the cube of the distance between a given ion and the surface. In this work, however, van der Waals interactions between ions and the monomeric units (instead of the surface of the nanogel) have been explicitly considered since ions can permeate the polymer network even in collapsed states. Such attractive interactions are inversely proportional to the six power of the distance between the interacting ions or molecules, whose minimum value depends on their ionic or molecular radii. Thus the phenomenon of charge inversion might happen not only for NaSCN and PNIPAM but also for other ions and polymers if these ionic species and the corresponding monomeric units have small sizes and high polarizability. It must also be stressed that this phenomenon disappears when the bare charge of the nanogel increases.

On the other hand, dispersion forces do not seem to have relevant effects on the net charge or the surface electrostatic potential for NaCl and $NaNO_3$. Moreover, the effects of the dispersive forces on the nanogel size are negligible for the three studied electrolytes. In any case, we should remark that here we have restricted ourselves to dispersion interactions, but Hofmeister effects can be driven by other forces.

Acknowledgments

The authors thank the Spanish "Ministerio de Economía y Competitividad (MINECO), Plan Nacional de Investigación, Desarrollo e Innovación Tecnológica (I + D + i)" (Projects FIS2016-80087-C2-1-P and FIS2016-80087-C2-2-P and European Regional Development Fund (ERDF). This study has also been

partially supported by "Consejería de Conocimiento, Investigación y Universidad, Junta de Andalucía", ref. SOMM17/6105/UGR.

5.5. References

[1] S. Seiffert, Sensitive microgels as model colloids and microcapsules, J. Polym. Sci. Part A Polym. Chem. 52 (2014) 435–449. doi:10.1002/pola.27024.

[2] K. Iwai, Y. Matsumura, S. Uchiyama, A.P. de Silva, Development of fluorescent microgel thermometers based on thermo responsive polymers and their modulation of sensitivity range, J. Mater. Chem. 15 (2005) 2796–2800. doi:10.1039/b502277k.

[3] S. Wu, J. Dzubiella, J. Kaiser, M. Drechsler, X. Guo, M. Ballauff, et al., Thermosensitive Au-PNIPA Yolk–Shell Nanoparticles with Tunable Selectivity for Catalysis, Angew. Chemie Int. Ed. 51 (2012) 2229–2233. doi:10.1002/anie.201106515.

[4] G. Zenkl, T. Mayr, I. Khmant, Sugar-responsive fluorescent nanospheres, Macromol. Biosci. 8 (2008) 146–152. doi:10.1002/mabi.200700174.

[5] Z.B. Hu, X.H. Lu, J. Gao, Hydrogel opals, Adv. Mater. 13 (2001) 1708–1712. doi:10.1002/1521-4095(200111)13:22<1708::AID-ADMA1708>3.0.CO;2-L.

[6] A. Pich, J. Hain, Y. Lu, V. Boyko, Y. Prots, H.J. Adler, Hybrid microgels with ZnS inclusions, Macromolecules. 38 (2005) 6610–6619. doi:10.1021/ma0505272.

[7] N. Welsch, M. Ballauff, Y. Lu, Microgels as Nanoreactors: Applications in Catalysis, in: Pich, A and Richtering, W (Ed.), Chem. Des. RESPONSIVE MICROGELS, SPRINGER-VERLAG BERLIN, HEIDELBERGER PLATZ 3, D-14197 BERLIN, GERMANY, 2010: pp. 129–163. doi:10.1007/12_2010_71.

[8] W. Kunz, P. Lo Nostro, B.W. Ninham, The present state of affairs with Hofmeister effects, Curr. Opin. Colloid Interface Sci. 9 (2004) 1–18. doi:10.1016/j.cocis.2004.05.004.

[9] E.R.A. Lima, D. Horinek, R.R. Netz, E.C. Biscaia, F.W. Tavares, W. Kunz, et al., Specific ion adsorption and surface forces in colloid science., J. Phys. Chem. B. 112 (2008) 1580–5.

http://www.scopus.com/inward/record.url?eid=2-s2.0-39849088157&partnerID=tZOtx3y1 (accessed January 13, 2015).

[10] D.F. Parsons, M. Boström, P. Lo Nostro, B.W. Ninham, Hofmeister effects: interplay of hydration, nonelectrostatic potentials, and ion size., Phys. Chem. Chem. Phys. 13 (2011) 12352–67. doi:10.1039/c1cp20538b.

[11] M. Boström, D. Parsons, A. Salis, Possible origin of the inverse and direct Hofmeister series for lysozyme at low and high salt concentrations, Langmuir. 27 (2011) 9504–9511. doi:10.1021/la202023r.

[12] P. Lo Nostro, B.W. Ninham, Hofmeister phenomena: an update on ion specificity in biology., Chem. Rev. 112 (2012) 2286–322. doi:10.1021/cr200271j.

[13] A. Salis, F. Cugia, D.F. Parsons, B.W. Ninham, M. Monduzzi, Hofmeister series reversal for lysozyme by change in pH and salt concentration: insights from electrophoretic mobility measurements, Phys. Chem. Chem. Phys. 14 (2012) 4343–4346. doi:10.1039/c2cp40150a.

[14] A. Salis, B.W. Ninham, Models and mechanisms of Hofmeister effects in electrolyte solutions, and colloid and protein systems revisited., Chem. Soc. Rev. 43 (2014) 7358–77. doi:10.1039/c4cs00144c.

[15] T. López-León, A. Elaïssari, J.L. Ortega-Vinuesa, D. Bastos-González, Hofmeister effects on poly(NIPAM) microgel particles: Macroscopic evidence of ion adsorption and changes in water structure, ChemPhysChem. 8 (2007) 148–156. doi:10.1002/cphc.200600521.

[16] M. Boström, D.R.M. Williams, B.W. Ninham, Surface tension of electrolytes: Specific ion effects explained by dispersion forces, Langmuir. 17 (2001) 4475–4478. doi:10.1021/la0102298.

[17] M. Boström, D.R.M. Williams, B.W. Ninham, Ion specificity of micelles explained by ionic dispersion forces, Langmuir. 18 (2002) 6010–6014. doi:10.1021/la0201220.

[18] M. Boström, D. Williams, B. Ninham, Specific ion effects: why the properties of lysozyme in salt solutions follow a Hofmeister series, Biophys. J. 85 (2003) 686–694. http://www.sciencedirect.com/science/article/pii/S0006349503745123 (accessed January 16, 2015).

[19] M. Boström, D.R.M. Williams, P.R. Stewart, B.W. Ninham, Hofmeister effects in membrane biology: The role of ionic dispersion potentials, Phys.

Rev. E - Stat. Physics, Plasmas, Fluids, Relat. Interdiscip. Top. 68 (2003) 1–6. doi:10.1103/PhysRevE.68.041902.

[20] W. Kunz, L. Belloni, O. Bernard, B.W. Ninham, Osmotic coefficients and surface tensions of aqueous electrolyte solutions: Role of dispersion forces, J. Phys. Chem. B. 108 (2004) 2398–2404. doi:10.1021/jp036113x.

[21] P. Koelsch, H. Motschmann, An experimental route to Hofmeister, Curr. Opin. Colloid Interface Sci. 9 (2004) 87–91. doi:10.1016/j.cocis.2004.05.009.

[22] S.A. Edwards, D.R.M. Williams, Hofmeister effects in colloid science and biology explained by dispersion forces: Analytic results for the double layer interaction, Curr. Opin. Colloid Interface Sci. 9 (2004) 139–144. doi:10.1016/j.cocis.2004.05.019.

[23] F. Tavares, D. Bratko, Ion-specific effects in the colloid-colloid or protein-protein potential of mean force: role of salt-macroion van der Waals interactions, J. Phys. Chem. B. 108 (2004) 9228–9235. http://pubs.acs.org/doi/abs/10.1021/jp037809t (accessed January 9, 2015).

[24] M. Boström, F.W. Tavares, B.W. Ninham, J.M. Prausnitz, Effect of salt identity on the phase diagram for a globular protein in aqueous electrolyte solution., J. Phys. Chem. B. 110 (2006) 24757–60. http://www.scopus.com/inward/record.url?eid=2-s2.0-33846061271&partnerID=tZOtx3y1 (accessed January 15, 2015).

[25] L.A. Moreira, M. Boström, B.W. Ninham, E.C. Biscaia, F.W. Tavares, Effect of the ion-protein dispersion interactions on the protein-surface and protein-protein interactions, J. Braz. Chem. Soc. 18 (2007) 223–230. doi:10.1590/S0103-50532007000100026.

[26] A. Martín-Molina, J.G. Ibarra-Armenta, M. Quesada-Pérez, Effect of ion dispersion forces on the electric double layer of colloids: a Monte Carlo simulation study., J. Phys. Chem. B. 113 (2009) 2414–21. doi:10.1021/jp8019792.

[27] M. Quesada-Pérez, R. Hidalgo-Álvarez, A. Martín-Molina, Effect of ionic van der Waals forces on the diffuse potential of model colloids, Colloid Polym. Sci. 288 (2010) 151–158.

[28] F. Vereda, A. Martín-Molina, R. Hidalgo-Alvarez, M. Quesada-Pérez, Specific ion effects on the electrokinetic properties of iron oxide nanoparticles: experiments and simulations, Phys. Chem. Chem. Phys. 17 (2015) 17069–17078. doi:10.1039/C5CP01011J.

[29] A.P. dos Santos, A. Diehl, Y. Levin, Surface Tensions, Surface Potentials, and the Hofmeister Series of Electrolyte Solutions, LANGMUIR. 26 (2010) 10778–10783. doi:10.1021/la100604k.

[30] A.P. dos Santos, Y. Levin, Surface and interfacial tensions of Hofmeister electrolytes, FARADAY Discuss. 160 (2013) 75–87. doi:10.1039/c2fd20067h.

[31] A.P. dos Santos, Y. Levin, Effective charges and zeta potentials of oil in water microemulsions in the presence of Hofmeister salts, J. Chem. Phys. 148 (2018). doi:10.1063/1.5019704.

[32] T. López-León, A.B. Jódar-Reyes, D. Bastos-González, J.L. Ortega-Vinuesa, Hofmeister effects in the stability and electrophoretic mobility of polystyrene latex particles, J. Phys. Chem. B. 107 (2003) 5696–5708. http://www.scopus.com/inward/record.url?eid=2-s2.0-0038576812&partnerID=tZOtx3y1.

[33] C.G. Lopez, W. Richtering, Does Flory-Rehner theory quantitatively describe the swelling of thermoresponsive microgels?, Soft Matter. 13 (2017) 8271–8280. doi:10.1039/c7sm01274h.

[34] M.S. Liu, C. Taylor, B. Chong, L. Liu, A. Bilic, N.S. Terefe, et al., Conformational transitions and dynamics of thermal responsive poly(N-isopropylacrylamide) polymers as revealed by molecular simulation, Eur. Polym. J. 55 (2014) 153–159. doi:10.1016/j.eurpolymj.2014.03.019.

[35] I. Adroher-Benitez, A. Moncho-Jorda, G. Odriozola, Conformation change of an isotactic poly (N-isopropylacrylamide) membrane: Molecular dynamics, J. Chem. Phys. 146 (2017). doi:10.1063/1.4983525.

[36] L. Tavagnacco, E. Zaccarelli, E. Chiessi, On the molecular origin of the cooperative coil-to-globule transition of poly(N-isopropylacrylamide) in water, Phys. Chem. Chem. Phys. 20 (2018) 9997–10010. doi:10.1039/c8cp00537k.

[37] H. Du, R. Wickramasinghe, X. Qian, Effects of Salt on the Lower Critical Solution Temperature of Poly (N -Isopropylacrylamide), J. Phys. Chem.

B. 114 (2010) 16594–16604. doi:10.1021/jp105652c.

[38] E.A. Algaer, N.F.A. Van Der Vegt, Hofmeister ion interactions with model amide compounds, J. Phys. Chem. B. 115 (2011) 13781–13787. doi:10.1021/jp208583w.

[39] G.C. Claudio, K. Kremer, C. Holm, Comparison of a hydrogel model to the Poisson-Boltzmann cell model, J. Chem. Phys. 131 (2009) 094903. doi:094903 10.1063/1.3207275.

[40] P.K. Jha, J.W. Zwanikken, F.A. Detcheverry, J.J. de Pablo, M.O. de la Cruz, Study of volume phase transitions in polymeric nanogels by theoretically informed coarse-grained simulations, Soft Matter. 7 (2011) 5965–5975. doi:10.1039/c1sm05264k.

[41] R. Schroeder, A.A. Rudov, L.A. Lyon, W. Richtering, A. Pich, I.I. Potemkin, Electrostatic Interactions and Osmotic Pressure of Counterions Control the pH-Dependent Swelling and Collapse of Polyampholyte Microgels with Random Distribution of Ionizable Groups, Macromolecules. 48 (2015) 5914–5927. doi:10.1021/acs.macromol.5b01305.

[42] H. Kobayashi, R. Winkler, Structure of Microgels with Debye–Hückel Interactions, Polymers (Basel). 6 (2014) 1602–1617. doi:10.3390/polym6051602.

[43] H. Kobayashi, R.G. Winkler, Universal conformational properties of polymers in ionic nanogels, Sci. Rep. 6 (2016). doi:10.1038/srep19836.

[44] H. Kobayashi, R. Halver, G. Sutmann, R.G. Winkler, Polymer Conformations in Ionic Microgels in the Presence of Salt: Theoretical and Mesoscale Simulation Results, Polymers (Basel). 9 (2017).

[45] N. Gnan, L. Rovigatti, M. Bergman, E. Zaccarelli, In Silico Synthesis of Microgel Particles, Macromolecules. 50 (2017) 8777–8786. doi:10.1021/acs.macromol.7b01600.

[46] L. Rovigatti, N. Gnan, E. Zaccarelli, Internal structure and swelling behaviour of in silico microgel particles, J. PHYSICS-CONDENSED MATTER. 30 (2018). doi:10.1088/1361-648X/aaa0f4.

[47] L. Rovigatti, N. Gnan, L. Tavagnacco, A.J. Moreno, E. Zaccarelli, Numerical modelling of non-ionic microgels: an overview, Soft Matter. 15 (2019) 1108–1119. doi:10.1039/c8sm02089b.

[48] A. Martín-Molina, M. Quesada-Pérez, A review of coarse-grained simulations of nanogel and microgel particles, J. Mol. Liq. 280 (2019) 374–381. doi:https://doi.org/10.1016/j.molliq.2019.02.030.

[49] J. Shin, A.G. Cherstvy, R. Metzler, Sensing Viruses by Mechanical Tension of DNA in Responsive Hydrogels, Phys. Rev. X. 4 (2014) 21002. http://link.aps.org/doi/10.1103/PhysRevX.4.021002.

[50] M. Quesada-Perez, J. Ramos, J. Forcada, A. Martin-Molina, Computer simulations of thermo-sensitive microgels: Quantitative comparison with experimental swelling data, J. Chem. Phys. 136 (2012) 244903–244909. http://dx.doi.org/10.1063/1.4729946.

[51] J.N. Israelachvili, Intermolecular and surface forces / Jacob N. Israelachvili, Academic Press, London ; San Diego :, 1991.

[52] A. Catenaccio, Y. Daruich, C. Magallanes, Temperature dependence of the permittivity of water, Chem. Phys. Lett. 367 (2003) 669–671. doi:10.1016/S0009-2614(02)01735-9.

[53] S. Schneider, P. Linse, Monte Carlo simulation of defect-free cross-linked polyelectrolyte gels, J. Phys. Chem. B. 107 (2003) 8030–8040. doi:10.1021/jp022336w.

[54] R.S. Dias, A. Pais, Polyelectrolyte condensation in bulk, at surfaces, and under confinement, Adv. Colloid Interface Sci. 158 (2010) 48–62. doi:10.1016/j.cis.2010.02.007.

[55] S.K. Ghosh, A.G. Cherstvy, R. Metzler, Deformation propagation in responsive polymer network films, J. Chem. Phys. 141 (2014). doi:http://dx.doi.org/10.1063/1.4893056.

[56] I. Adroher-Benitez, A. Martin-Molina, S. Ahualli, M. Quesada-Perez, G. Odriozola, A. Moncho-Jorda, Competition between excluded-volume and electrostatic interactions for nanogel swelling: effects of the counterion valence and nanogel charge, Phys. Chem. Chem. Phys. 19 (2017) 6838–6848. doi:10.1039/c6cp08683g.

[57] J. Estelrich, M. Quesada-Perez, J. Forcada, J. Callejas-Fernandez, CHAPTER 1 Introductory Aspects of Soft Nanoparticles, in: Soft Nanoparticles Biomed. Appl., The Royal Society of Chemistry, 2014: pp. 1–18. doi:10.1039/9781782625216-00001.

[58] M.O. Khan, S.M. Mel'nikov, B. Jonsson, Anomalous salt effects on DNA

conformation: Experiment and theory, Macromolecules. 32 (1999) 8836–8840. doi:10.1021/ma9905627.

[59] F.A. Escobedo, J.J. de Pablo, Monte Carlo simulation of branched and crosslinked polymers, J. Chem. Phys. 104 (1996) 4788–4801. http://link.aip.org/link/?JCP/104/4788/1.

[60] M. Quesada-Perez, J. Alberto Maroto-Centeno, J. Forcada, R. Hidalgo-Alvarez, Gel swelling theories: the classical formalism and recent approaches, Soft Matter. 7 (2011) 10536–10547. doi:10.1039/c1sm06031g.

[61] M. Quesada-Perez, A. Martin-Molina, Monte Carlo simulation of thermoresponsive charged nanogels in salt-free solutions, Soft Matter. 9 (2013) 7086–7094. doi:10.1039/c3sm00093a.

[62] M. Quesada-Pérez, S. Ahualli, A. Martín-Molina, Temperature-sensitive nanogels in the presence of salt: Explicit coarse-grained simulations, J. Chem. Phys. 141 (2014) 124903. doi:10.1063/1.4895960.

[63] F.W. Tavares, M. Boström, E.R.A. Lima, E.C. Biscaia, Ion-specific thermodynamic properties of colloids and proteins, Fluid Phase Equilib. 296 (2010) 99–105. doi:10.1016/j.fluid.2010.02.031.

[64] G.D. Mahan, van der Waals coefficient between closed shell ions, J. Chem. Phys. 76 (1982) 493. doi:10.1063/1.442750.

[65] S. Ahualli, A. Martin-Molina, J. Alberto Maroto-Centeno, M. Quesada-Perez, Interaction between Ideal Neutral Nanogels: A Monte Carlo Simulation Study, Macromolecules. 50 (2017) 2229–2238. doi:10.1021/acs.macromol.6b02333.

[66] L. Pérez-Fuentes, D. Bastos-González, J. Faraudo, C. Drummond, Effect of organic and inorganic ions on the lower critical solution transition and aggregation of PNIPAM, Soft Matter. 14 (2018) 7818–7828. doi:10.1039/c8sm01679h.

[67] M. V. Manilo, N.I. Lebovka, S. Barany, Effects of sort and concentration of salts on the electrosurface properties of aqueous suspensions containing hydrophobic and hydrophilic particles: Validity of the Hofmeister series, J. Mol. Liq. 276 (2019) 875–884. doi:10.1016/j.molliq.2018.12.058.

[68] T. López-León, a. Fernández-Nieves, Macroscopically probing the

entropic influence of ions: Deswelling neutral microgels with salt, Phys. Rev. E. 75 (2007) 011801. doi:10.1103/PhysRevE.75.011801.

6. Coarse-grained Monte Carlo simulations of nanogel-polyelectrolite complexes: electrostatic and steric effects.

L. Pérez-Mas, A. Martín-Molina and M. Quesada-Pérez

The content of this chapter is published in: *Physical Chemistry Chemical Physics*, **2020**, *16*, 3022.

https://doi.org/10.1039/D0SM00173B

6. Paper III *Physical Chemistry Chemical Physics*, **2020**, *16*, 3022.

Abstract

Coarse-grained Monte-Carlo simulations of nanogel-polyelectrolyte complexes have been carried out. The results presented here capture two phenomena reported in experiments with real complexes: i) the reduction in size after absorbing just a few chains; ii) the charge inversion detected through electrophoretic mobility data. Our simulations reveal that charge inversion occurs if the polyelectrolyte charge is large enough. In addition, the distribution of chains inside the nanogel strongly depends on whether charge inversion takes place. It should be also stressed that the size and surface electrostatic potential depends on the number of monomers per chain. However, the chain topology has very scarce influence on the properties studied here.

6.1. Introduction

Nanogels are crosslinked polymer (or polyelectrolyte) networks with sizes of just a few tens of nanometers.[1,2] One of their more outstanding characteristics is that these colloidal particles are able to swell or shrink in response to environmental properties, such as temperature or pH. As a result of this responsiveness and their high loading capacity, nanogels are very promising as drug-delivery carriers.[3–8] In particular, ionic nanogels can incorporate oppositely charged macromolecules, polyelectrolytes or inorganic nanoparticles due to attractive electrostatic forces. In fact, this principle can be exploited to immobilize oligonucleotides and plasmid DNA in cationic nanogels, which protect such polyelectrolytes from enzymatic degradation.[9–17] In addition, these nanogels can be used to deliver genes into a cell. Apart from that, nanogels have been proposed as a soft and porous alternative to solid substrates and, what is more, some research groups have experimentally investigated the absorption of some polyelectrolytes (such as poly(diallydimethylammoniumchloride) (PDADMAC), miktoarm star polymers, peptides or polystyrene suphonate) into micro- or nanogels.[18–23]

In order to control the uptake of polyelectrolytes by nanogels, we should fully understand the role played by electrostatic and excluded-volume interactions, which are present in all charged systems. However, some counterintuitive electrostatic phenomena continue challenging many theorists of colloid science and soft matter. Widely known examples of this are charge inversion and the existence of attractive electrostatic forces between like-charged

macroions. Strong electrostatic correlations and charge fluctuations neglected by mean-field theories are responsible in many cases for such striking phenomena.[24–29]

It is appropriate to mention in this regard that coarse-grained simulations of nanogels are particularly useful to consider these and other aspects which are not included in many theoretical models, such as the presence of nodes in the polyelectrolyte network or the flexibility of the chains. In addition, these simulations have significantly contributed to elucidate some aspects of the behavior of nanogels,[30–47] such as size and charge effects. For instance, a previous work has recently showed that the deswelling and charge inversion observed after the absorption of spherical hard nanoparticles into nanogels can be explained in terms of electrostatic and excluded volume interactions.[48] The simulations performed therein also revealed that: i) charge inversion only takes place if the nanoparticle charge is large enough; ii) the distribution of hard nanoparticles inside the nanogel depends on whether charge inversion occurs.

Some experimental works assume that the formation of polyelectrolyte-microgel complexes is driven largely by electrostatic interactions to draw some conclusions about the role of these interactions.[20,22] In real systems, however, the presence of other interactions depending on the specific chemical nature of the microgel and polyelectrolyte chains is very likely. Commonly, such interactions are not known a priori and therefore it is difficult to reach firm conclusions. In this respect, computer simulations can be extremely helpful since they employ tailor-made systems, whose structure and interactions between their constituents are specified at the beginning.

According to the preceding paragraphs, one of the main goals of this work is to find out the precise role played by electrostatic forces in complexes formed by nanogels and soft polyelectrolyte chains incorporated into them. To tackle this issue, the absorption of linear and ring polyelectrolyte chains into nanogels has been simulated using the bead-spring model for both species. In this way, the complex topology of nanogels and the fluctuations of polyelectrolyte chains are explicitly considered. Different properties of the polyelectrolyte/nanogel complexes formed are analyzed paying special attention to size and charge effects. Linear and ring polyelectrolyte chains are inspired in oligonucleotides and plasmid DNA, since the latter it has been proved to be much more efficiently transfected than linear DNA (when cationic lipids as used as vectors in gene therapy).[49,50] However, the results obtained here go far beyond DNA arrangements and can be relevant for a huge variety of

polyelectrolyte/nanogel complexes given the generality of the model. Apart from this, ring polymers were also included in our study because two polyelectrolytes with the same charge but different architecture or topology exhibit different charge distributions. Therefore, the comparison between ring and linear polyelectrolytes will help us to discover if the chain charge distribution has important effects.

6.2. Model and simulations

The coarse-grained picture employed here for polyelectrolyte chains and nanogels is the so-called bead-spring model. According to this representation of reality, monomer units and ions are modeled as spheres, whereas the solvent is modeled as a dielectric continuum. The short-range repulsion between any pair of these beads (monomers or ions) due to excluded volume effects is modeled by means of the Weeks–Chandler–Andersen potential:

$$u_{LJ}(r) = \begin{cases} 4\varepsilon_{LJ}\left(\frac{d^{12}}{r^{12}} - \frac{d^6}{r^6} + \frac{1}{4}\right) & r \leq \sqrt[6]{2}(a_i + a_j) \\ 0 & r > \sqrt[6]{2}(a_i + a_j) \end{cases} \quad (6.1)$$

Here r is the center-to-center distance between a given pair of particles, $\varepsilon_{LJ} = 4.11 \times 10^{-21}$ J, a_i stands for the radius of species i and $d = a_i + a_j$. We assumed that the monomers of the nanogel and the monomers of the free chains have similar but slightly different diameters ($d = 0.65$ and 0.7 nm, respectively). Estimates of the diameters of different monomers yield values of this order.[51] A diameter of 0.7 nm was also employed for ions. The hydration shell of ions is included in the corresponding spheres.

Consecutive monomers of a chain are connected by harmonic bonds, whose interaction potential is:

$$u_{bond}(r) = 0.5k_{bond}(r - r_0)^2 \quad (6.2)$$

where k_{bond} is the elastic constant and r_0 is the equilibrium length corresponding to this harmonic potential. The r_0-values used for monomers of the nanogel and the free polyelectrolyte chains were identical to their respective diameters, but the same k_{bond}-value was employed for both, 0.4 Nm^{-1}. This value was also employed by Schneider and Edgecombe *et al.* in coarse-grained simulations of polyelectrolyte gels.[52-54] Other authors proposed elastic constants much greater than k_BT/d_m^2, where d_m is the diameter of monomers, k_B is Boltzmann's constant and T is the absolute temperature.[30,55] This ensures

that thermal fluctuations undergone by the monomers are much smaller than their diameter. The elastic constant employed in this work also satisfies this condition.

Some monomers of the free polyelectrolyte chains and nanogels carry electric charge. These beads and ions interact through the Coulomb potential:

$$u_{elec}(r) = \frac{Z_i Z_j e^2}{4\varepsilon_0 \varepsilon_r r} \tag{6.3}$$

where $Z_i e$ is the charge of species i, e denotes the positive elementary charge and $\varepsilon_0 \varepsilon_r$ is the dielectric permittivity of the medium (water at 293 K in this case).

The topology of the nanogel is the same as we employed in previous works:[48] 100 polyelectrolyte chains connect through 66 crosslinkers. Inner crosslinkers (40%) were connected to the ends four polyelectrolyte chains. However, the most external crosslinkers were connected only to three or even two chains. The nanogel lacks chains with a free end. Each chain of the nanogel is formed by 15 monomers whereas the free polyelectrolyte chains are made of 12 or 24 monomers. The bare charge of the nanogel is $+100e$ (one charged group per chain). This is a representative sample of a slightly charged nanogel. As we are interested in charge effects, four families of free chains with different bare charges were employed in our simulations. Linear and ring polyelectrolyte chains with 12 monomers carry bare charges of $-3e$, $-6e$, $-12e$ and $-24e$, whereas the bare charge of linear and ring polyelectrolytes with 24 monomers can be $-4e$, $-8e$, $-16e$, $-24e$ or $-48e$. Figure 6.1 shows the nanogel and some 24-monomer linear polyelectrolyte chains whose charge is $-8e$.

The simulation cell contains the cationic nanogel in the middle, a given number of free anionic polyelectrolyte chains and the monovalent anions and cations required to neutralize the charge of the nanogel and the polyelectrolyte chains, respectively. The simulation box also contains additional cations and anions corresponding to a fixed concentration of monovalent electrolyte (0.1 mM). The length of the cell (L_c) was estimated as $L \approx 2(R_{NG0} + 3l_D)$, where R_{NG0} is an estimate of the radius of the nanogel in the absence of free polyelectrolyte chains and l_D is the Debye screening length. The definition of l_D is not a trivial issue. In fact, Claudio *et al.* admitted in their pioneering work on coarse-grained simulations of nanogels that different criteria might be employed to define the Debye length.[30] Here, we have adopted the simplest criterion: to consider the total number of ionic species in the simulation box (including free

polyelectrolyte chains), which gives us a lower bound for the Debye length. After simulation, we confirmed that the cell contained a significant portion of electrical double layer around the nanogel. In any case, the cell lengths employed in our simulations were greater than 100 nm.

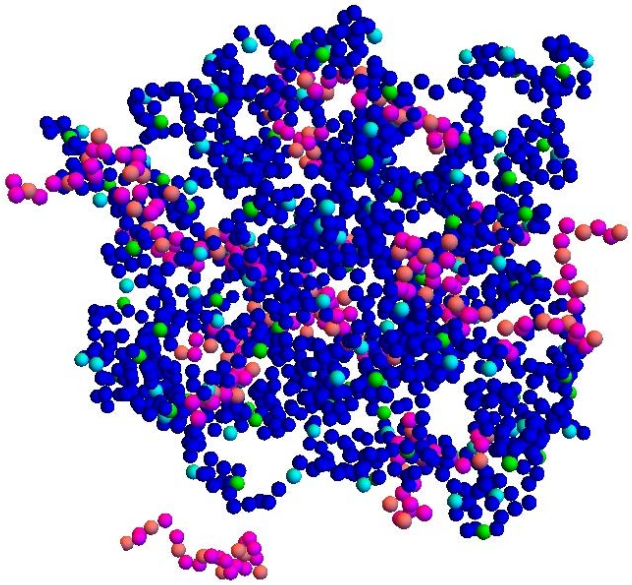

Figure 6.1: Nanogel and some 24-monomer linear polyelectrolyte chains whose charge is −8*e*. Blue, light blue and green beads represent neutral monomers, charged monomers and crosslinkers of the nanogel. Magenta and pink beads stand for neutral and charged monomers of the polyelectrolyte chains.

Monte Carlo (MC) simulations were performed using the canonical ensemble, in which volume, temperature and number of particles are kept constant. Different kinds of MC moves were executed in our simulations according to the conventional Metropolis algorithm: i) 88% of the total number of trial moves are single-particle moves of the beads forming the nanogel and the free polyelectrolyte chains; ii) 10% are translations of the free chains as a whole; iii) 2% are rotations of these free chains. Polyelectrolyte chains were translated and rotated together with their nearest counterions (as if they formed a cluster). Simulations with higher percentages for translations and rotation of free chains were also performed in a preliminary study obtaining almost identical results (within the statistical uncertainty). It should be mentioned, however, that the simulation time considerably increases with these percentages. For

that reason, low percentages are preferred. The maximum displacement corresponding to each bead and cluster was individually adjusted so that its respective acceptance ratio was close to 50%. But in the case of clusters, this maximum displacement could not be larger than the diameter of monomers. Periodic boundary conditions were employed. Long-range Coulomb forces were handled through Ewald sums, which were implemented with the recommendations reported in previous works.[40]

Simulations can be split into three stages. First, the nanogel is equilibrated in the absence of free polyelectrolytes. This stage takes 3×10^8 moves. Then, the polyelectrolyte chains are added to the simulation box and equilibrated (1×10^8 moves). Finally, a set of statistically independent configuration for averaging was extracted from 3×10^8 MC moves. The correlation functions of different properties revealed that such configurations should be sampled at least every 10^5 moves (in round numbers). According to this, 300 statistically independent configurations were obtained. There are efficient simulation packages for coarse-grained models of soft matter, but these simulations were performed using a home-made computer code (in C).

6.3. Results and discussion

As mentioned previously, four families of free polyelectrolyte chains were employed in our simulations. Figure 6.2 shows the radius of gyration of all these chains as a function of the magnitude of their bare charge. As can be seen the radius of gyration grows with the bare charge and the number of monomers of the chain. In addition, the two families of linear chains exhibit radii of gyration greater than the families of ring polyelectrolytes with the same number of monomers. This figure also shows that the families of ring chains with 24 monomers and linear chains with 12 monomers exhibit very similar sizes.

In a first set of simulations, we employed four polyelectrolyte chains with the same bare charge ($-24e$) but different numbers of monomers (12 or 24) and topology (linear or ring). Figure 6.3 displays the number of free chains absorbed by the nanogel as a function of the number of in the simulation cell, which can also be thought of as the number of chains per nanogel particle in the reservoir. A chain is considered to be absorbed if the distance between its center of mass (CM) and the CM of the nanogel is smaller than the effective radius. Here, the effective radius of the polymer network that constitutes a nanogel (or a complex) is $R_{eff} = \sqrt{5/3}R_g$, where R_g is its radius of gyration.[30,56]

6. Paper III *Physical Chemistry Chemical Physics*, **2020**, *16*, 3022.

It can be shown that the radius of gyration of a solid sphere of radius R is $R_g = \sqrt{5/3}R$. Consequently, R_{eff} provides us an idea of the geometrical radius of the polymer network considered as a sphere in a first approximation. In fact, an imaginary sphere of radius R_{eff} centered at the CM of the polymer network contains 90% of its monomers.[56] Such an imaginary sphere is also considered the border between the interior and the exterior of the nanogel. As can be inferred from Figure 6.3, if this number of chains in the simulation cell is small enough (two or four chains in our case), all the chains are absorbed. But if the number of chains in the simulation cell goes on increasing, the number of chains absorbed seems to reach a plateau (saturated complexes). This behavior has been experimentally found for complexes formed by poly(*N*-isopropylacrylamide) (PNIPAm) microgels and PDADMAC.[20] It is worth stressing that the maximum number of chains absorbed characterizing the saturated complexes slightly decreases when the radius of gyration increases, as can be concluded comparing Figure 6.2 and 6.3

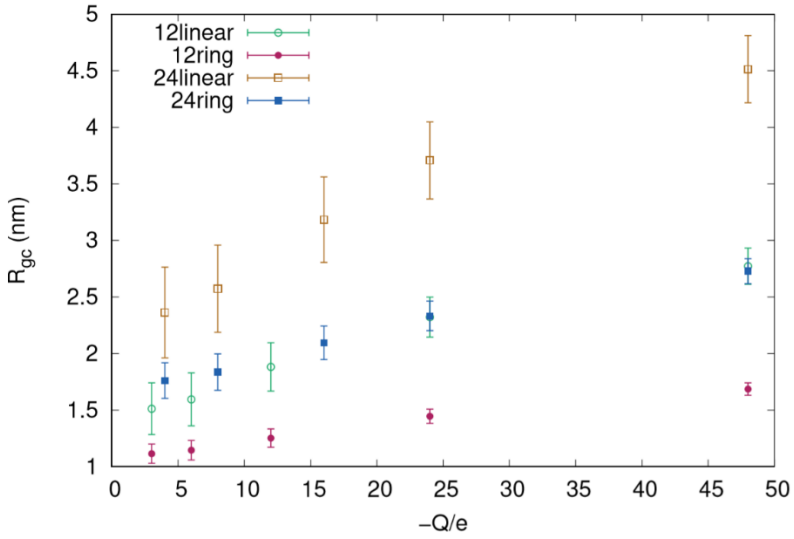

Figure 6.2: Radius of gyration of the polyelectrolyte chains (R_{gc}) as a function of the magnitude of their charge (in elementary units, $-Q/e$) for: 12-monomer linear chain (open circle), 12-monomer ring chain (closed circle), 24-monomer linear chain (open square), 24-monomer ring chain (closed square).

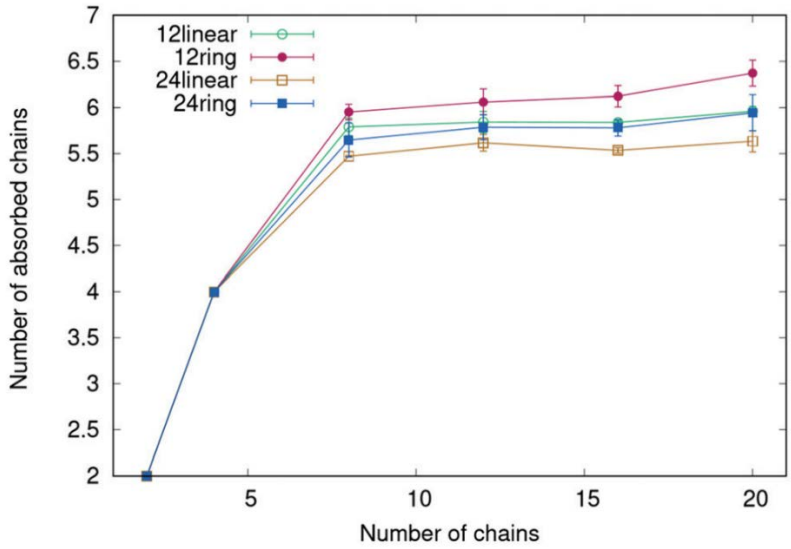

Figure 6.3: Number of chains absorbed as a function of the number of chains per nanogel for the four chains whose charge is $-24e$: 12-monomer linear chain (open circle), 12-monomer ring chain (closed circle), 24-monomer linear chain (open square), 24-monomer ring chain (closed square).

At this point, it is interesting to find out if the nanogel-polyelectrolyte complexes differ in size from the nanogel. The answer to this question can be found in Figure 6.4, which shows the effective radius of the complexes as a function of the number of chains in the cell. The error bars were estimated as the standard deviation of the effective diameters obtained in three simulations. A similar criterion was employed for other properties (number of absorbed chains, net charge and electrostatic potential).

As can be seen in Figure 6.4, first the size of the complexes decreases markedly, then it goes through a minimum and finally it increases slightly. A similar behavior has been reported by Kleinen *et al.*[18] from experiments with microgel-PDADMAC complexes.

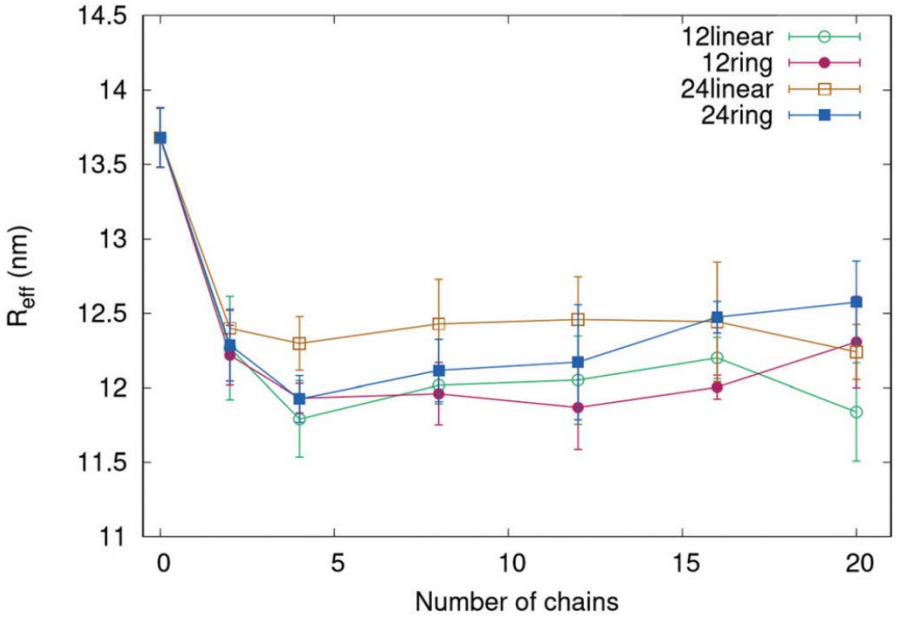

Figure 6.4: Effective radius of the nanogel-polyelectrolyte complexes as a function of the number of chains in the simulation cell for the four chains whose charge is –24*e*: 12-monomer linear chain (open circle), 12-monomer ring chain (closed circle), 24-monomer linear chain (open square), 24-monomer ring chain (closed square). The radius at 0 is the effective radius of the nanogel in the absence of chains.

The reduction in the size of the polyelectrolyte network observed when the nanogel absorbs just a few chains can be explained as follows. In the absence of chains, the nanogel contains some monovalent counterions that partly

neutralize its bare charge. For instance, the bare charge of the nanogel employed in this work is +100*e*, which means that its polymer backbone carries 100 ionized monovalent groups. In addition, the nanogel contains around 22 monovalent counterions. Thus its net charge is +78*e*. When the nanogel absorbs a few highly charged polyelectrolytes, a considerable fraction of these monovalent counterions are expelled, which brings about a fall in the osmotic pressure that swells the polyelectrolyte network, which in turn causes the reduction in size.

Now let us turn our attention to electric properties of these complexes. Figure 6.5 displays their net charge as a function of the number of chains in the simulation cell for the four polyelectrolytes studied previously. The net charge of the complexes includes the bare charge of the nanogel as well as the charge of the polyelectrolyte chains and small ions inside. As can be seen, the net charge varies from a positive value for the nanogel without chains (+78*e*) to a negative value of the order of −30*e* for saturated complexes. Indeed, the most outstanding feature of this figure is the change of sign in the electric charge. This phenomenon, which has been reported for a wide variety of complex fluids, is known as charge inversion or overcharging.

6. Paper III *Physical Chemistry Chemical Physics*, **2020**, *16*, 3022.

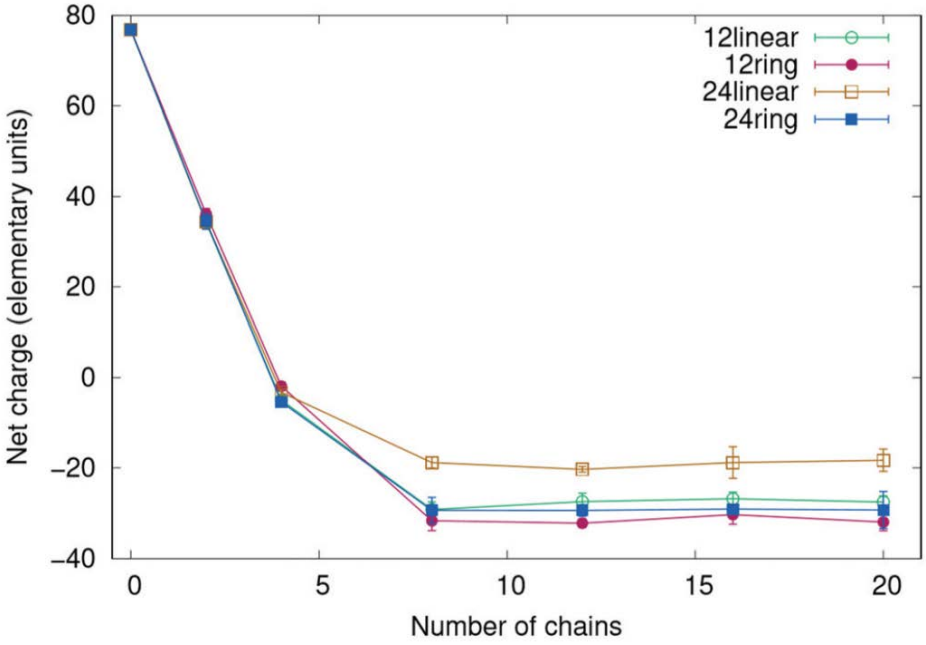

Figure 3.5: Net charge of the nanogel-polyelectrolyte complexes as a function of the number of chains in the simulation cell for the four chains whose charge is −24*e*: 12-monomer linear chain (open circle), 12-monomer ring chain (closed circle), 24-monomer linear chain (open square), 24-monomer ring chain (closed square). The net charge at 0 is the net charge in the absence of chains.

Figure 6.5 also shows that the neutralization point is reached when the nanogel absorbs about four polyelectrolyte chains. As each of them carries an electric charge of −24*e*, we can conclude that the charge neutralization can be attributed to these four chains to a great extent. We should also keep in mind that this can also be mathematically expressed by means of the quotient between the magnitude of the bare charge of the nanogel and the magnitude of the total charge of the absorbed polyelectrolyte. Such a quotient is called nominal charge ratio by some authors.[18,20] In our case, this ratio is around one.

Regarding charge inversion, the question is: why does the nanogel continue to absorb chains beyond the neutralization point? In the last two decades, several mechanisms have been put forward to justify the existence of charge inversion. Previous simulations of complexes formed by nanogels and hard spherical nanoparticles suggest that strong electrostatic correlations between such nanoparticles can induce charge inversion.[48] Certainly, this idea can also

be applied when these nanoparticles are replaced by highly charged polyelectrolyte chains.

Some experiments performed with PDADMAC,[18,20] miktoarm star polymers,[21] polystyrene sulphonate[23] and siRNA[9] have clearly suggested that polyelectrolyte-microgel complexes undergo charge inversion. Nominal charge ratios close to one were also reported. However, it should be stressed that such experiments are based on electrophoretic mobility measurements. In the case of hard colloids, it is well established that electrokinetic properties are directly related to the zeta-potential, the electrostatic potential at the slipping surface, very close to the particle surface. For that reason, we have also computed the dimensionless electrostatic potential at the imaginary border of the nanogel, $e\psi(R_{eff})/k_BT$, where ψ is the electrostatic potential, k_B is Boltzmann's constant and T the absolute temperature. The electrostatic potential at a distance R_{eff} from the CM, $\psi(R_{eff})$, was computed by integrating from the border of the simulation cell to R_{eff}:

$$\psi(R_{eff}) = -\int_{L_c/2}^{R_{eff}} E(r)\mathrm{d}r \qquad (6.4)$$

Here, $E(r)$ is the spherically averaged electric field at a distance r from the CM, which in turn can be obtained from the net charge enclosed by a sphere of radius r by applying Gauss' law.

Figure 6.6 shows the dimensionless electrostatic potential as a function of the number of chains. The error bars were computed as the standard deviation of the ψ-values obtained in three simulations. As expected, the electrostatic potential also exhibits a change in sign for saturated complexes, which would be straightforwardly related to an inversion in the electrophoretic mobility detected in experiments. It should be mentioned that the electrostatic potential does not depend on the topology of the complexes. This behavior contrasts with that found for lipoplexes (complexes formed by liposomes and DNA). The charge of ionic liposomes is mainly placed on their surface and the complexation of DNA by liposomes results in complexes in which the topology of nucleic acid molecules plays an important role.[49,50]

6. Paper III *Physical Chemistry Chemical Physics*, **2020**, *16*, 3022.

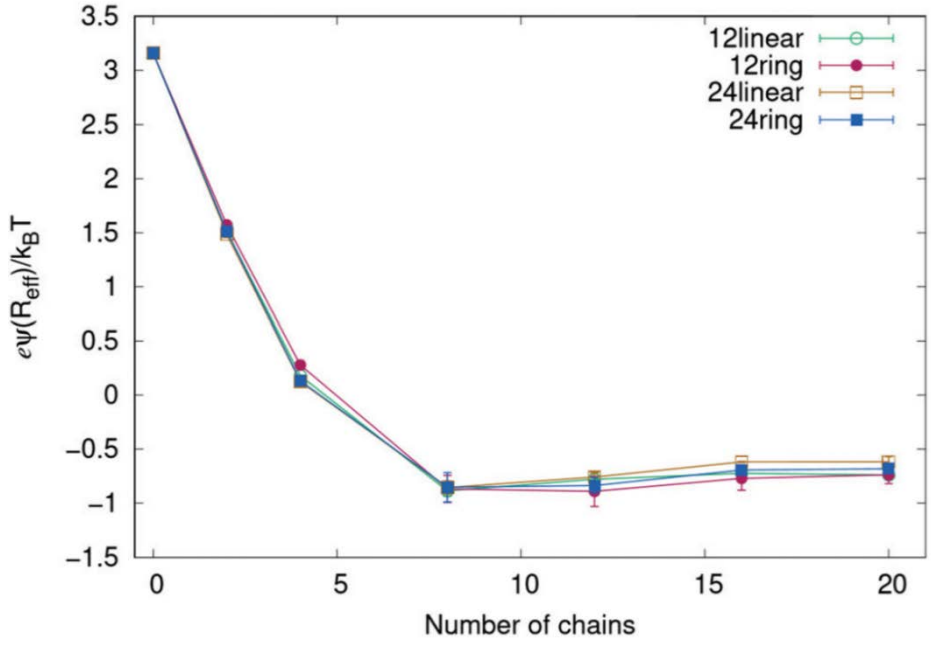

Figure 6.6: Dimensionless electrostatic potential at the imaginary surface of the nanogel-polyelectrolyte complexes as a function of the number of chains per nanogel in the reservoir for the four chains whose charge is –24*e*: 12-monomer linear chain (open circle), 12-monomer ring chain (closed circle), 24-monomer linear chain (open square), 24-monomer ring chain (closed square).

So far, we have commented results of simulations in which the polyelectrolyte chains had the same charge (–24*e*). It would be interesting to analyze how the electrostatic potential depends on the charge of the chains. In practice, this could be the case of polyelectrolytes with weak acid/basic groups, whose charge varies with pH. Consequently, simulations were performed with the four families of polyelectrolytes but setting the number of chains in the simulation cell to 20. Figure 6.7 displays the normalized electrostatic potential obtained for the four families of chains as a function of their electric charge.

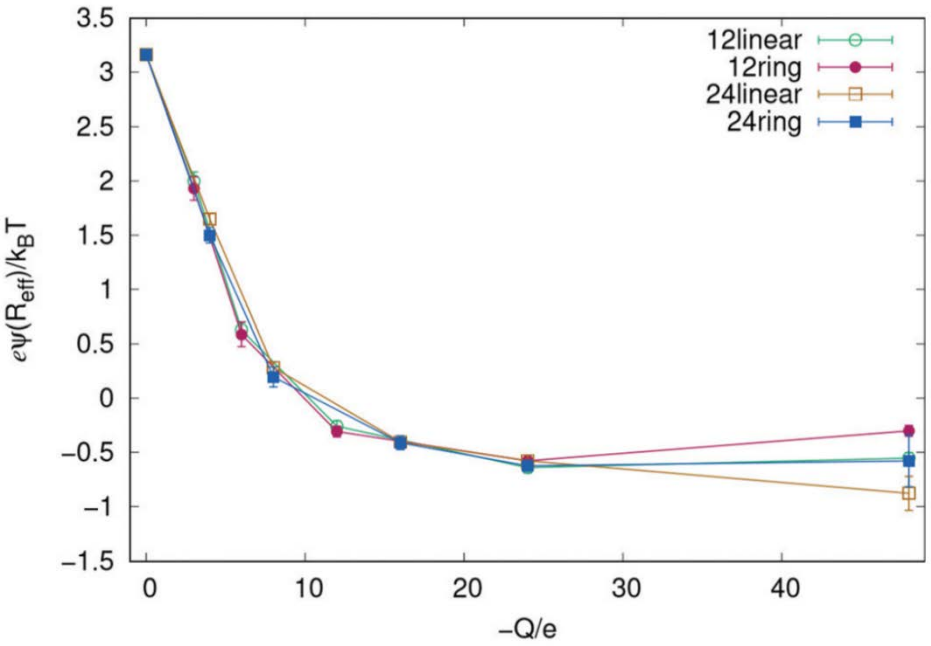

Figure 6.7: Dimensionless electrostatic potential at the imaginary surface of the nanogel-polyelectrolyte complexes as a function of the chain charge for: 12-monomer linear chains (open circle), 12-monomer ring chains (closed circle), 24-monomer linear chains (open square), 24-monomer ring chains (closed square). The value at 0 stands for the normalized electrostatic potential in the absence of chains.

This figure clearly shows that the electrostatic potential of the complexes exhibits inversion only if the magnitude of the charge of chains is greater than 10*e*. This threshold seems to be similar for the four families of polyelectrolytes simulated here and it is also very close to the charge required for inversion in nanogel-nanoparticles composites with sizes ranging from 2 to 6 nm previously simulated.[48] This suggests that the charge required for inversion of several species encapsulated by a nanogel is not very sensitive to the charge distribution since polyelectrolytes chains with different lengths and topology and spherical nanoparticles exhibit similar values. The net charge also displays a threshold of about 10*e* for charge inversion (figure not shown).

Finally, it is quite instructive to analyze where the polyelectrolyte chains encapsulated by the nanogel are located (depending on their charge). In fact, Gelissen *et al.* has recently employed simulations to compute the distribution of polystyrene sulfonate chains inside polyampholyte core-shell microgels.[23] In our case, Figure 6.8 and 6.9 show the spherically averaged local chain number

density, $\rho_{ch}(r)$, as a function of chain-nanogel center-to-center distance r for different polyelectrolyte chains of 12 (Figure 6.8) and 24 (Figure 6.9) monomers per chain. The most remarkable feature of both figures is that the preferential location of the chains inside the nanogel strongly depends on their electric charge. Chains with charges (in magnitude) smaller than 10e are preferentially located at the center of the nanogel. Chains with $-3e$, $-4e$, $-6e$ or $-8e$ are illustrative examples of this behavior. In contrast, chains with greater charges leave empty the center of the nanogel and are structured in shells at different distances from it. Given that the threshold charge for inversion in the electrostatic potential is $-10e$ we can also state that the distribution of chains inside the nanogel strongly depends on the existence of charge inversion in the complex.

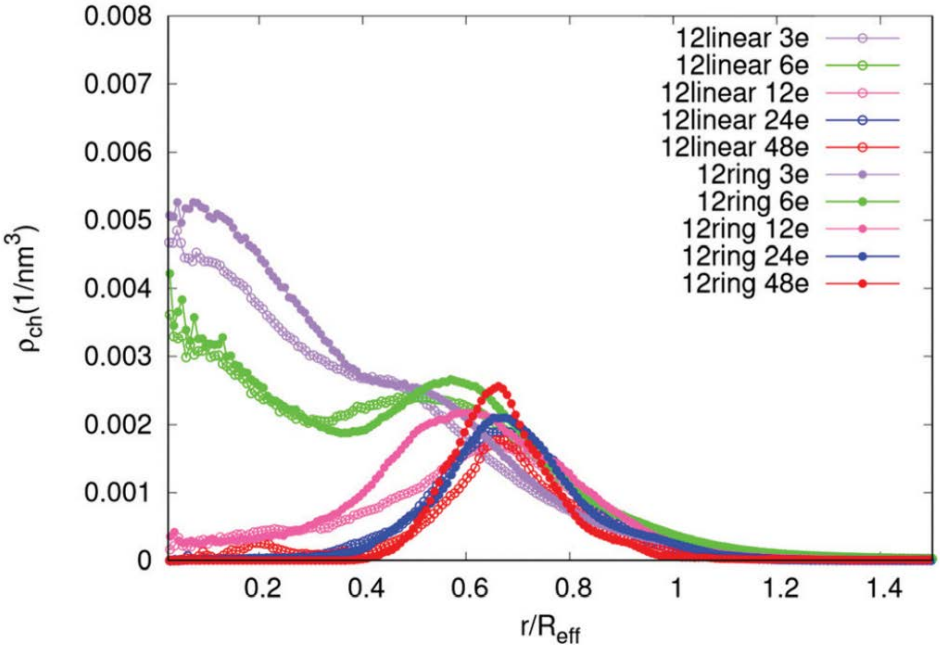

Figure 6.8: Spherically averaged local chain number density, $\rho_{ch}(r)$, as a function of the chain-nanogel center-to-center distance r for linear and ring polyelectrolytes of 12 monomers per chain.

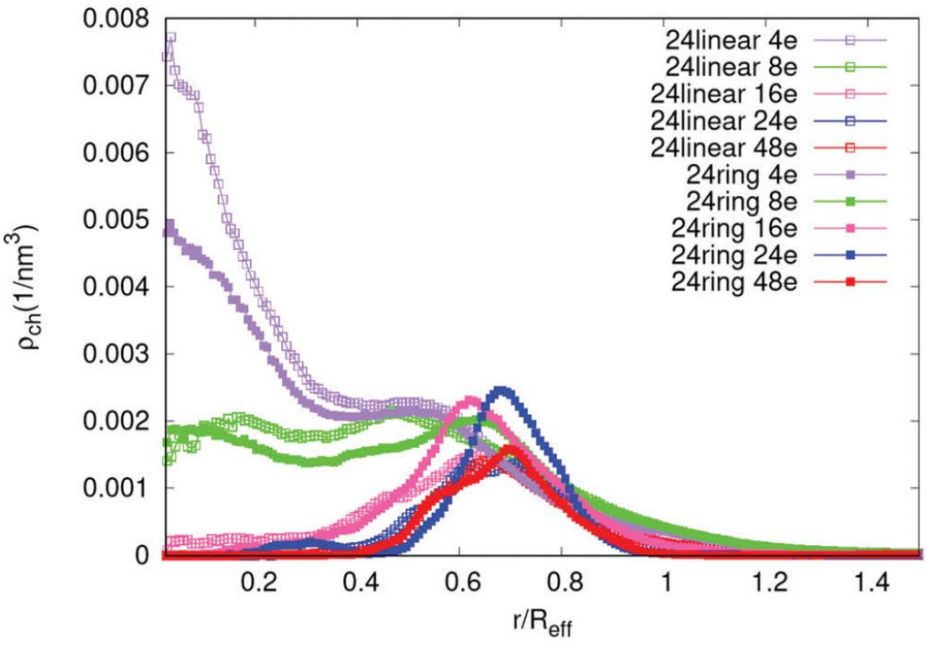

Figure 6.9: Spherically averaged local chain number density, $\rho_{ch}(r)$, as a function of the chain-nanogel center-to-center distance r for linear and ring polyelectrolytes of 24 monomers per chain.

6.4. Conclusions

In this work, we have performed coarse-grained Monte Carlo simulations of complexes formed by a nanogel and oppositely charged polyelectrolyte chains with different charge, number of monomers per chain and topology. Given that the model employed only involves nonspecific forces (electrostatic and excluded volume forces), the results can be extrapolated to a wide variety of nanogel-polyelectrolyte complexes to a great extent. Special attention has been paid to two phenomena observed in experiments with microgel-polyelectrolyte complexes: the deswelling and charge inversion undergone after absorption.

Our results reveal that the net charge of the complexes and their surface electrostatic potential are almost identical for linear and ring chains. In other words, the topology of the polyelectrolytes has little or no influence on many of these properties. This also implies that the distribution of charge in

polyelectrolyte chains is not a determining feature in phenomena such as charge inversion or the reduction of the complex size after absorbing some chains.

According to our results, charge inversion only takes place if the charge of the polyelectrolytes exceeds a threshold value, which suggests that strong electrostatic correlations between highly charged polyelectrolyte chains are responsible for such a phenomenon. It should also be stressed that the existence of charge inversion has a profound influence on the distribution of chains inside the nanogel. Slightly charged polyelectrolytes are preferentially located in the center of the nanogel. However, highly charged chains (which give rise to charge inversion) leave the center of the nanogel empty and form shells at different distances from it.

Conflicts of interest

There are no conflicts of interest to declare.

Acknowledgements

The authors thank the financial support from the following institutions: (i) 'Ministerio de Economía y Competitividad, Plan Estatal de Investigación-Científica y Técnica y de Innovación 2013-2016', Project FIS2016-80087-C2-2-P; (ii) European Regional Development Fund (ERDF).

6.5. References

1. R. Pelton, *Adv. Colloid Interface Sci.*, 2000, **85**, 1–33.
2. S. Seiffert, *J. Polym. Sci. Part A Polym. Chem.*, 2014, **52**, 435–449.
3. M. D. Blanco, S. Guerrero, C. Teijón, R. Olmo, L. Pastrana, I. Katime, and J. M. Teijón, *Polym. Int.*, 2008, **57**, 1215–1225.
4. A. V Kabanov and S. V Vinogradov, *Angew. CHEMIE-INTERNATIONAL Ed.*, 2009, **48**, 5418–5429.
5. J. K. Oh, R. Drumright, D. J. Siegwart, and K. Matyjaszewski, *Prog. Polym. Sci.*, 2008, **33**, 448–477.
6. K. Raemdonck, J. Demeester, and S. De Smedt, *Soft Matter*, 2009, **5**, 707–715.
7. M. Karg, A. Pich, T. Hellweg, T. Hoare, L. A. Lyon, J. J. Crassous, D. Suzuki,

R. A. Gumerov, S. Schneider, I. I. Potemkin, and W. Richtering, *Langmuir*, 2019, **35**, 6231–6255.

8. T. Casalini and G. Perale, *Gels*, 2019, 5, 28.
9. A. Tamura, M. Oishi, and Y. Nagasaki, *Biomacromolecules*, 2009, **10**, 1818–1827.
10. W. H. Blackburn, E. B. Dickerson, M. H. Smith, J. F. McDonald, and L. A. Lyon, *Bioconjug. Chem.*, 2009, **20**, 960–968.
11. R. Sunasee, P. Wattanaarsakit, M. Ahmed, F. B. Lollmahomed, and R. Narain, *Bioconjug. Chem.*, 2012, **23**, 1925–1933.
12. M. Ahmed, P. Wattanaarsakit, and R. Narain, *Polym. Chem.*, 2013, **4**, 3829–3836.
13. C. Vauthier, C. Zandanel, and A. L. Ramon, *Curr. Opin. Colloid Interface Sci.*, 2013, **18**, 406–418.
14. S. L. Goh, N. Murthy, M. Xu, and J. M. J. Fréchet, *Bioconjug. Chem.*, 2004, **15**, 467–474.
15. E. Mauri, G. Perale, and F. Rossi, *ACS Appl. Nano Mater.*, 2018, **1**, 6525–6541.
16. D. Huang, H. Qian, H. Qiao, W. Chen, J. Feijen, and Z. Zhong, *Expert Opin. Drug Deliv.*, 2018, **15**, 703–716.
17. R. Kandil and O. M. Merkel, *Curr. Opin. Colloid Interface Sci.*, 2019, **39**, 11–23.
18. J. Kleinen and W. Richtering, *Macromolecules*, 2008, **41**, 1785–1790.
19. J. Kleinen and W. Richtering, *J. Phys. Chem. B*, 2011, **115**, 3804–3810.
20. J. Kleinen and W. Richtering, *Colloid Polym. Sci.*, 2011, **289**, 739–749.
21. S. Walta, D. V. Pergushov, A. Oppermann, A. A. Steinschulte, K. Geisel, L. V. Sigolaeva, F. A. Plamper, D. Wöll, and W. Richtering, *Polymer (Guildf).*, 2017, **119**, 50–58.
22. H. Bysell, P. Hansson, and M. Malmsten, *J. Phys. Chem. B*, 2010, **114**, 7207–7215.
23. A. P. H. Gelissen, A. Scotti, S. K. Turnhoff, C. Janssen, A. Radulescu, A. Pich, A. A. Rudov, I. I. Potemkin, and W. Richtering, *Soft Matter*, 2018, **14**,

4287–4299.

24. W. M. Gelbart, R. F. Bruinsma, P. A. Pincus, and V. A. Parsegian, *Phys. Today*, 2000, **53**, 38–44.
25. Y. Levin, *Reports Prog. Phys.*, 2002, **65**, 1577–1632.
26. A. Y. Grosberg, T. T. Nguyen, and B. I. Shklovskii, *Rev. Mod. Phys.*, 2002, **74**, 329–345.
27. M. Quesada-Perez, E. Gonzalez-Tovar, A. Martin-Molina, M. Lozada-Cassou, and R. Hidalgo-Alvarez, *CHEMPHYSCHEM*, 2003, **4**, 234–248.
28. Y. Levin, *BRAZILIAN J. Phys.*, 2004, **34**, 1158–1176.
29. J. Faraudo and A. Martin-Molina, *Curr. Opin. Colloid Interface Sci.*, 2013, **18**, 517–523.
30. G. C. Claudio, K. Kremer, and C. Holm, *J. Chem. Phys.*, 2009, **131**, 094903.
31. P. K. Jha, J. W. Zwanikken, F. A. Detcheverry, J. J. de Pablo, and M. O. de la Cruz, *Soft Matter*, 2011, **7**, 5965–5975.
32. L. Rovigatti, N. Gnan, and E. Zaccarelli, *J. PHYSICS-CONDENSED MATTER*, 2018, **30**.
33. L. Rovigatti, N. Gnan, L. Tavagnacco, A. J. Moreno, and E. Zaccarelli, *Soft Matter*, 2019, **15**, 1108–1119.
34. A. Martín-Molina and M. Quesada-Pérez, *J. Mol. Liq.*, 2019, **280**, 374–381.
35. E. S. Minina, P. A. Sánchez, C. N. Likos, and S. S. Kantorovich, *J. Mol. Liq.*, 2019, **289**, 111066.
36. T. Colla, R. Blaak, and C. N. Likos, *Soft Matter*, 2018, **14**, 5106–5120.
37. T. Colla, P. S. Mohanty, S. Nojd, E. Bialik, A. Riede, P. Schurtenberger, and C. N. Likos, *ACS Nano*, 2018, **12**, 4321–4337.
38. J. Riest, L. Athanasopoulou, S. A. Egorov, C. N. Likos, and P. Ziherl, *Sci. Rep.*, 2015, **5**.
39. H. Lowen, A. Esztermann, A. Wysocki, E. Allahyarov, R. Messina, A. Jusufi, N. Hoffmann, D. Gottwald, G. Kahl, M. Konieczny, and C. N. Likos, in *Kinetic Theory of Nonideal Plasmas*, ed. Bonitz, M and Kraeft, WD, IOP PUBLISHING LTD, DIRAC HOUSE, TEMPLE BACK, BRISTOL BS1 6BE, ENGLAND, 2005, vol. 11, pp. 207–222.

40. M. Quesada-Perez and A. Martin-Molina, *Soft Matter*, 2013, **9**, 7086–7094.

41. M. Quesada-Pérez, S. Ahualli, and A. Martín-Molina, *J. Chem. Phys.*, 2014, **141**, 124903.

42. R. Schroeder, A. A. Rudov, L. A. Lyon, W. Richtering, A. Pich, and I. I. Potemkin, *Macromolecules*, 2015, **48**, 5914–5927.

43. H. Kobayashi and R. Winkler, *Polymers (Basel).*, 2014, **6**, 1602–1617.

44. A. Moncho-Jorda and I. Adroher-Benitez, *Soft Matter*, 2014, **10**, 5810–5823.

45. H. Kobayashi and R. G. Winkler, *Sci. Rep.*, 2016, **6**.

46. H. Kobayashi, R. Halver, G. Sutmann, and R. G. Winkler, *Polymers (Basel).*, 2017, **9**.

47. N. Gnan, L. Rovigatti, M. Bergman, and E. Zaccarelli, *Macromolecules*, 2017, **50**, 8777–8786.

48. M. D. M. Ramos-Tejada and M. Quesada-Pérez, *Macromolecules*, 2019, **52**, 2223–2230.

49. M. Muñoz-Úbeda, S. K. Misra, A. L. Barrán-Berdón, C. Aicart-Ramos, M. B. Sierra, J. Biswas, P. Kondaiah, E. Junquera, S. Bhattacharya, and E. Aicart, *J. Am. Chem. Soc.*, 2011, **133**, 18014–18017.

50. M. Muñoz-Úbeda, A. Rodríguez-Pulido, A. Nogales, O. Llorca, M. Quesada-Pérez, A. Martín-Molina, E. Aicart, and E. Junquera, *Soft Matter*, 2011, **7**, 5991.

51. M. Quesada-Perez and A. Martin-Molina, *Soft Matter*, 2013, **9**, 7086–7094.

52. S. Schneider and P. Linse, *J. Phys. Chem.* B, 2003, **107**, 8030–8040.

53 S. Schneider and P. Linse, *Macromolecules*, 2004, **37**, 3850–3856.

54 S. Edgecombe, S. Schneider and P. Linse, *Macromolecules*, 2004, **37**, 10089–10100.

55 B. A. Mann, C. Holm and K. Kremer, *J. Chem. Phys*., 2005, **122**, 154903.

52. S. Ahualli, A. Martin-Molina, J. Alberto Maroto-Centeno, and M. Quesada-Perez, *Macromolecules*, 2017, **50**, 2229–2238.

6. Paper III *Physical Chemistry Chemical Physics*, **2020**, *16*, 3022.

7. Conclusions

A long this thesis we have carried out simulations of gels and nanogels, exploring their use for encapsulation of spherical cosolutes (which could represent therapeutic drugs, reactants, globular proteins and other biomacromolecules), different electrolytes or even polyelectrolyte chains. Let us review the most important results we have obtained throughout this work.

7.1. Paper I

In this work, we have performed coarse-grained Monte Carlo simulations of the absorption of diluted spherical cosolutes inside a neutral hydrogel for different swelling states. The competition between the excluded-volume repulsion and the solvent-induced hydrophobic attraction between the monomeric units and the cosolute particle has been analyzed. The simulations results show two well-defined regimes depending on the strength of the attractive forces. For small hydrophobic attractions, the steric exclusion dominates and the partition coefficient decreases monotonically with the polymer volume fraction.

On the other hand, for sufficiently large hydrophobic attractions, a maximum of the partition coefficient at some intermediate polymer volume fraction is found. This is a result of the competition between steric exclusion and hydrophobic adhesion. The location and height of the peak increase with the depth and range of the hydrophobic interaction, but decrease with the cosolute

radius, due to the increase of the volume exclusion effect. The existence of this peak in the partition coefficient means that the uptake of some specific hydrophobic cosolutes can be maximized by adjusting its swelling state, its internal morphology (for instance, modifying the cross-linker density) or the nature of the polymer chains.

The simulation results are consistent with the theoretical model based on the calculation of the volumes of the regions of exclusion and attraction around the polymer chains, specially, in the regime of swollen hydrogels, where we achieved a very good quantitative agreement between theory and simulations. The theoretical model is able to provide the conditions required for the maximum absorption of a cosolute.

7.2. Paper II

In this work, we have studied the effects of dispersion forces on the absorption of different electrolytes into nanogels by means of coarse-grained Monte Carlo simulations. Our results prove that dispersion forces can induce charge inversion and electrostatic potential inversion for slightly charged cationic nanogels in the presence of NaSCN. This phenomenon has also been observed experimentally with PNIPAM microgels even at low NaSCN concentrations (such as 0.01 M). Charge inversion might also be observed for other ions and polymers if these ionic species and the corresponding monomeric units have small sizes and high polarizability. It should also be noted that this phenomenon disappears when the bare charge of the nanogel increases.

On the other hand, dispersion forces do not seem to have relevant effects on the net charge or the surface electrostatic potential when NaCl or $NaNO_3$ are present. Furthermore, the effects of dispersion forces on nanogel size are negligible for the three electrolytes studied.

7.3. Paper III

In this work, we have carried out coarse-grained Monte Carlo simulations of complexes consisting of a nanogel and oppositely charged polyelectrolyte chains with different charges, numbers of monomers per chain and topology. The results obtained can be extrapolated to a great extent to a wide variety of nanogel–polyelectrolyte complexes since the model employed only involves nonspecific forces (electrostatic and excluded volume forces). Our simulation results explain two phenomena observed experimentally with different

microgel-polyelectrolyte complexes: the deswelling and charge inversion undergone after absorption.

Additionally, it has been observed that topology of the polyelectrolytes has little or no influence on properties like the net charge or the surface electrostatic potential of these complexes. Moreover, the existence of charge inversion has a profound effect on the chain distribution inside the nanogel. Highly charged chains (which give rise to charge inversion) leave the center of the nanogel empty and form shells at different distances from it. However, slightly charged polyelectrolytes are preferentially located in the center of the nanogel.